

## ***In situ* modification of nanostructure configuration through the manipulation of hydrogen bonded amphiphile self-association**

Jennifer R. Hiscock,<sup>a\*</sup> Gianluca P. Bustone,<sup>a</sup> Ben Wilson,<sup>a</sup> Kate E. Belsey<sup>a</sup> and Laura R. Blackholly<sup>b</sup>

<sup>a</sup>*School of Physical Sciences, University of Kent, Park Wood Road, Canterbury, Kent, CT2 7NH, UK;*  
*Email: [J.R.Hiscock@Kent.ac.uk](mailto:J.R.Hiscock@Kent.ac.uk); Tel: +44 (0)1227 823043.*

<sup>b</sup>*School of Biosciences, University of Kent, Park Wood Road, Canterbury, Kent, CT2 7NH, UK.*

### **Electronic Supplementary Information**

## **Table of Contents**

Experimental .....	2
Characterisation NMR .....	4
Further NMR experiments .....	10
2D NMR experiments .....	11
<sup>1</sup> H NMR Binding Studies .....	18
<sup>1</sup> H NMR Job plot studies .....	24
DLS data .....	26
Count rate .....	26
Correlation data .....	27
Size distribution calculated by DLS .....	50
UV-Vis spectra .....	62
Powder X-ray diffraction .....	64
General procedure .....	64
Compound 4 .....	64
Compound 5 .....	65
TEM data .....	66
Sample preparation .....	66
Images .....	66
Filtered DMSO only .....	66
Compound 1 only .....	67
Compound 1 and 2 .....	69
Compound 1 and 6 .....	72
References .....	73

## Experimental

**General remarks:** All reactions were performed under slight positive pressure of nitrogen using oven dried glassware. NMR spectra were determined on a Jeol ECS-400 or a Bruker AV3 600 MHz spectrometer with the chemical shifts reported in parts per million (ppm), calibrated to the centre of the solvent peak set. All solvents and starting materials were purchased from chemical stores where available. High resolution mass spectra were collected by a Bruker micrOTOF-Q mass spectrometer. Samples were run by School of Biosciences, University of Kent. TEM images were obtained on a Jeol 1230 equipped with a Gatan multiscan digital camera. It was operated at an accelerating voltage of 80kV. Melting points were recorded in open capillaries on a Stuart SMP10 melting point apparatus and are uncorrected. Infrared (IR) spectra were recorded on a Shimadzu IR-Affinity 1, and reported in wavenumbers ( $\text{cm}^{-1}$ ). DLS studies were performed on a Malvern Zetasizer Nano ZS. UV-Vis were recorded on a Shimadzu UV-1800, and reported in nm.

**DLS studies:** The studies conducted with compound **1** were done in series with an aliquot of the most concentrated solution undergoing serial dilution. The studies conducted with compounds **1**, **6** and various TBA halide salts were done in series with compound **6** added to previously annealed solutions of compound **1** and TBA halide. Sample sizes were kept to 1 mL. All solvents used for DLS studies were filtered to remove particulates from the solvents. Samples were heated to the appropriate temperature and allowed to equilibrate for 2 minutes and then a series of 10 'runs' were performed with each sample to give enough data to derive an appropriate average. In some instances the raw correlation data indicated that a greater amount of time may be needed for the samples to reach a stable state. For this reason only the last 9 'runs' were included in the average size distribution calculations.

**HRMS studies:** Samples were dissolved in DMSO at a concentration of 1 mg/ml before being diluted 1 in 100 in methanol. 10  $\mu\text{l}$  of sample was injected into a flowing stream of 10 mM ammonium acetate in 95% methanol in water (flow rate: 0.02 ml/min) and the flow directed into the electrospray source of the mass spectrometer. Mass spectra were acquired in the positive ion mode and data processed in Bruker's Compass Data Analysis software utilising a lock mass.

**UV-Vis studies:** Sample were prepared in series with an aliquot of the most concentrated solution undergoing serial dilution. All solutions underwent an annealing process and were allowed to rest for approximately 2 minutes before undergoing analysis.

**Compound 1:** 1-Isocyanato-4-(trifluoromethyl)benzene (0.32 g, 1.82 mM) was added to a stirring solution of aminomethanesulfonic acid (0.21 g, 1.82 mM) in anhydrous pyridine (10 mL) under an inert atmosphere. The mixture was heated to 60 °C overnight. The pyridinium salt was then removed by filtration. Yield: 82 % (0.56 g, 1.49 mM). The pyridinium salt (0.20 g, 0.53 mM) was dissolved in a 1M solution of tetrabutylammonium hydroxide in methanol (0.53 mL). This solution was then taken to dryness and dissolved in DCM (20 mL) and washed with water (50 mL). The organic fraction was then dried with magnesium sulfate and then taken to dryness to give the pure product as a white solid. Yield: 100 % (2.85 g, 0.53 mM); mp: 142 °C;  $^1\text{H}$  NMR (400 MHz,  $\text{DMSO}-d_6$ ):  $\delta$ : 0.92 (t,  $J_1 = 7.36$  Hz, 12H), 1.25-1.35 (br m, 8H), 1.52-1.60 (br m, 8H), 3.14-3.18 (br m, 8H), 3.93 (d,  $J_1 = 5.96$  Hz, 2H), 6.98 (t,  $J_1 = 5.96$  Hz, 1H, NH), 7.49 (d,  $J_1 = 9.16$  Hz,  $J_2 = 8.72$ Hz, 2H), 7.56 (d,  $J_1 = 8.72$  Hz, 2H), 9.26 (s, 1H, NH);  $^{13}\text{C}\{^1\text{H}\}$  NMR (100 MHz,  $\text{DMSO}-d_6$ ):  $\delta$ : 13.5 ( $\text{CH}_3$ ), 19.2 ( $\text{CH}_2$ ), 23.1 ( $\text{CH}_2$ ), 55.9 ( $\text{CH}_2$ ), 57.5 ( $\text{CH}_2$ ), 117.1 (ArCH), 121.0 (ArC), 124.7 (q,  $J = 269.8$  Hz,  $\text{CF}_3$ ), 125.8 (q,  $J = 4.0$  Hz, ArC), 144.3 (ArC), 154.2 (CO); IR (film):  $\nu = 3277$  (NH stretch), 1693, 1230, 1107, 840; HRMS for the sulfonate-urea ion ( $\text{C}_9\text{H}_8\text{F}_3\text{N}_2\text{O}_4\text{S}$ ) (ESI):  $m/z$ : act: 297.0170 [ $\text{M}$ ] $^-$  cal: 297.0162 [ $\text{M}$ ] $^-$ .

**Compound 2:** This compound was synthesised in line with previously published methods.<sup>1</sup>

**Compound 3:** Ethylanesulfonic acid (0.25 g, 2.27 mM) was dissolved in a 1M solution of tetrabutylammonium hydroxide in methanol (2.27 mL). The solution was then taken to dryness to give the tetrabutylammonium salt of the acid as a white crystalline solid. Yield: 100 % (0.78 g, 2.27 mM);  $^1\text{H}$  NMR (400 MHz, DMSO- $d_6$ ):  $\delta$ : 0.93 (t,  $J$  = 7.32 Hz, 12H), 1.04 (t,  $J$  = 7.32 Hz, 3H), 1.31 (dt,  $J_1$  = 14.64 Hz,  $J_2$  = 7.52 Hz, 3H), 1.53-1.60 (br m, 8H), 2.35 (q,  $J$  = 7.80 Hz, 2H), 3.15-3.19 (br m, 8H).

**Compound 4:** The compound was produced with an analogous method to that described with the synthesis of compound 1. A single equivalent of KOH (0.03 g, 0.53 mM) was added to an aqueous solution (1 mL) of the pyridium salt (0.20 g, 0.53 mM) described in the synthesis of compound 1. The water and remaining pyridine was then removed by slow evaporation giving the crude potassium salt of compound 1. The proton spectrum was found to correlate with that observed for compound 1.  $^1\text{H}$  NMR (400 MHz, DMSO- $d_6$ ):  $\delta$ : 3.93 (d,  $J_1$  = 5.96 Hz, 2H), 6.83 (s, 1H, NH), 7.50-7.57 (m, 4H), 9.21 (s, 1H, NH).

**Compound 5:** Aminomethanesulfonic acid (0.35 g, 3.05 mM) in acetonitrile (6 mL) was added to a stirring solution of 1-isocyanato-4-nitrobenzene (0.50 g, 3.05 mM) in a 1N solution of tetrabutylammonium hydroxide in methanol (3.05 mL). The solution was allowed to stir overnight at room temperature. The mixture was then taken to dryness and the resulting oil, dissolved in DCM (20 mL), was washed twice with water (20 mL). The organic phase was dried with magnesium sulfate, taken to dryness and the pure product obtained by flash chromatography 100 % ethyl acetate followed by 100 % methanol. The methanol fraction was taken to dryness to give the pure product as a yellow solid. Yield: 29 % (0.46 g, 0.89 mM); mp: 167 °C;  $^1\text{H}$  NMR (400 MHz, DMSO- $d_6$ ):  $\delta$ : 0.92 (t,  $J_1$  = 7.36 Hz, 12H), 1.25-1.35 (br m, 8H), 1.52-1.60 (br m, 8H), 3.14-3.18 (br m, 8H), 3.96 (d,  $J_1$  = 5.96 Hz, 2H), 7.30 (t,  $J_1$  = 5.96 Hz, 1H, NH), 7.58 (d,  $J_1$  = 9.16 Hz, 2H), 8.04 (d,  $J_1$  = 9.16 Hz, 2H), 9.63 (s, 1H, NH);  $^{13}\text{C}\{^1\text{H}\}$  NMR (100 MHz, DMSO- $d_6$ ):  $\delta$ : 13.5 (CH<sub>3</sub>), 19.2 (CH<sub>2</sub>), 23.1 (CH<sub>2</sub>), 55.8 (CH<sub>2</sub>), 57.5 (CH<sub>2</sub>), 116.8 (ArCH), 124.9 (ArCH), 140.3 (ArC), 147.3 (ArC), 153.8 (CO); IR (film):  $\nu$  = 3271 (NH amide stretch), 1697, 1220, 1111, 851; HRMS for the sulfonate-urea ion (C<sub>8</sub>H<sub>8</sub>N<sub>3</sub>O<sub>6</sub>S) (ESI<sup>-</sup>):  $m/z$ : act: 274.0141 [M]<sup>-</sup> cal: 274.0139 [M]<sup>-</sup>.

**Compound 6:** This compound was synthesised by previously published, well established methods.<sup>2</sup>

# Characterisation NMR

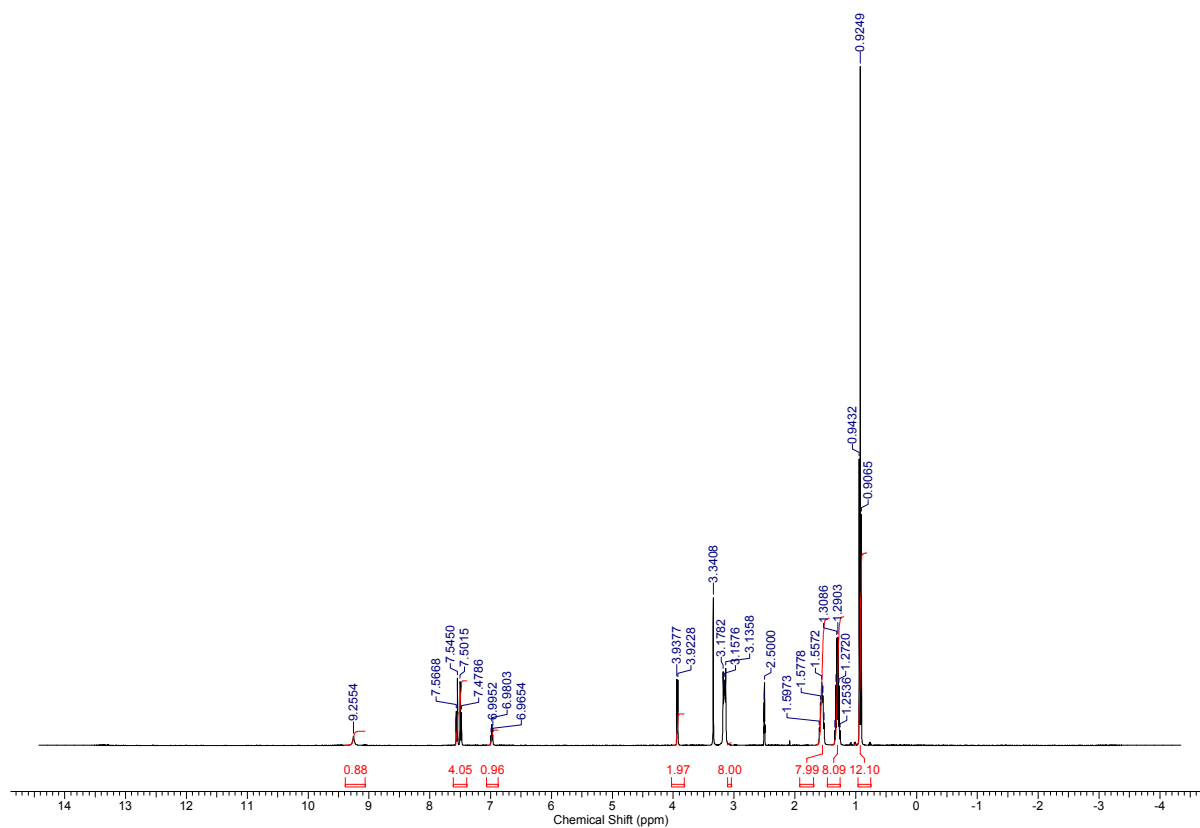


Figure S1 –  $^1\text{H}$  NMR of compound **1** in  $\text{DMSO-d}_6$ .

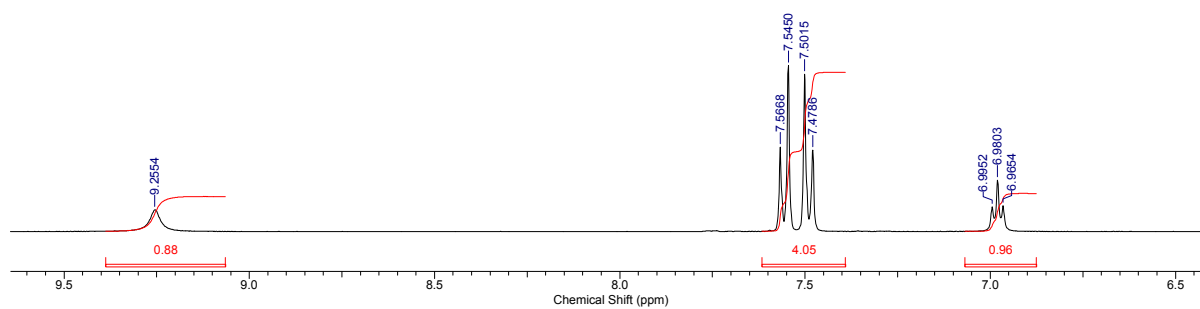


Figure S2 –  $^1\text{H}$  NMR of compound **1** in  $\text{DMSO-d}_6$ .

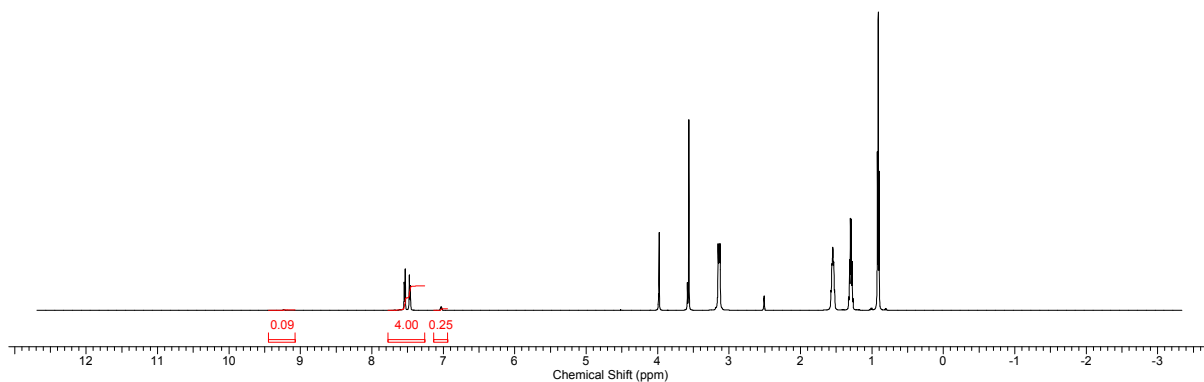


Figure S3 –  $^1\text{H}$  NMR of compound **1** in a  $\text{DMSO-d}_6/\text{D}_2\text{O}$  (10%) mixture. Proton NMR analysis showed 75 % to 91 % exchange for the two NH protons of **1** within 30 minutes.

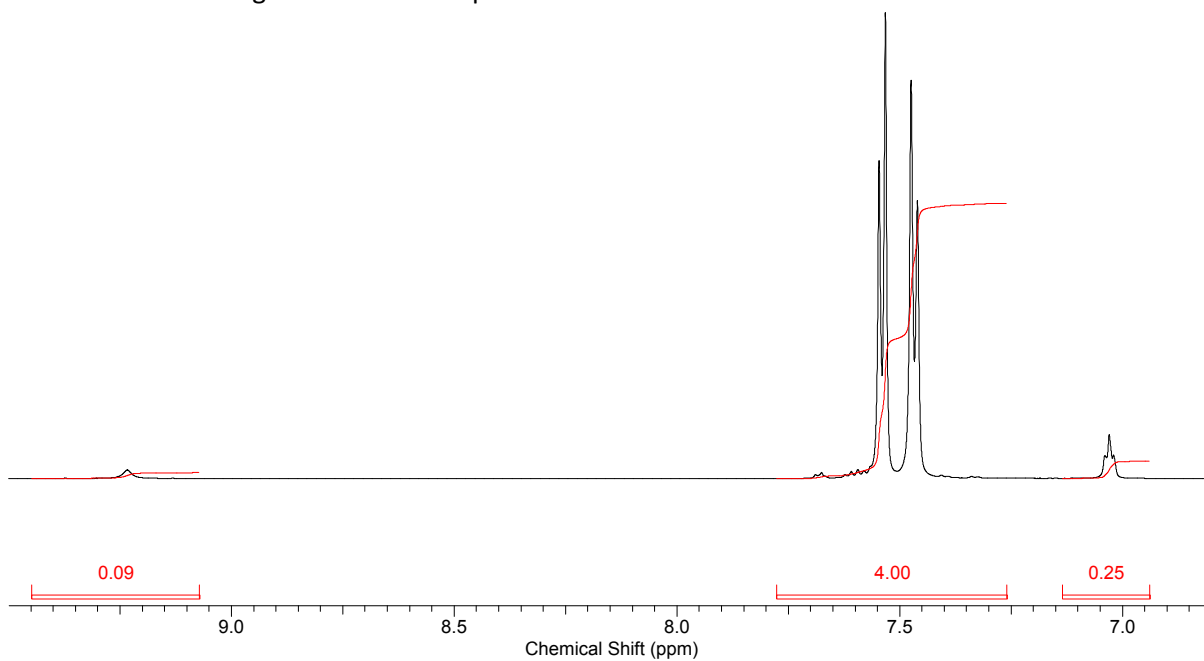


Figure S4 –  $^1\text{H}$  NMR of compound **1** in a  $\text{DMSO-d}_6/\text{D}_2\text{O}$  (10%) mixture. Proton NMR analysis showed 75 % to 91 % exchange for the two NH protons of **1** within 30 minutes.

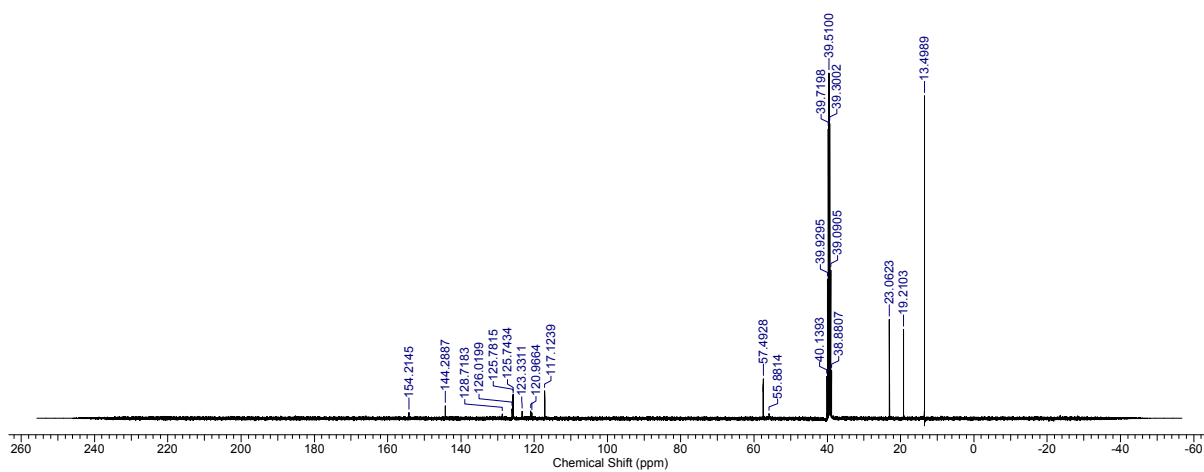
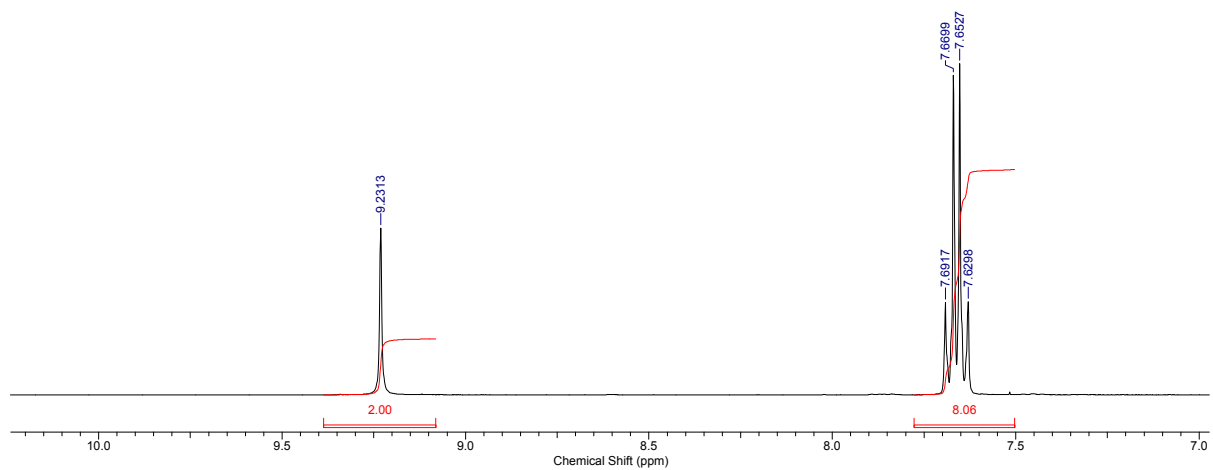
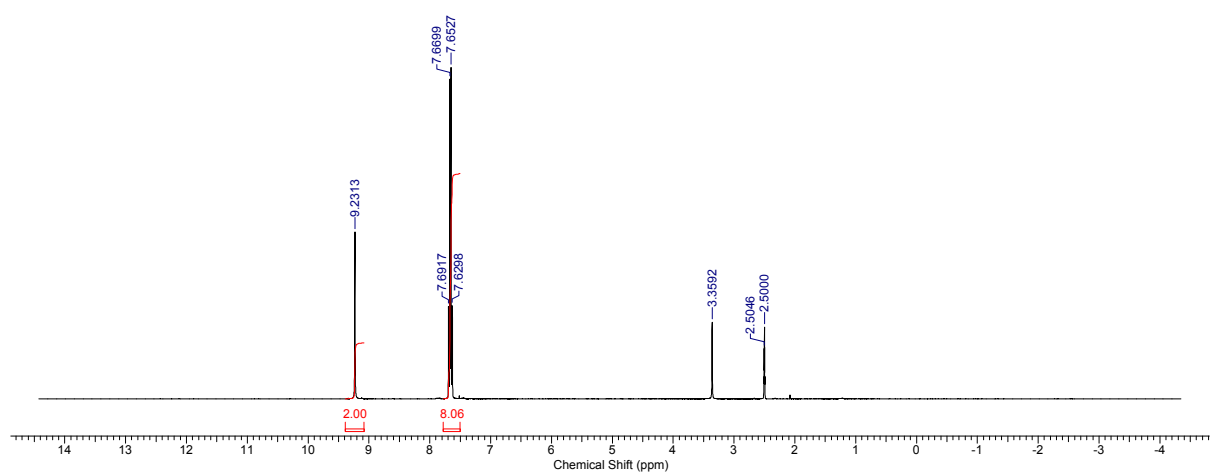
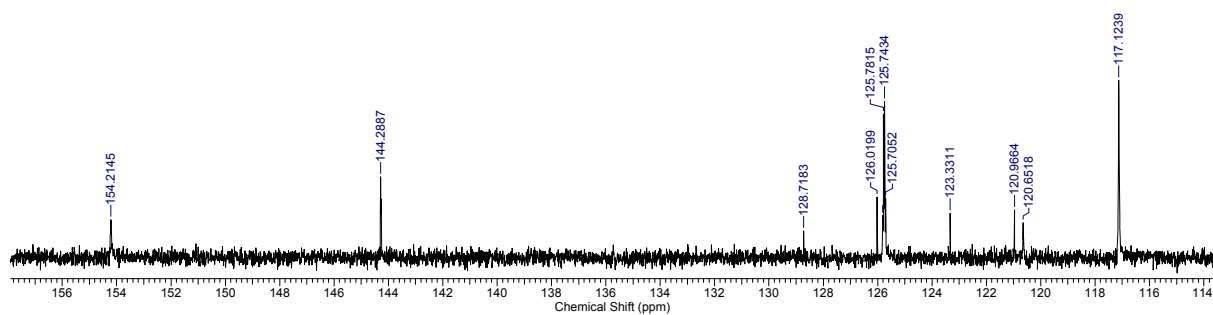
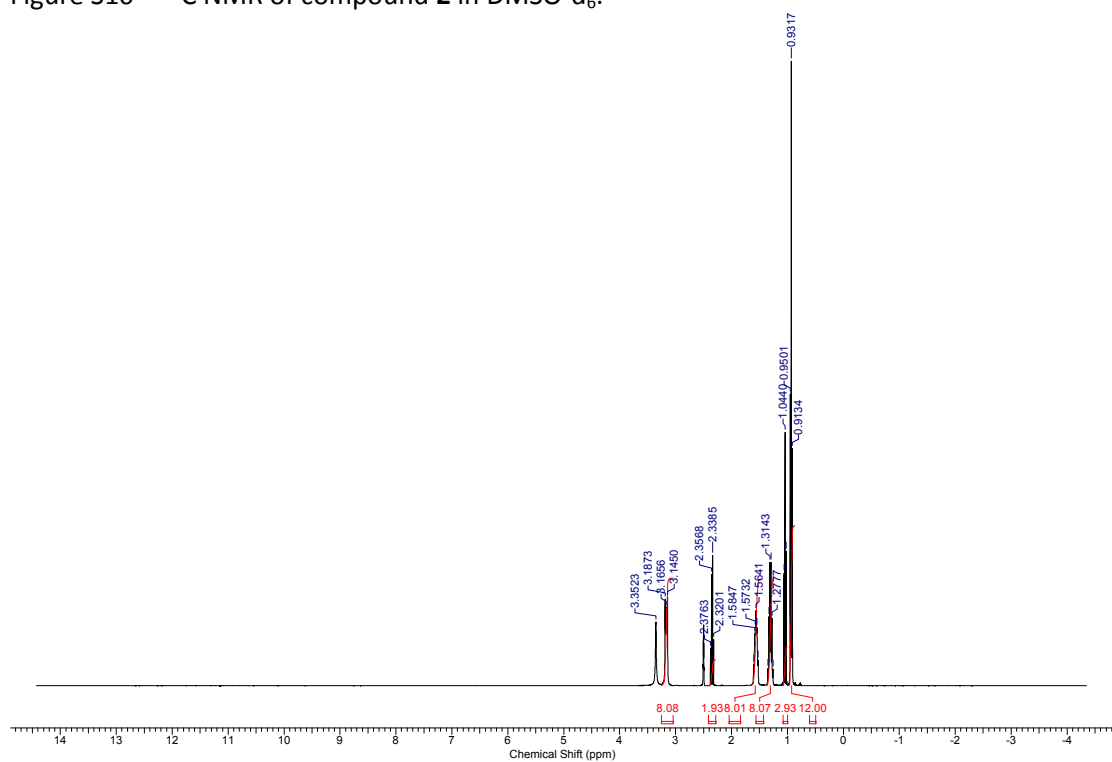
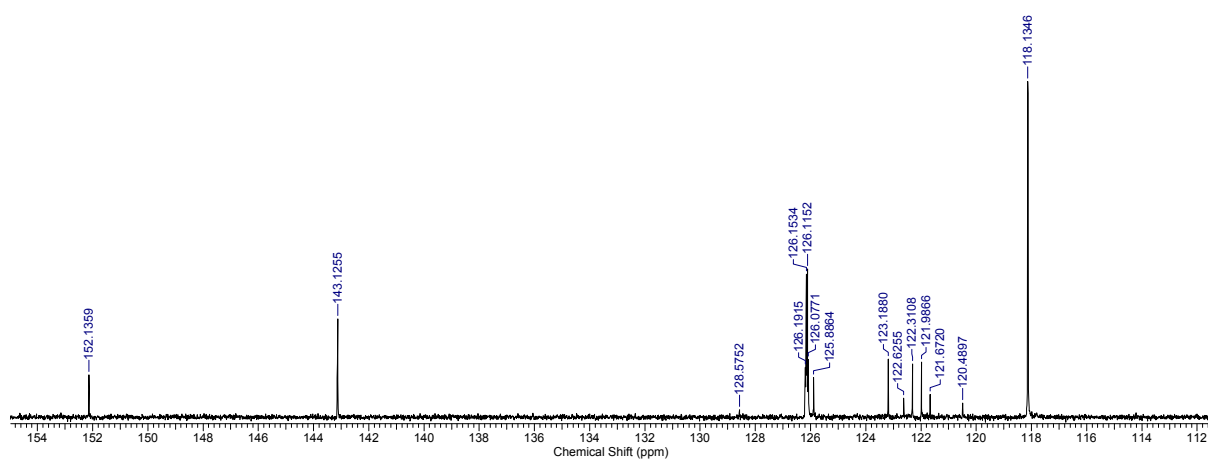
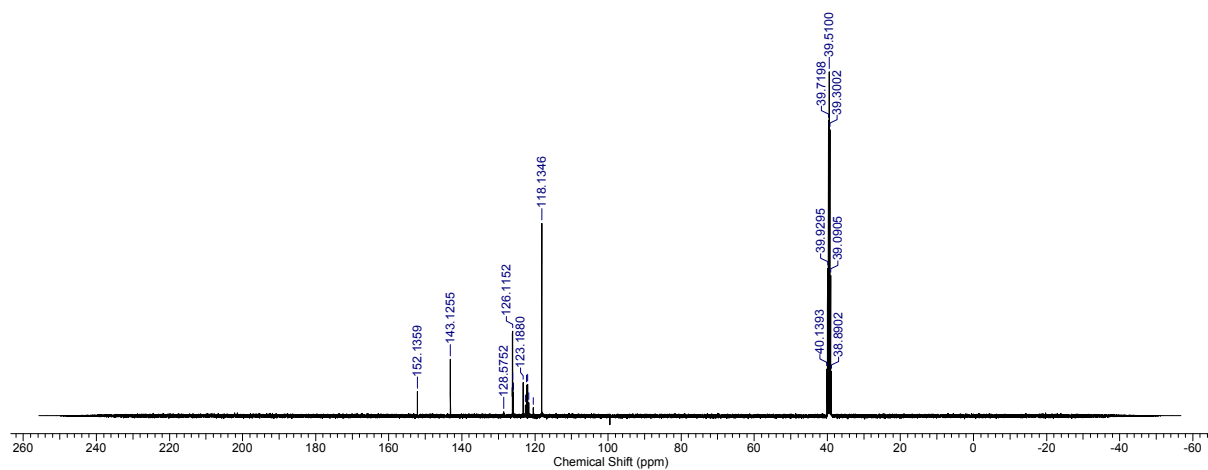


Figure S5 –  $^{13}\text{C}$  NMR of compound **1** in  $\text{DMSO-d}_6$ .





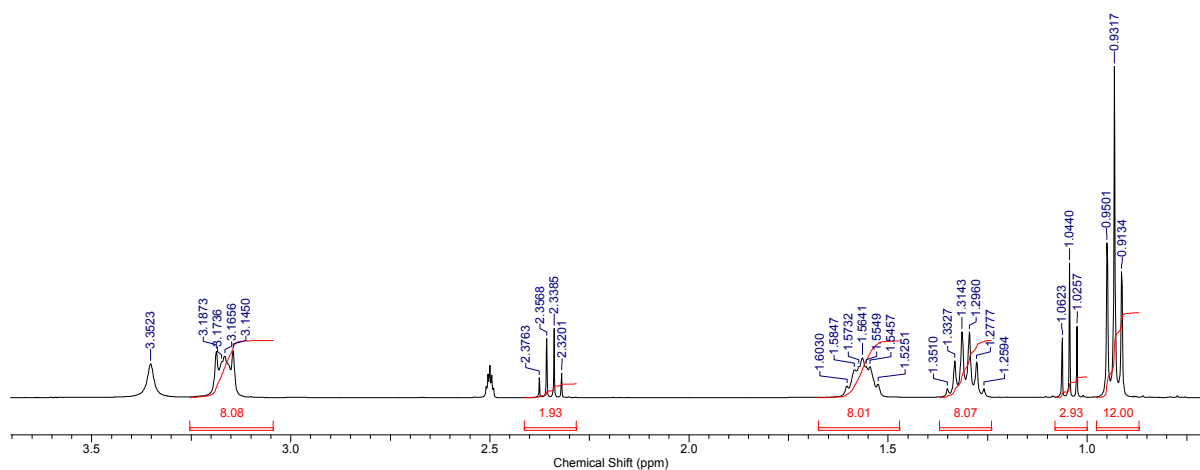


Figure S12 –  $^1\text{H}$  NMR of compound **3** in  $\text{DMSO-d}_6$ .

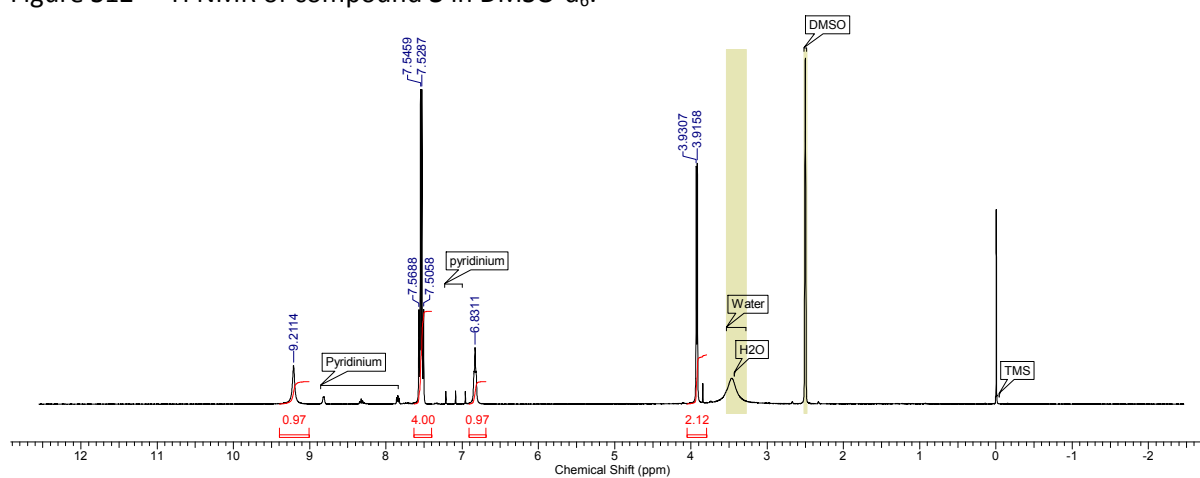


Figure S13 –  $^1\text{H}$  NMR of crude compound **4** in  $\text{DMSO-d}_6$ .

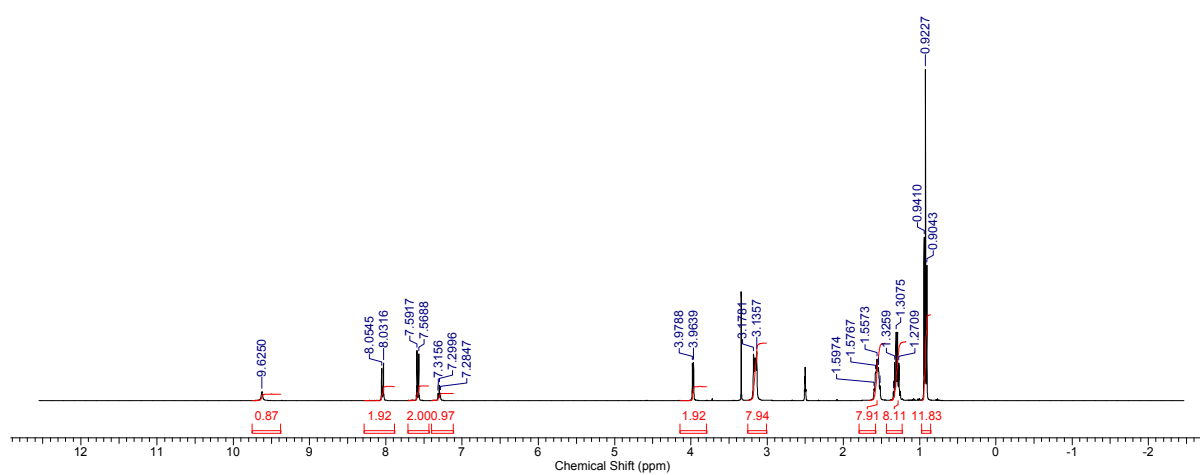


Figure S14 –  $^1\text{H}$  NMR of compound **5** in  $\text{DMSO-d}_6$ .

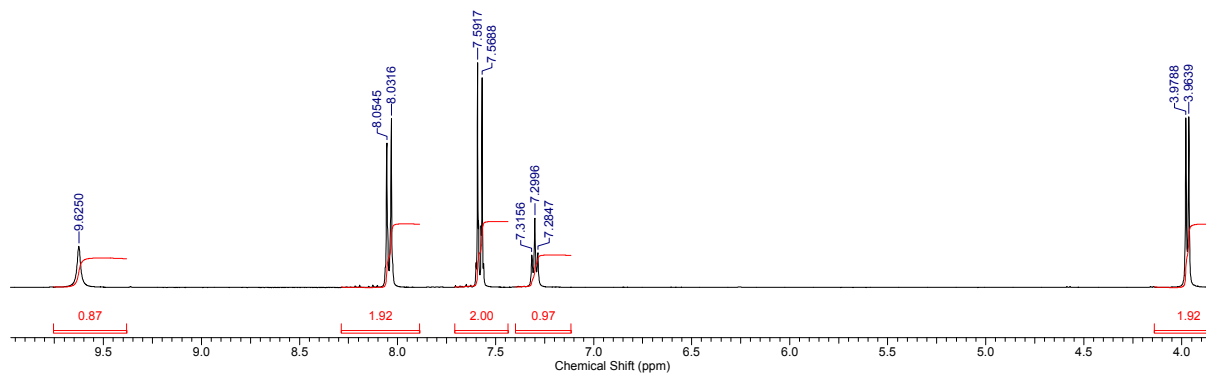


Figure S15 –  $^1\text{H}$  NMR of compound **5** in  $\text{DMSO-d}_6$ .

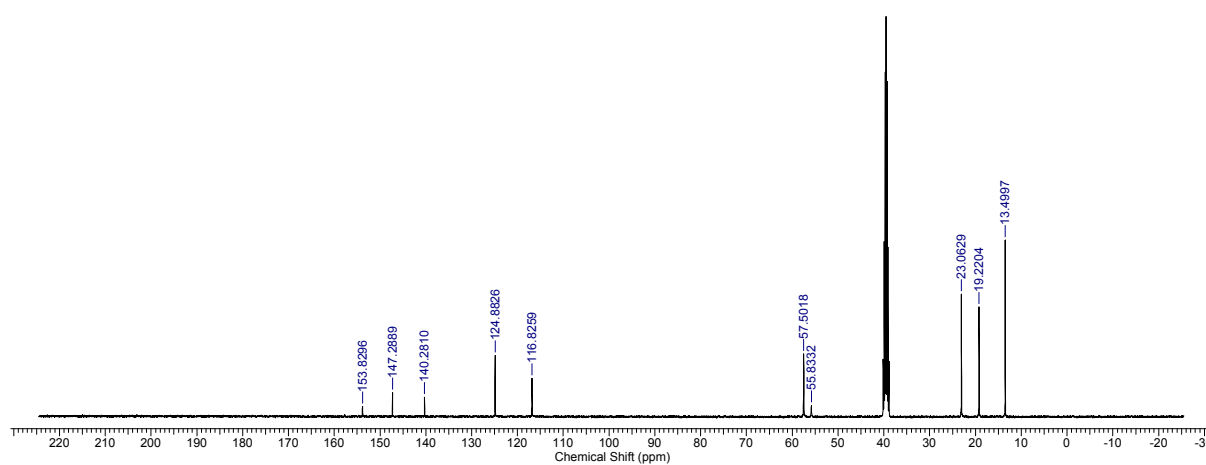


Figure S16 –  $^{13}\text{C}$  NMR of compound **5** in  $\text{DMSO-d}_6$ .

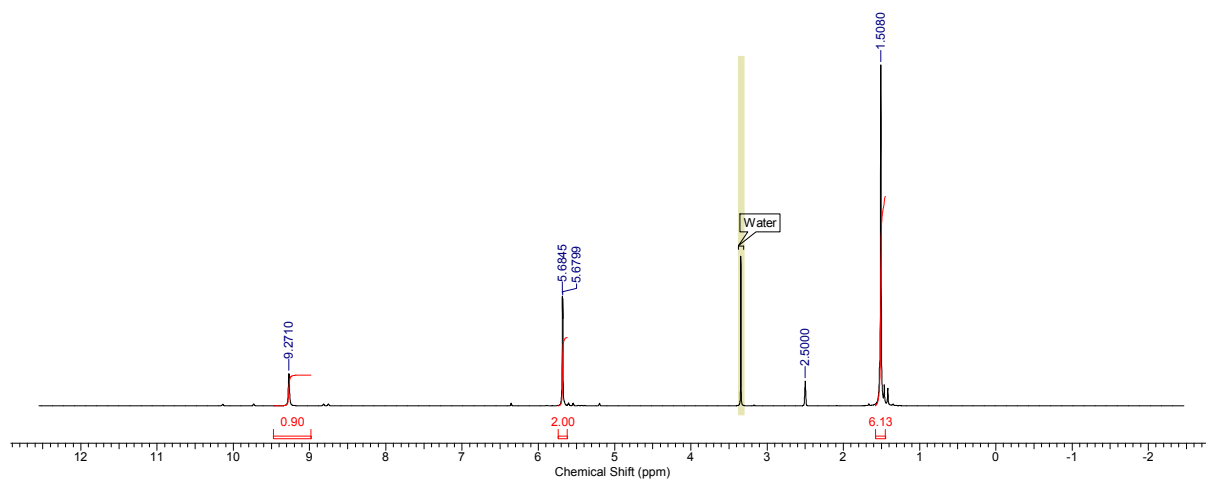


Figure S17 –  $^1\text{H}$  NMR of compound **6** in  $\text{DMSO-d}_6$ .

## Further NMR experiments

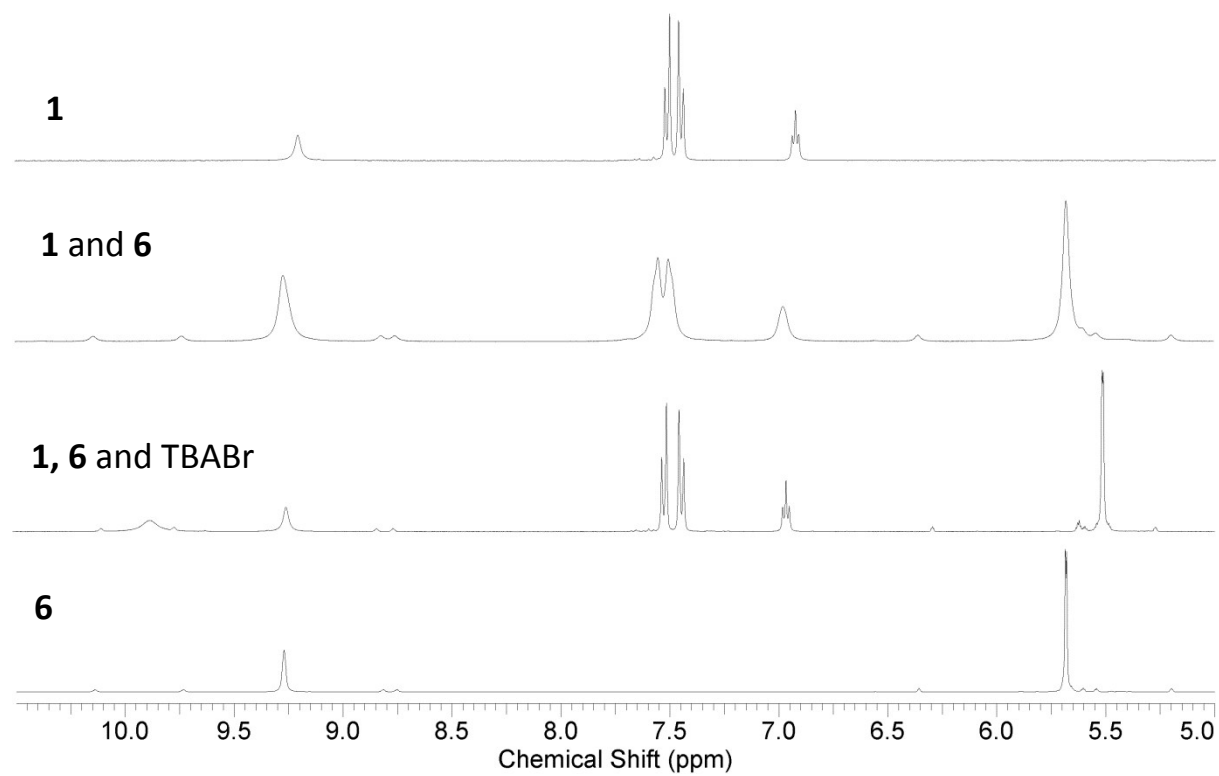


Figure S18 – Comparative  $^1\text{H}$  NMR stack plot of compound **1**, **6** and TBABr in  $\text{DMSO-d}_6$ .

## 2D NMR experiments

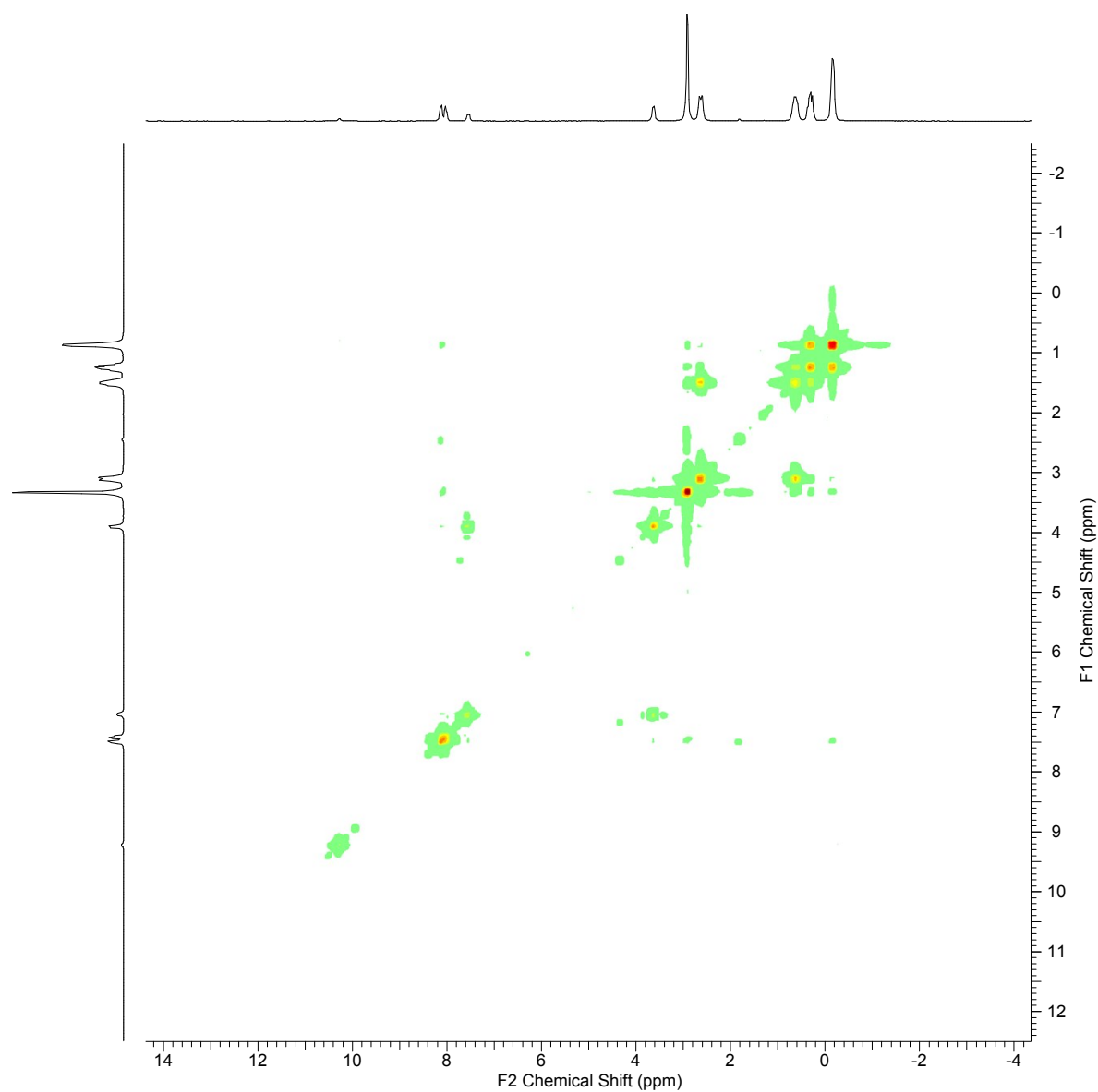


Figure S19 –  $^1\text{H}$  COSY NMR of an equimolar solution of compound **1** in  $\text{DMSO-d}_6$ .

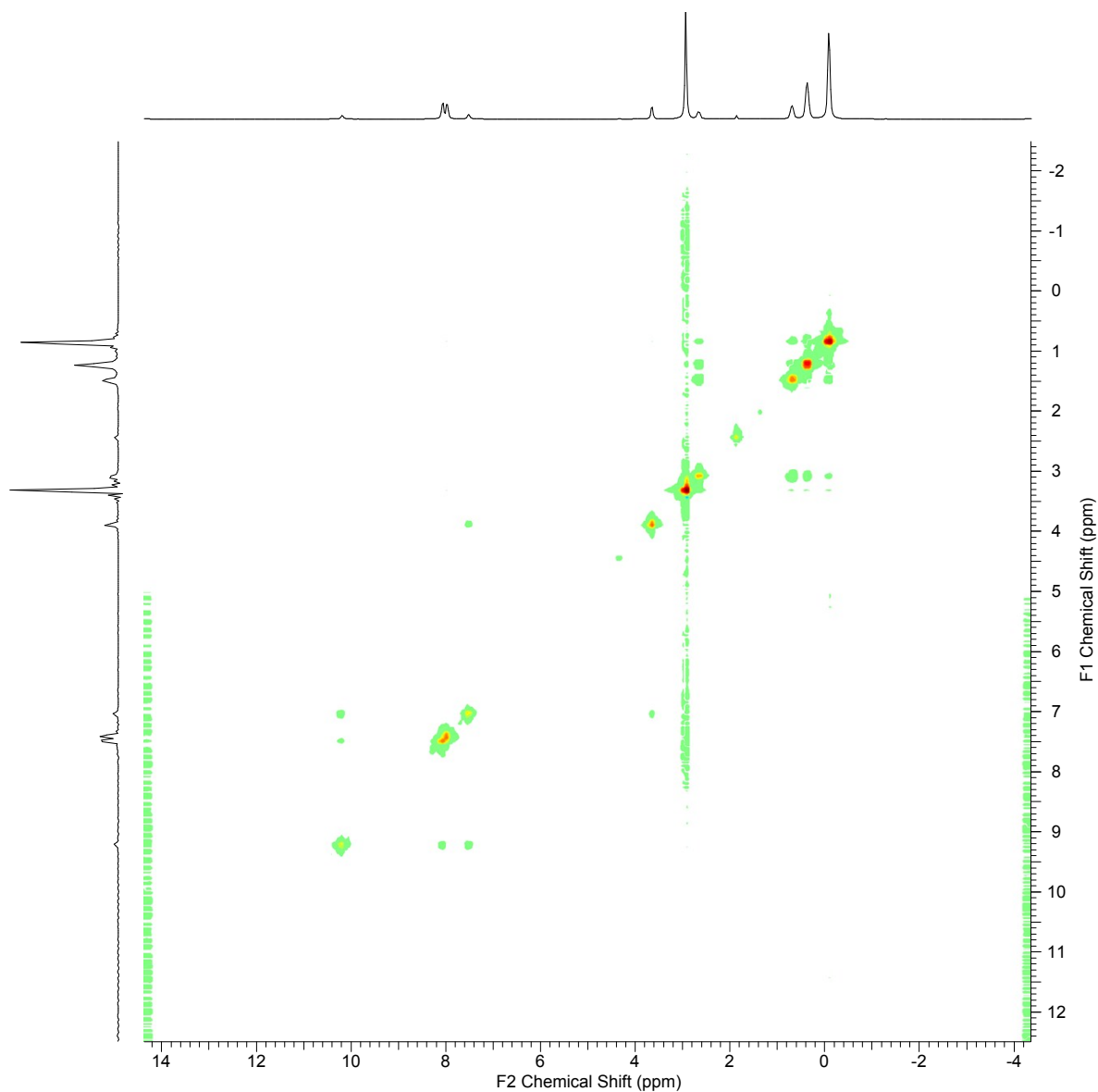


Figure S20 –  $^1\text{H}$  NOESY NMR of an equimolar solution of compound **1** in  $\text{DMSO-d}_6$ .

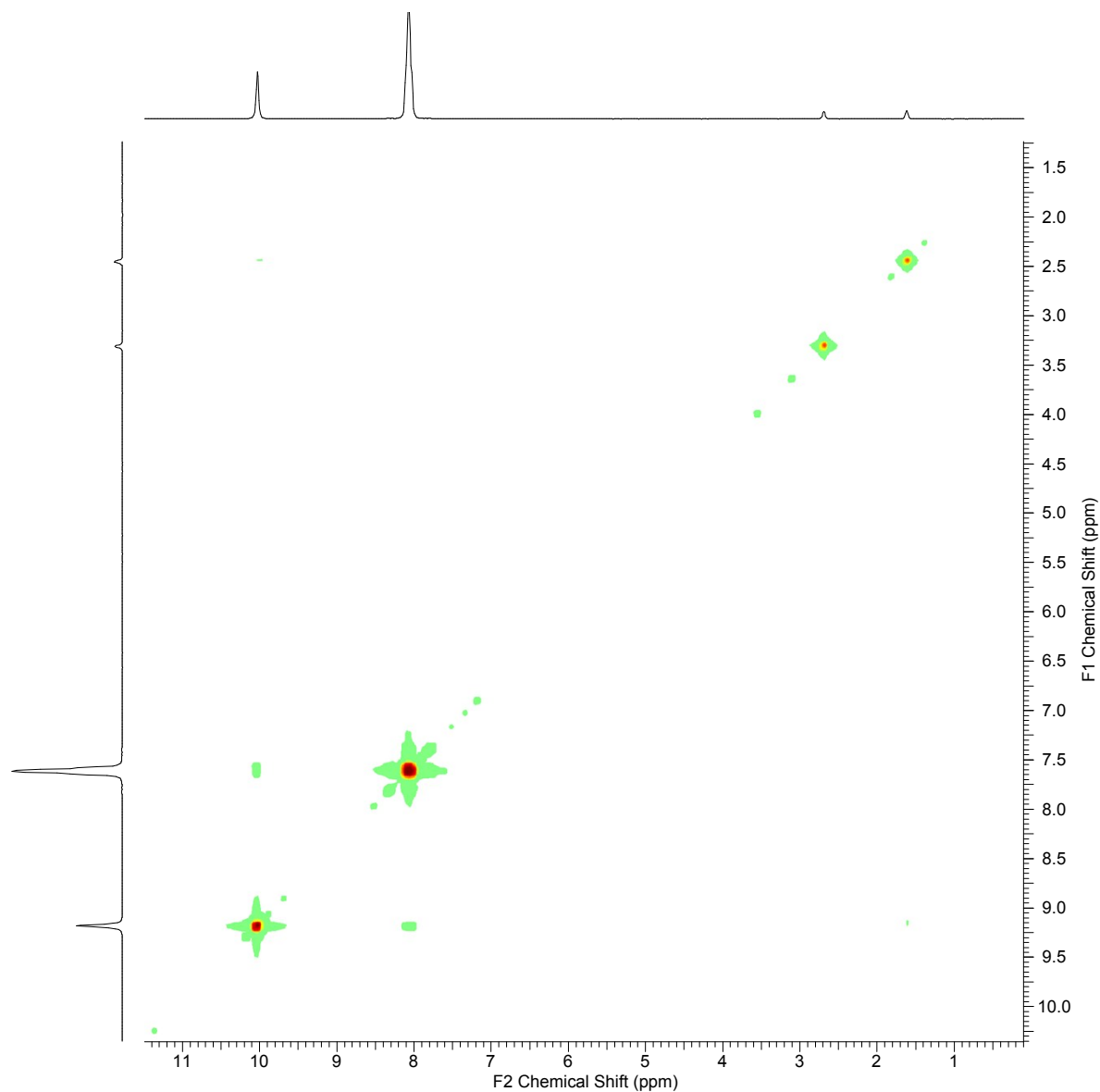


Figure S21 –  $^1\text{H}$  COSY NMR of an equimolar solution of compound **2** in  $\text{DMSO-d}_6$ .

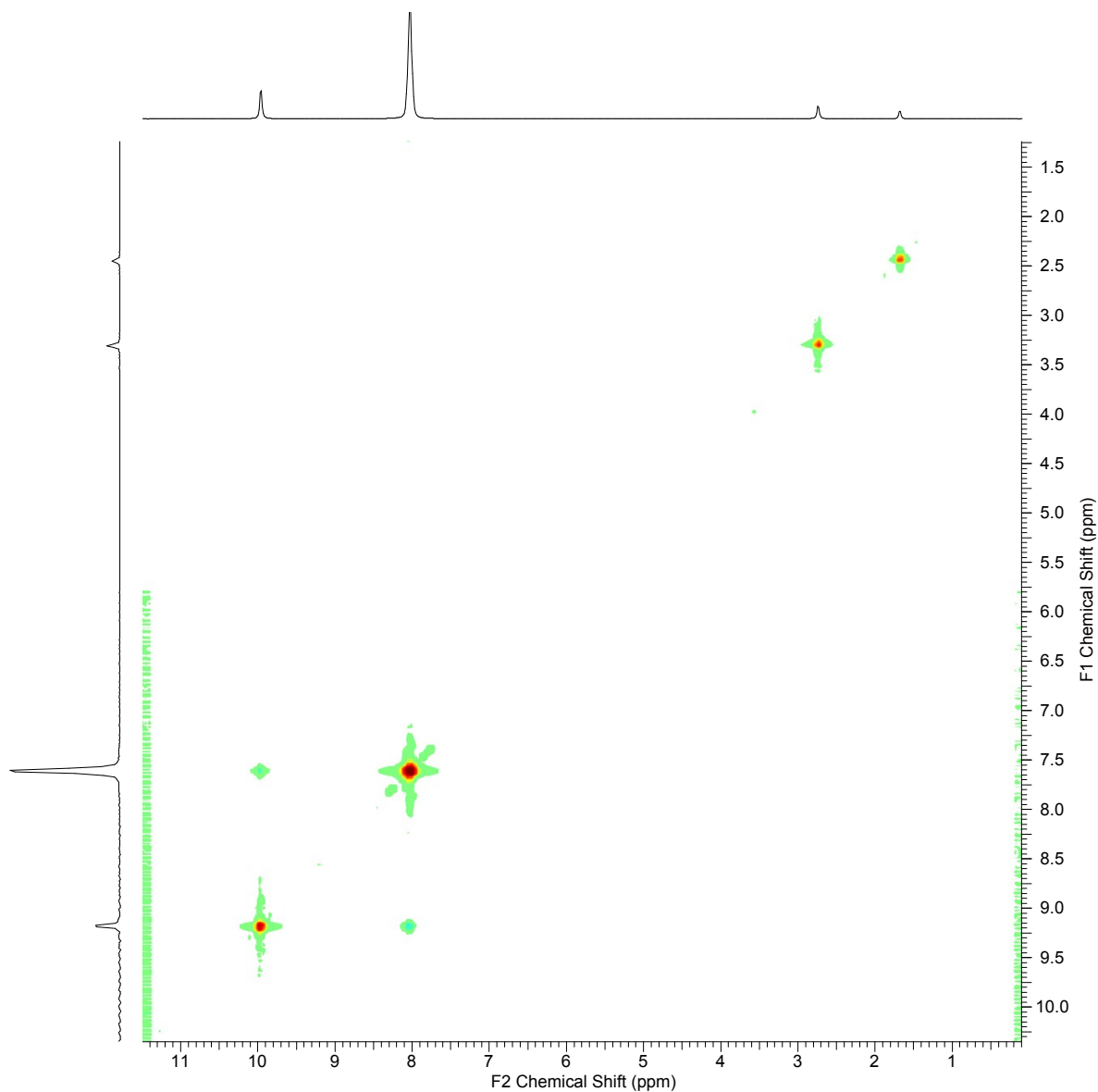


Figure S22 – <sup>1</sup>H NOESY NMR of an equimolar solution of compound **2** in DMSO-d<sub>6</sub>.

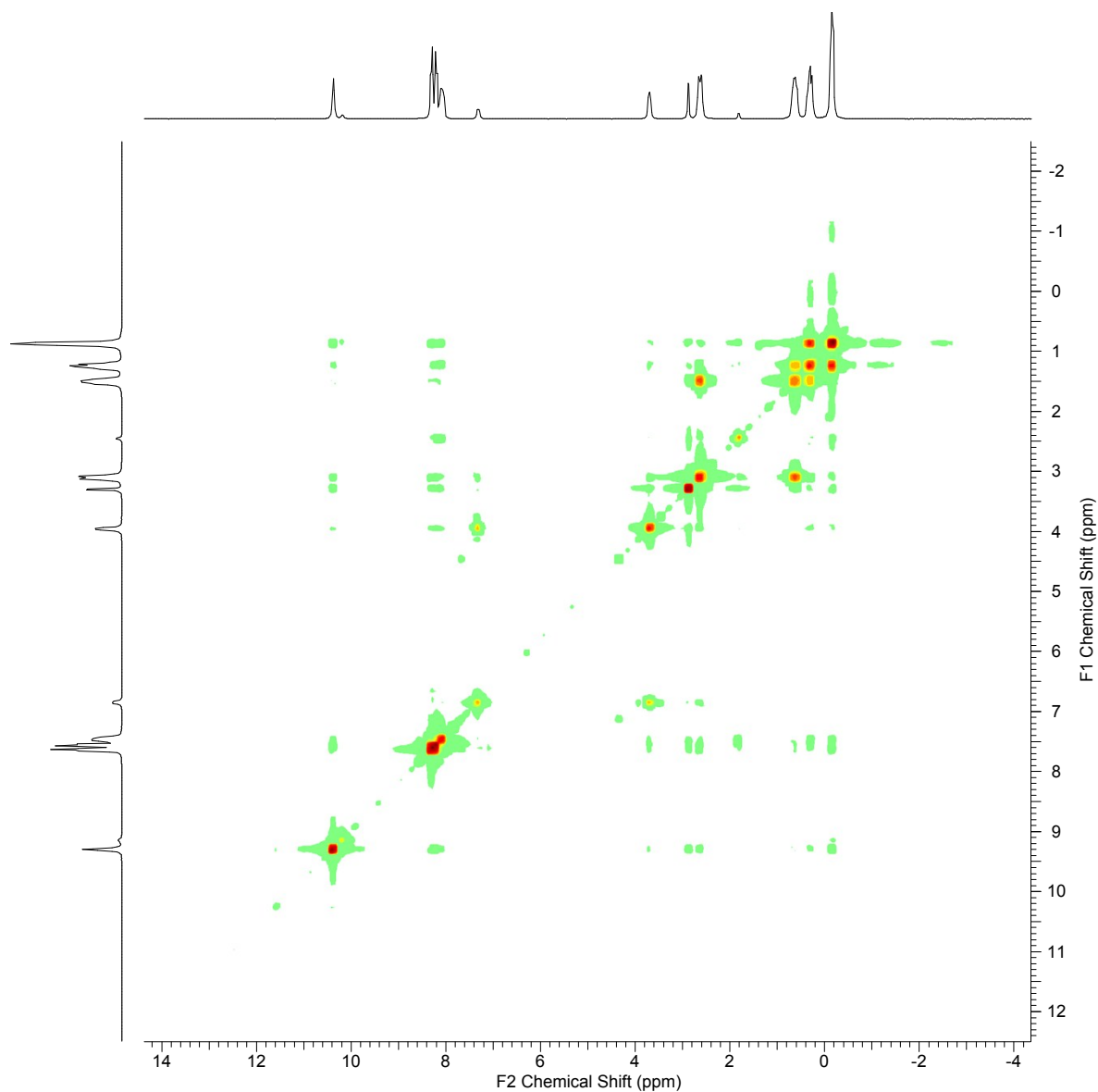


Figure S23 –  $^1\text{H}$  COSY NMR of an equimolar solution of compounds **1** and **2** in  $\text{DMSO-d}_6$ .

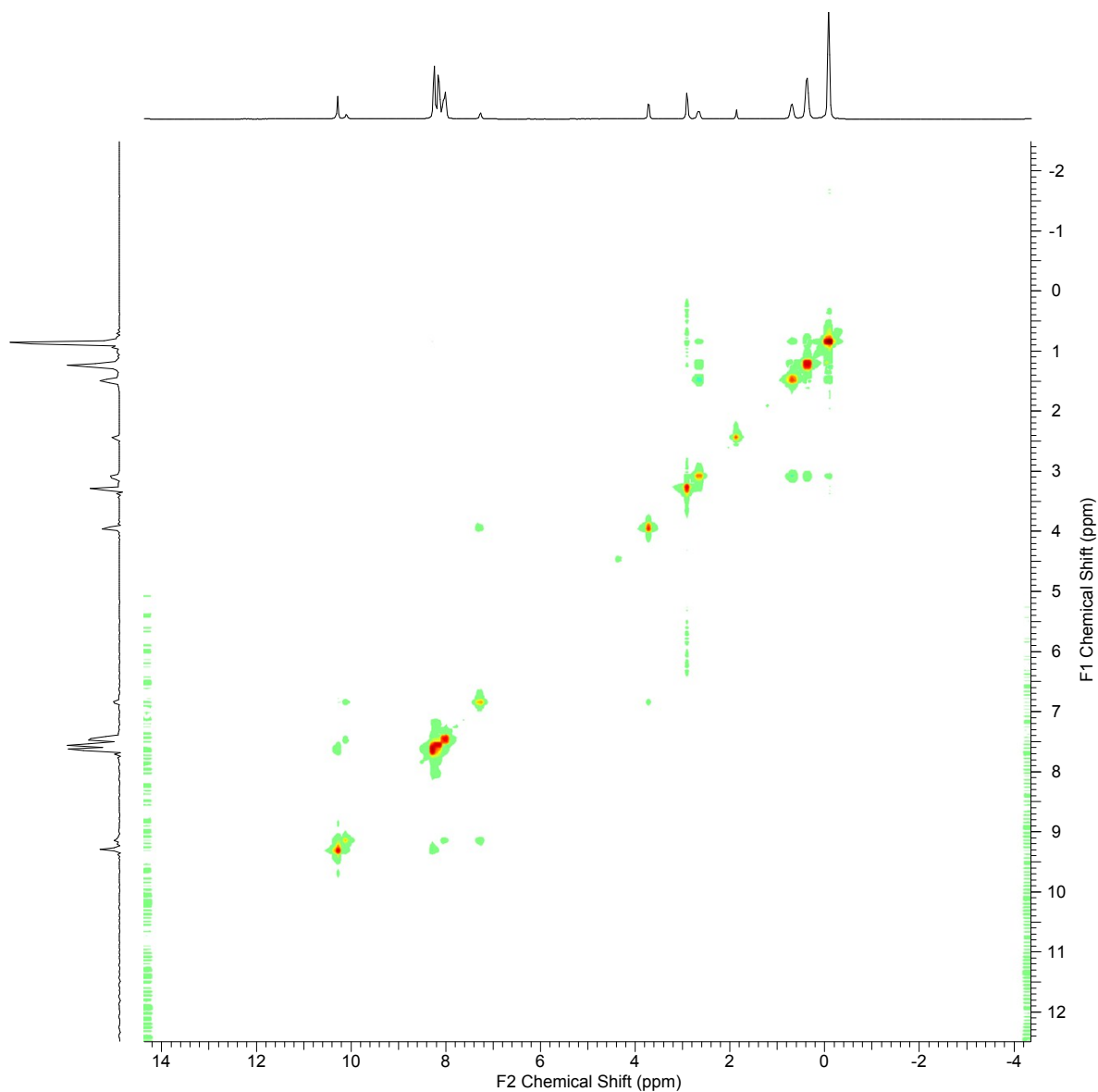


Figure S24 – <sup>1</sup>H NOESY NMR of an equimolar solution of compounds **1** and **2** in DMSO-d<sub>6</sub>.

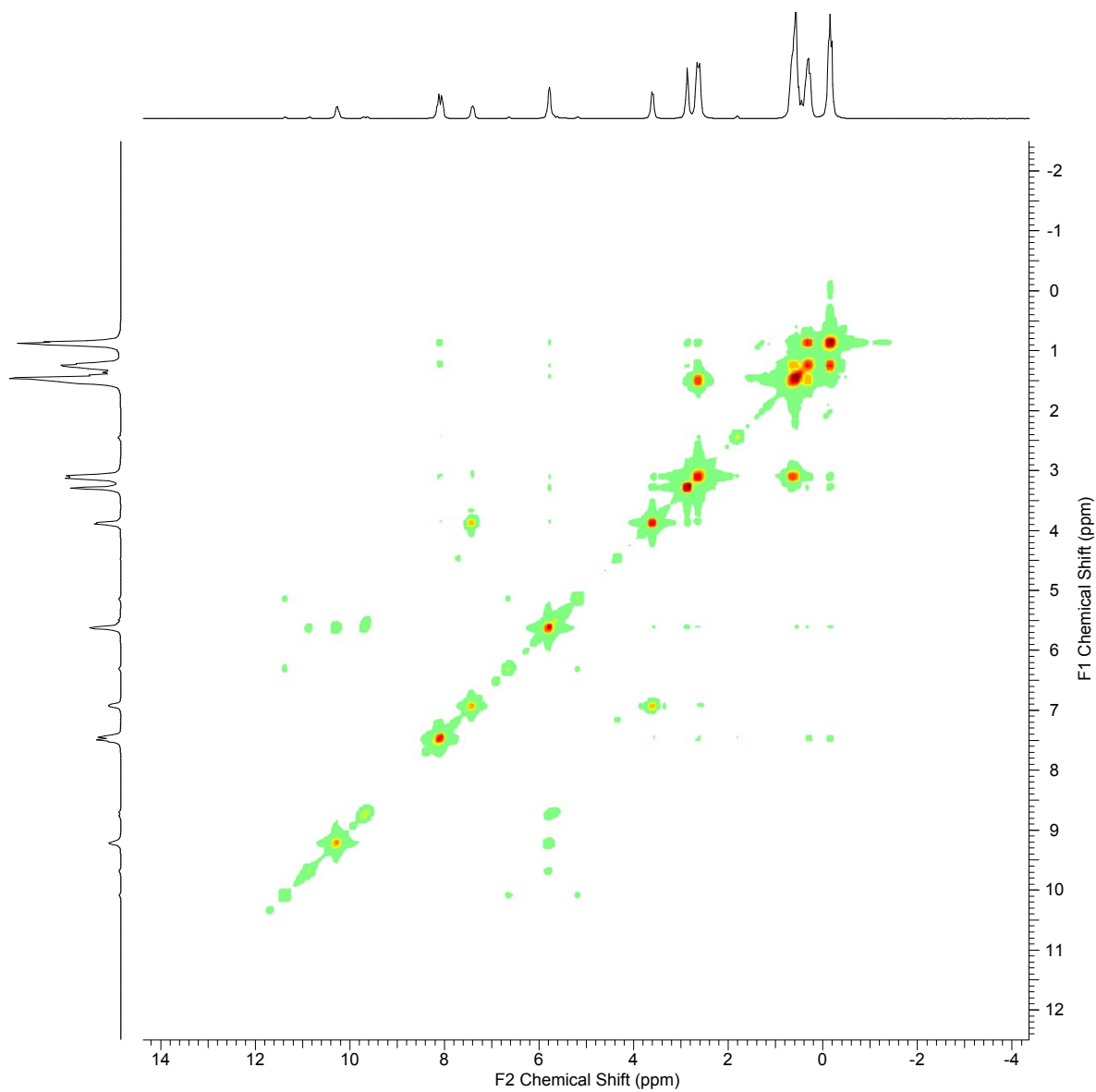


Figure S25 –  $^1\text{H}$  COSY NMR of an equimolar solution of compounds **1** and **6** in  $\text{DMSO-d}_6$ .

## <sup>1</sup>H NMR Binding Studies

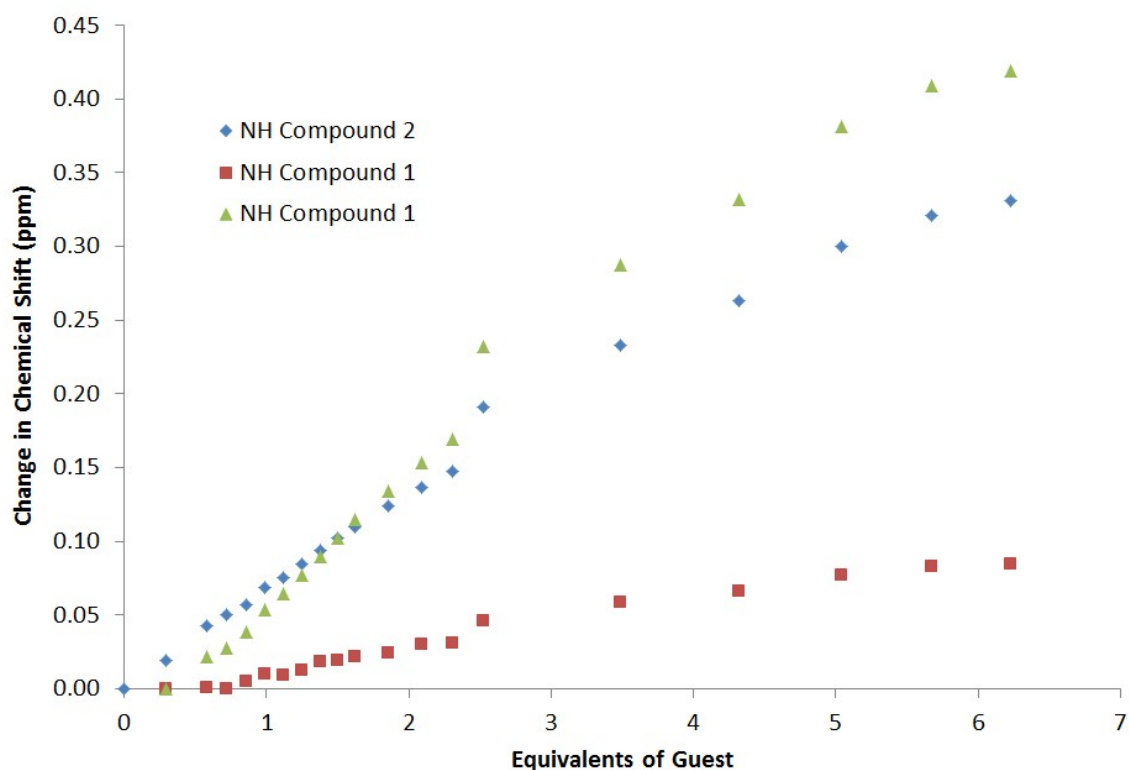


Figure S26 – Graph illustrating the change in chemical shift <sup>1</sup>H NMR titration of **2** vs. **1** in DMSO-d<sub>6</sub>/0.5 % H<sub>2</sub>O.

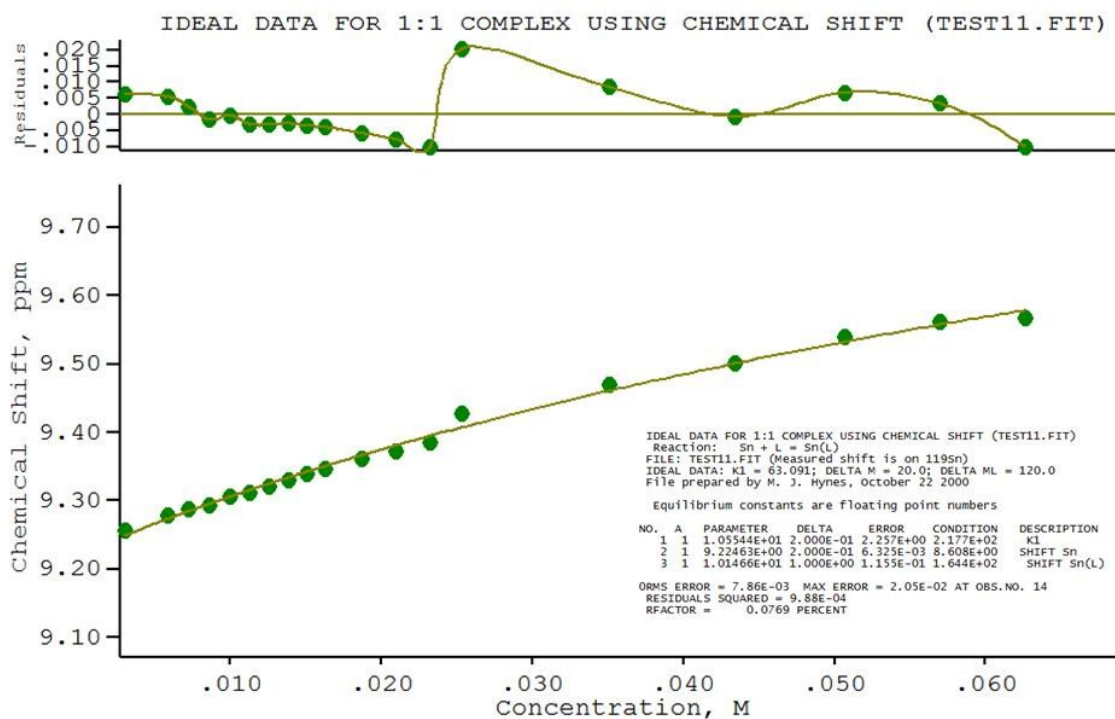


Figure S27 – <sup>1</sup>H NMR titration in in DMSO-d<sub>6</sub>/0.5 % H<sub>2</sub>O with receptor **2** vs. **1**. Values calculated using the urea NH of compound **2**.

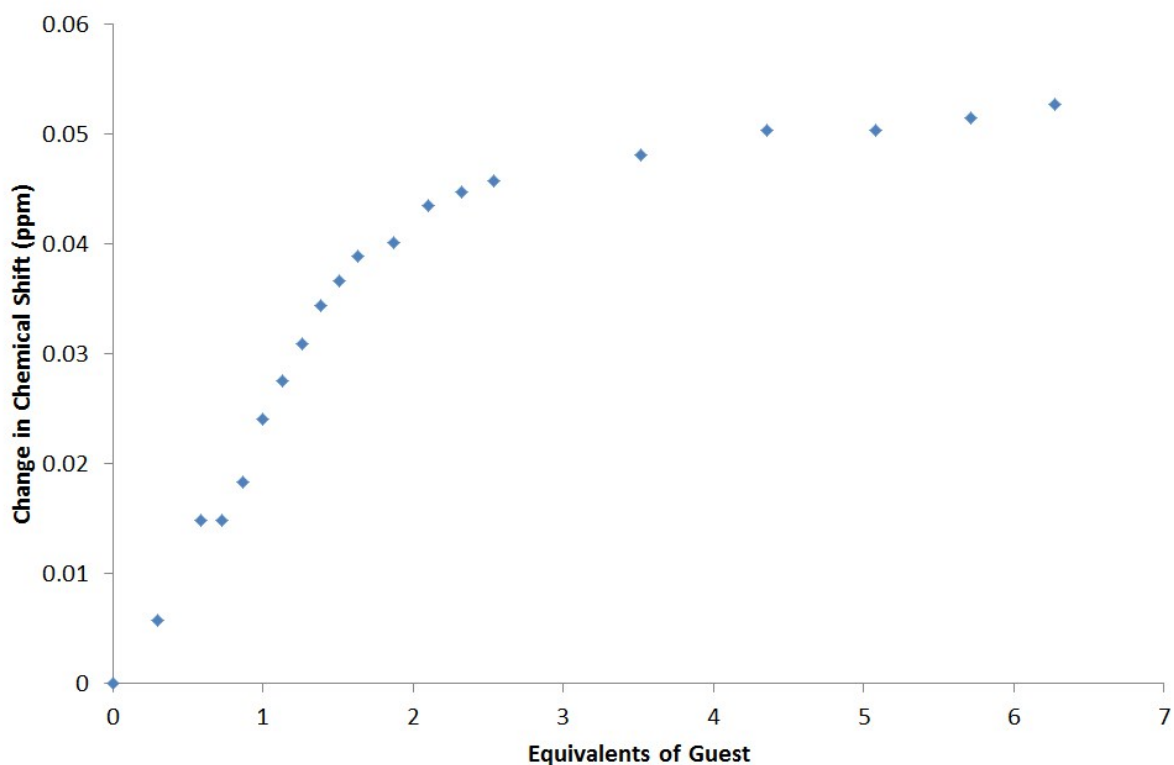


Figure S28 – Graph illustrating the change in chemical shift  $^1\text{H}$  NMR titration of **1** vs. TBAF in  $\text{DMSO-d}_6/0.5\% \text{H}_2\text{O}$ , following an aromatic CH due to NH peak broadening.

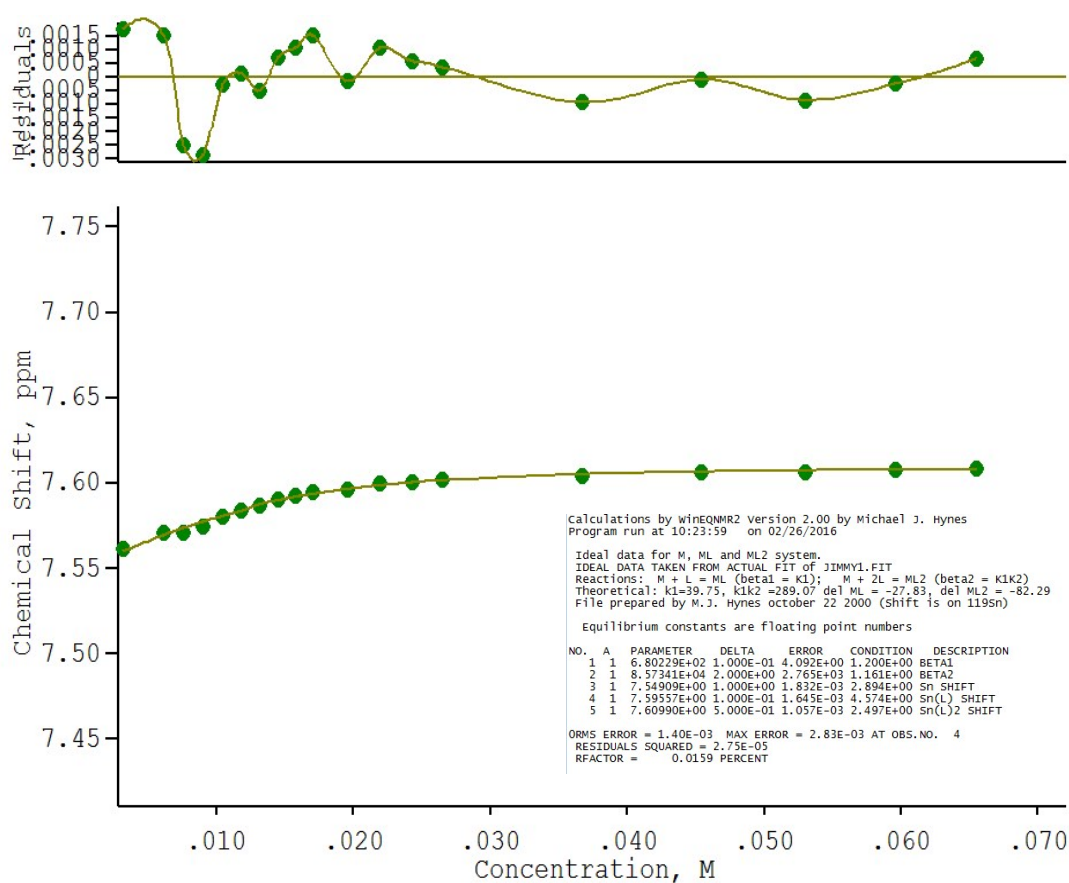


Figure S29 –  $^1\text{H}$  NMR titration of **1** vs. TBAF in  $\text{DMSO-d}_6/0.5\% \text{H}_2\text{O}$ , following an aromatic CH due to NH peak broadening.

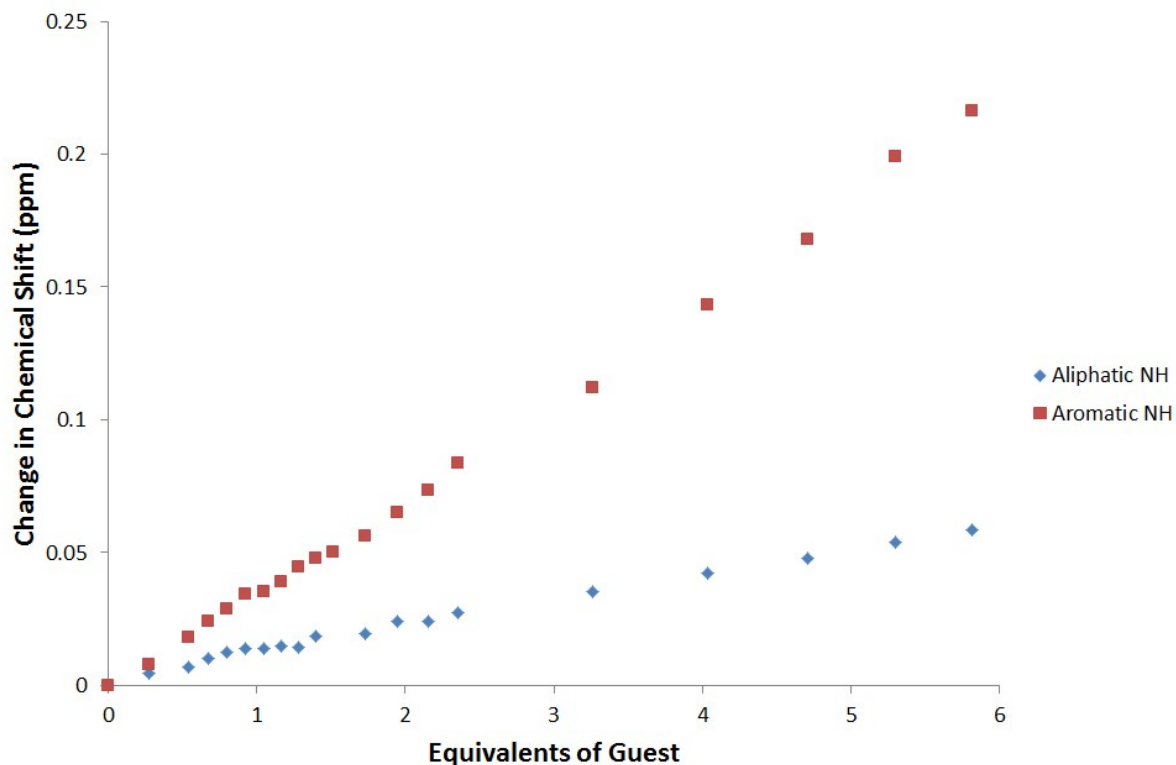


Figure S30 – Graph illustrating the change in chemical shift  $^1\text{H}$  NMR titration of **1** vs. TBACl in  $\text{DMSO-d}_6/0.5\% \text{H}_2\text{O}$ , following the urea NHs.

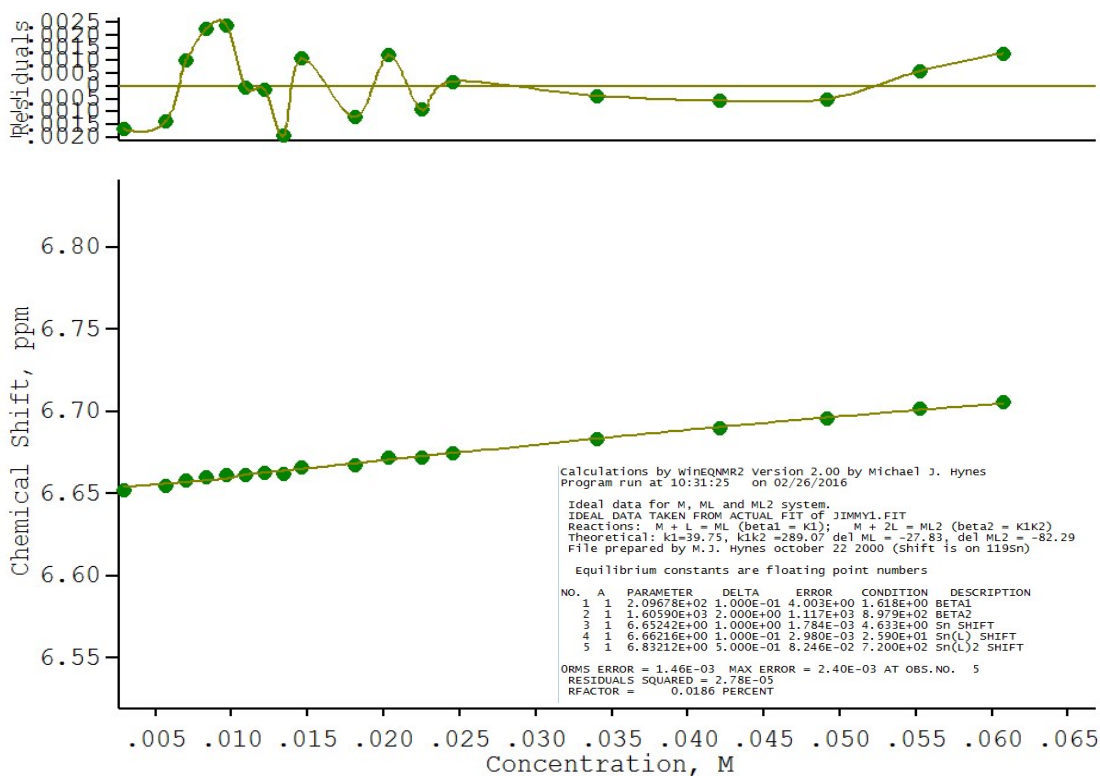


Figure S31 –  $^1\text{H}$  NMR titration of **1** vs. TBACl in  $\text{DMSO-d}_6/0.5\% \text{H}_2\text{O}$ , following a urea NH.

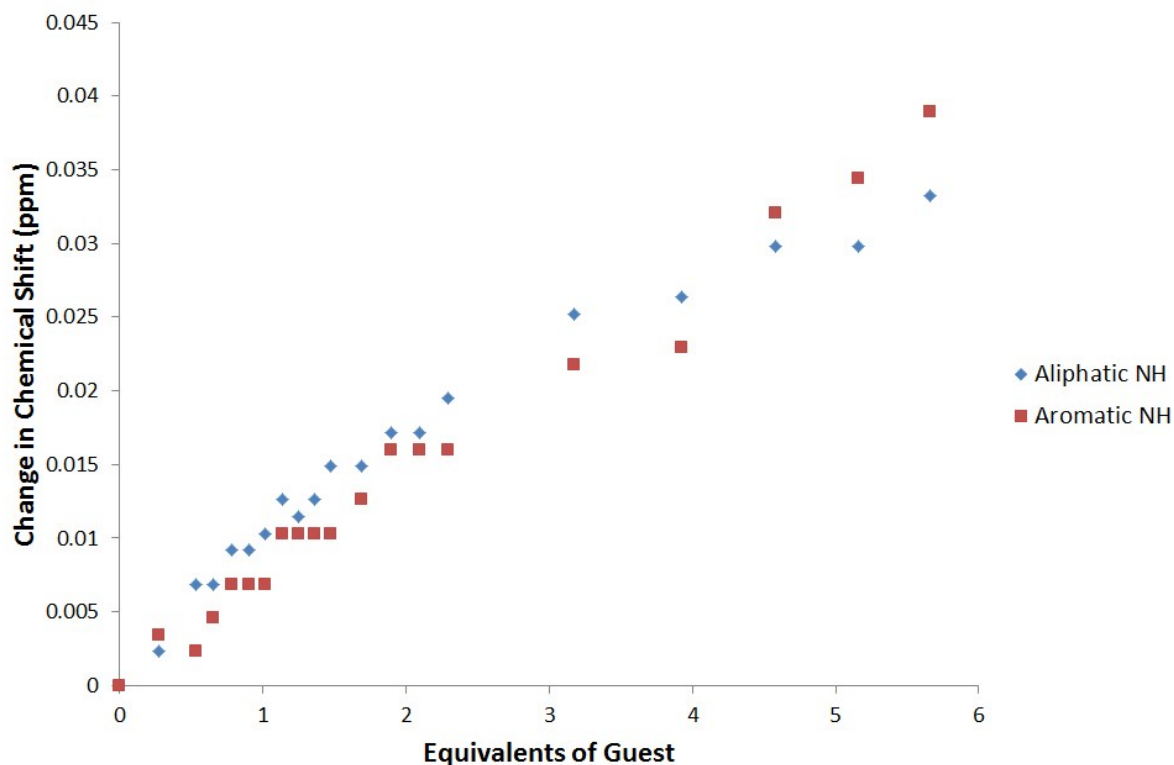


Figure S32 – Graph illustrating the change in chemical shift  $^1\text{H}$  NMR titration of **1** vs. TBABr in  $\text{DMSO-d}_6/0.5\% \text{H}_2\text{O}$ , following the urea NHs.

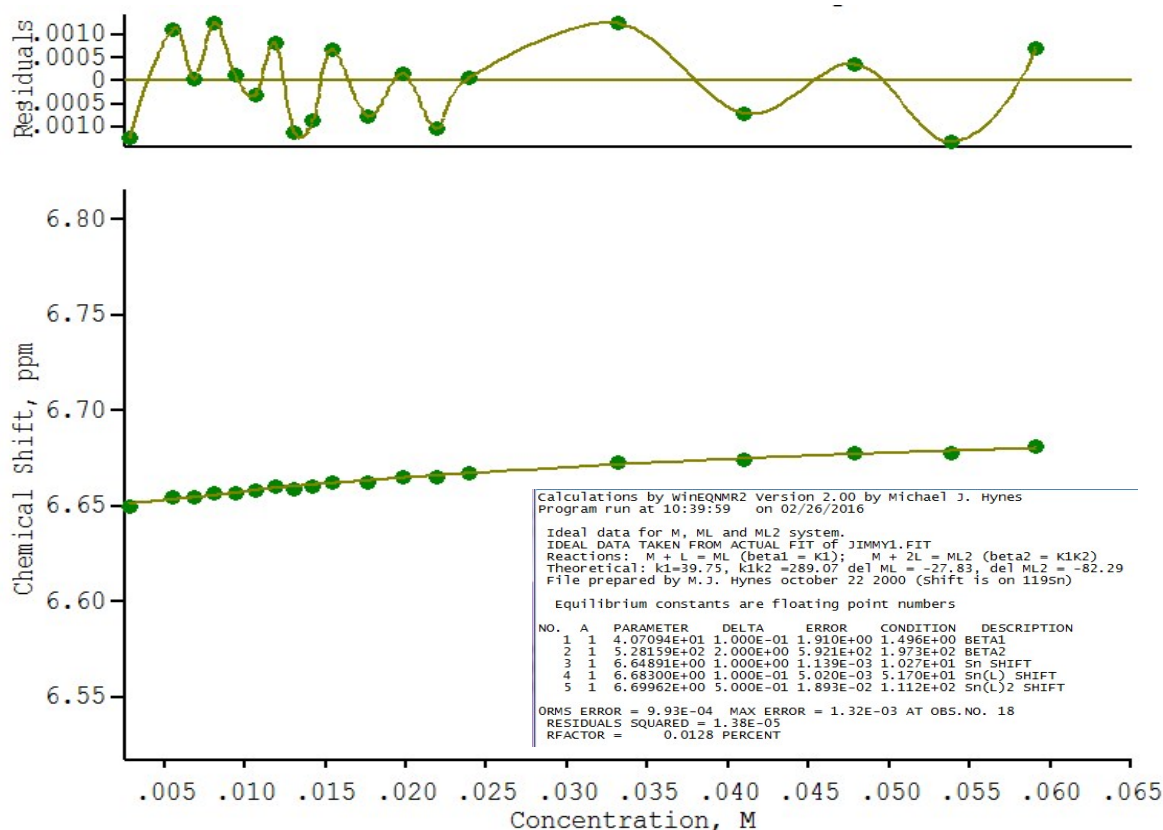


Figure S33 –  $^1\text{H}$  NMR titration of **1** vs. TBABr in  $\text{DMSO-d}_6/0.5\% \text{H}_2\text{O}$ , following a urea NHs.

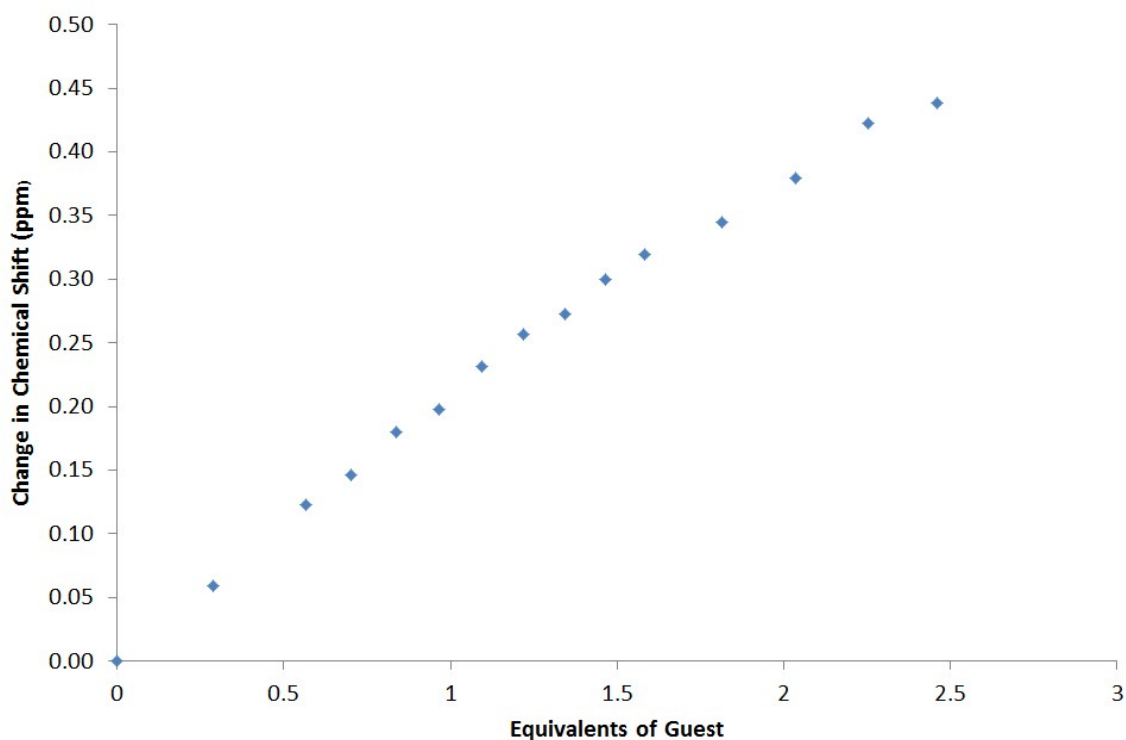


Figure S34 – Graph illustrating the change in chemical shift  $^1\text{H}$  NMR titration of **2** vs. **3** in  $\text{DMSO-d}_6/0.5\% \text{H}_2\text{O}$ .

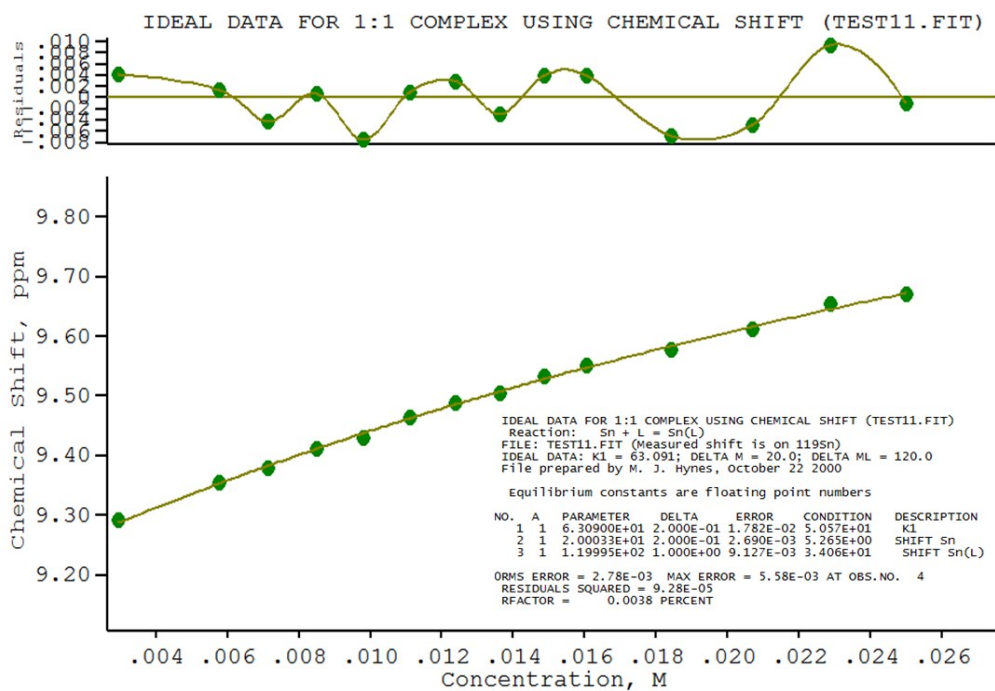


Figure S35 –  $^1\text{H}$  NMR titration in in  $\text{DMSO-d}_6/0.5\% \text{H}_2\text{O}$  with receptor **2** vs. **3**.

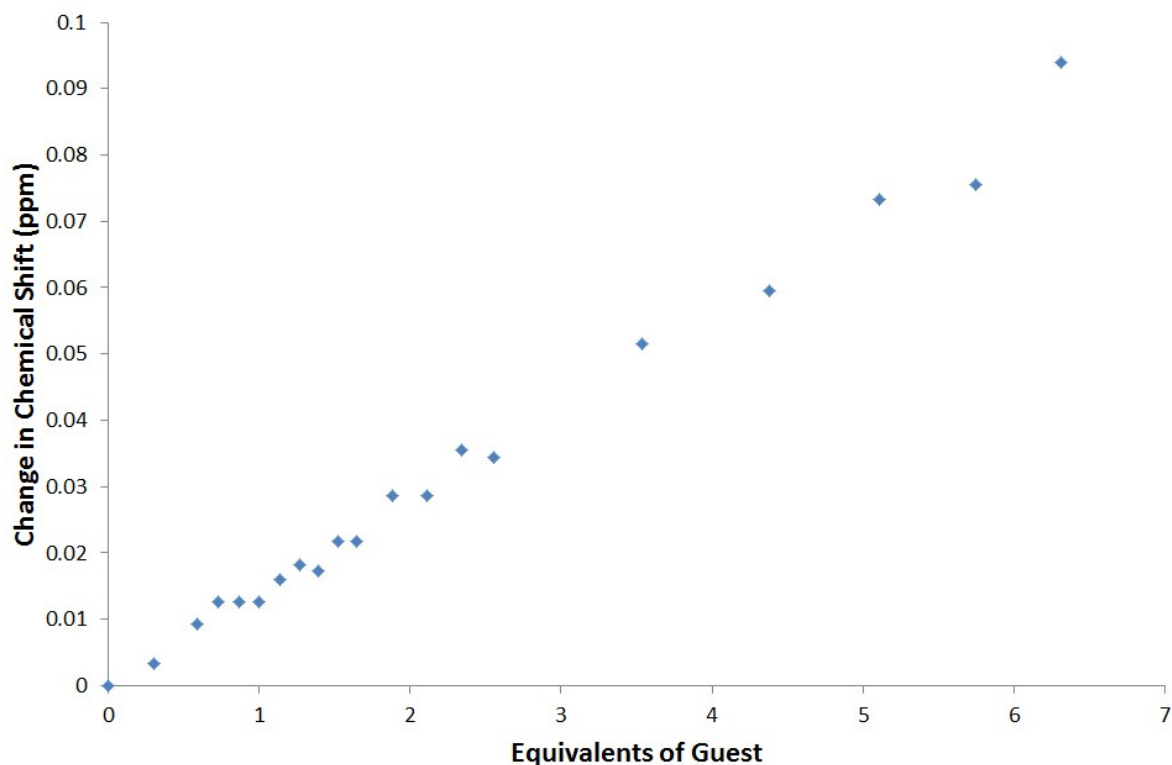


Figure S36 – Graph illustrating the change in chemical shift  $^1\text{H}$  NMR titration of **6** vs. **3** in  $\text{DMSO-d}_6/0.5\% \text{H}_2\text{O}$ . Following the pyrrole NH.

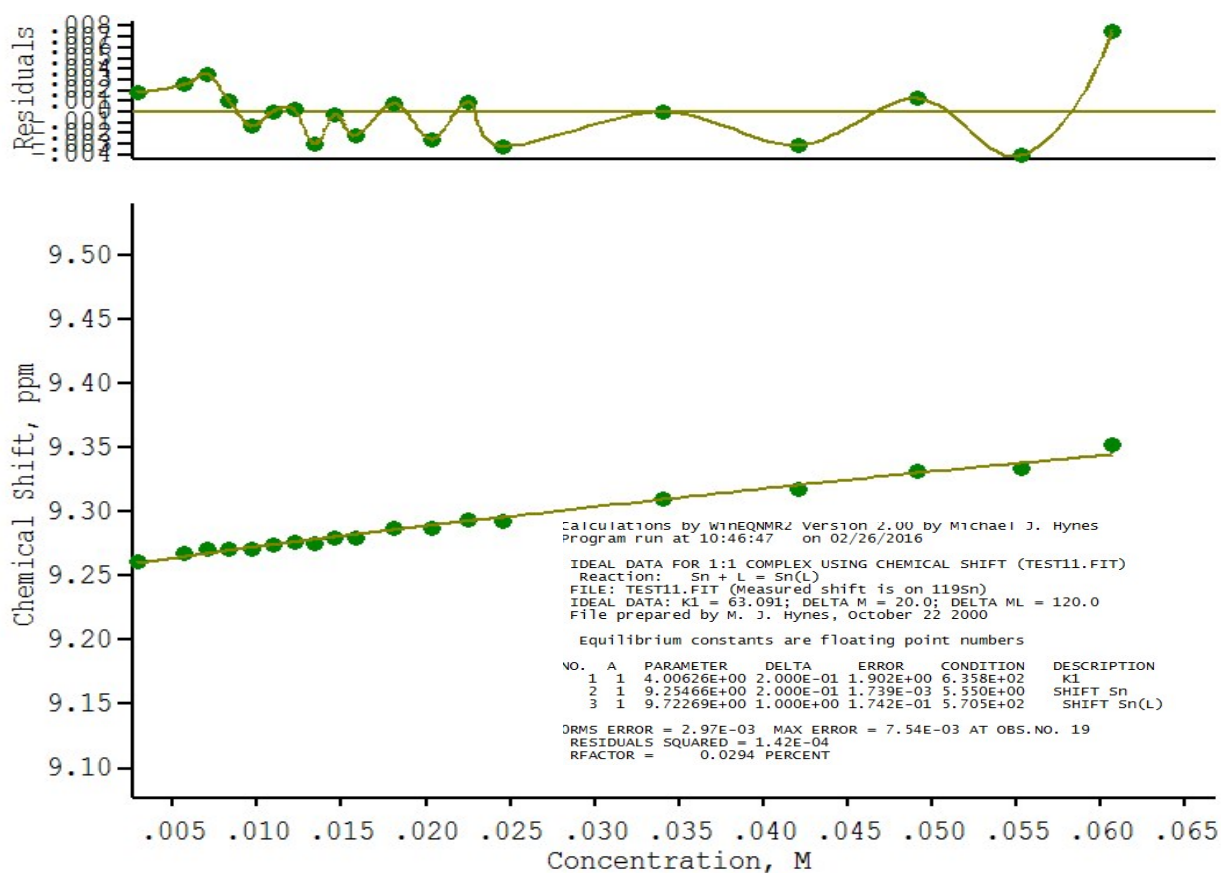


Figure S37 –  $^1\text{H}$  NMR titration of **6** vs. **3** in  $\text{DMSO-d}_6/0.5\% \text{H}_2\text{O}$ . Following the pyrrole NH.

## <sup>1</sup>H NMR Job plot studies

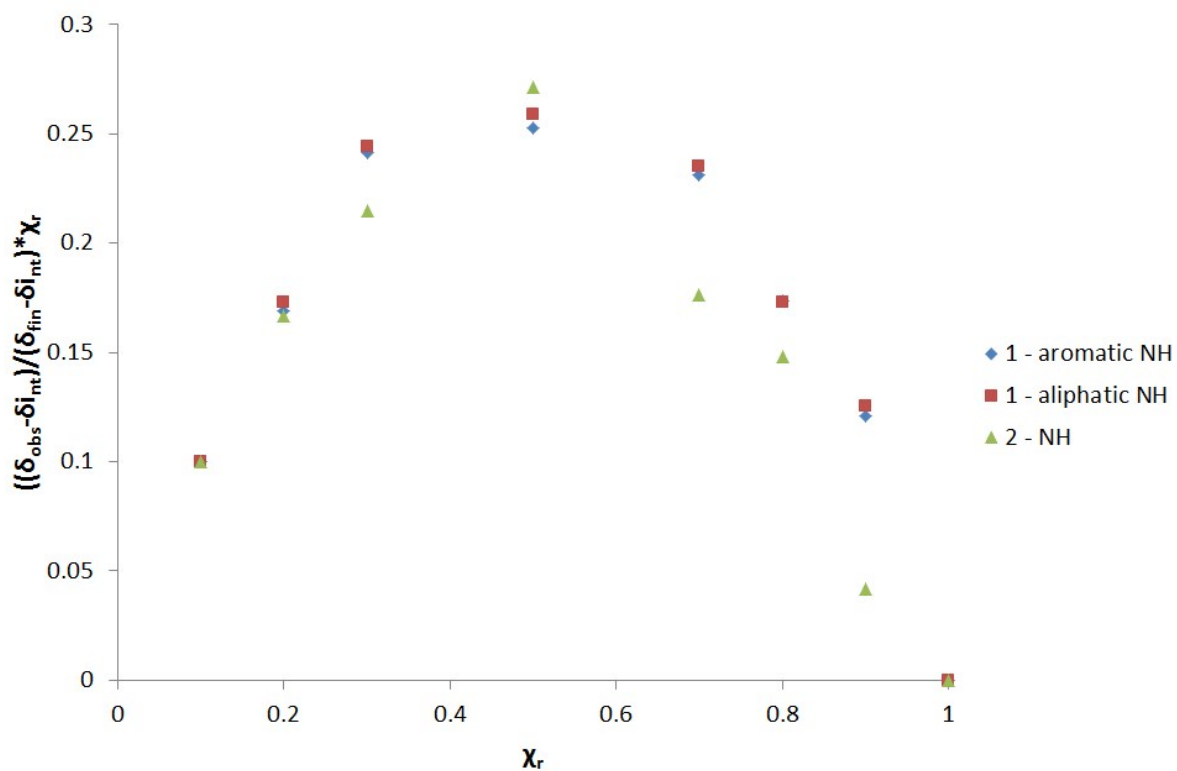


Figure S38 – <sup>1</sup>H NMR Job Plot in in DMSO-d<sub>6</sub>/ 0.5 % H<sub>2</sub>O with receptor **2** vs. **1**.

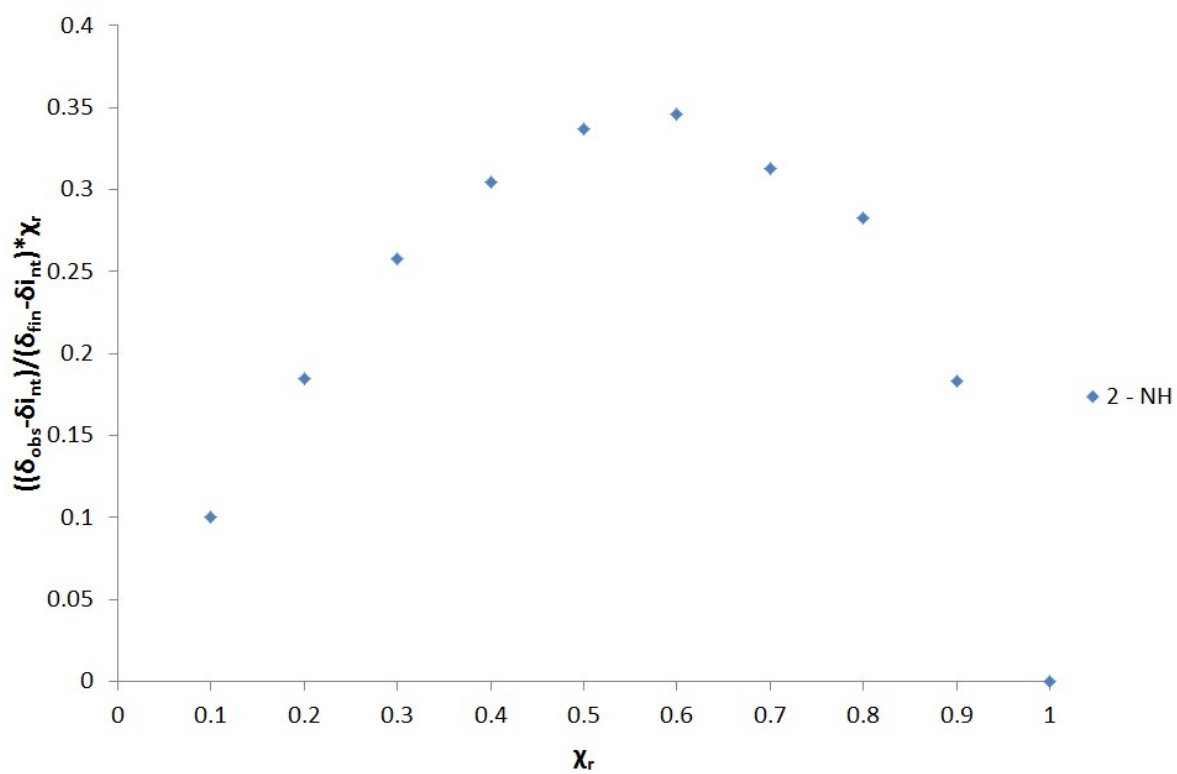


Figure S39 – <sup>1</sup>H NMR Job Plot in in DMSO-d<sub>6</sub>/ 0.5 % H<sub>2</sub>O with receptor **2** vs. **3**.

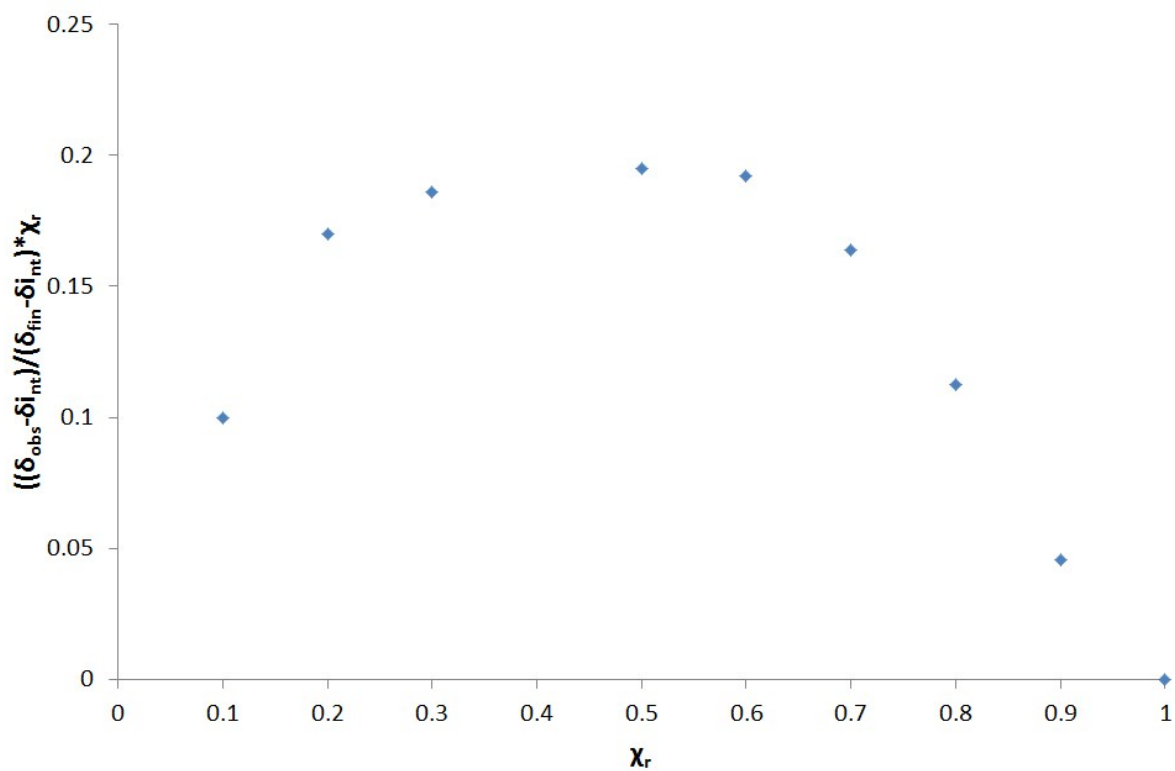


Figure S40 –  $^1\text{H}$  NMR Job Plot in in DMSO- $d_6$ / 0.5 %  $\text{H}_2\text{O}$  with receptor **1** vs. TBACl. Following the aromatic urea NH.

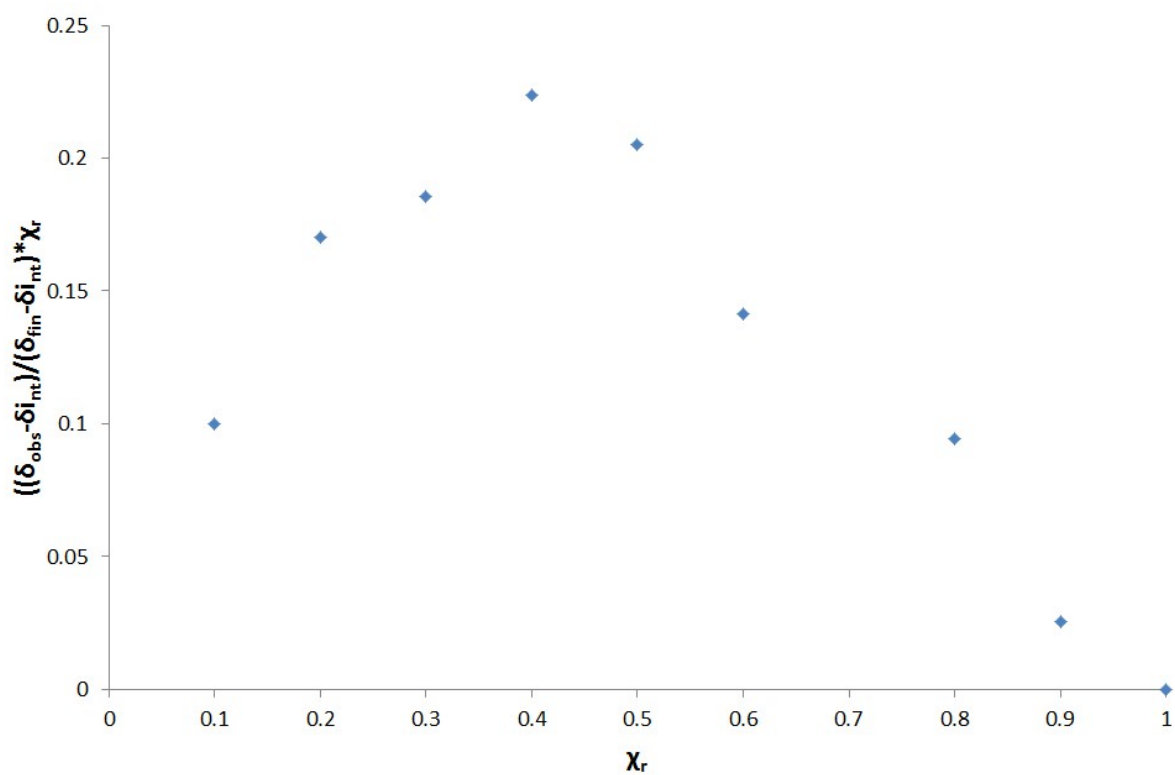


Figure S41 –  $^1\text{H}$  NMR Job Plot in in DMSO- $d_6$ / 0.5 %  $\text{H}_2\text{O}$  with receptor **1** vs. TBABr. Following the aromatic urea NH.

## DLS data

### Count rate

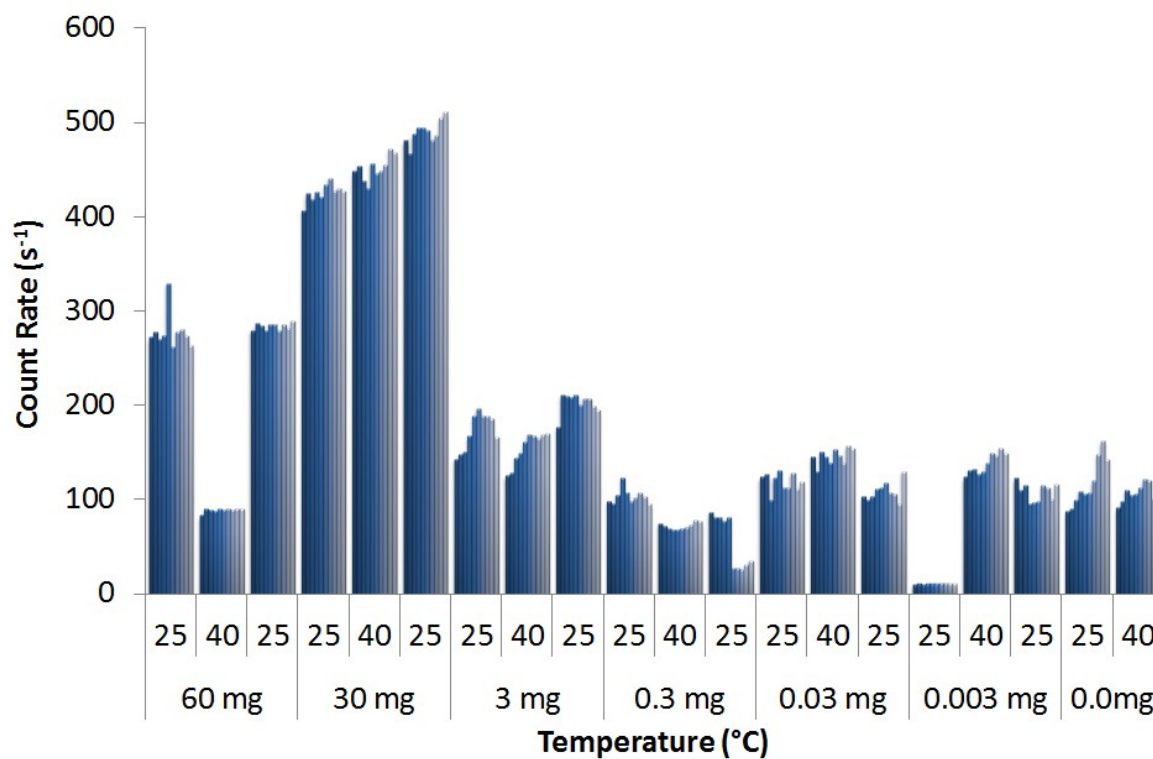


Figure S42 – Graph illustrating the count rate for each DLS run at a specific temperature with compound 1 in DMSO (1 mL).

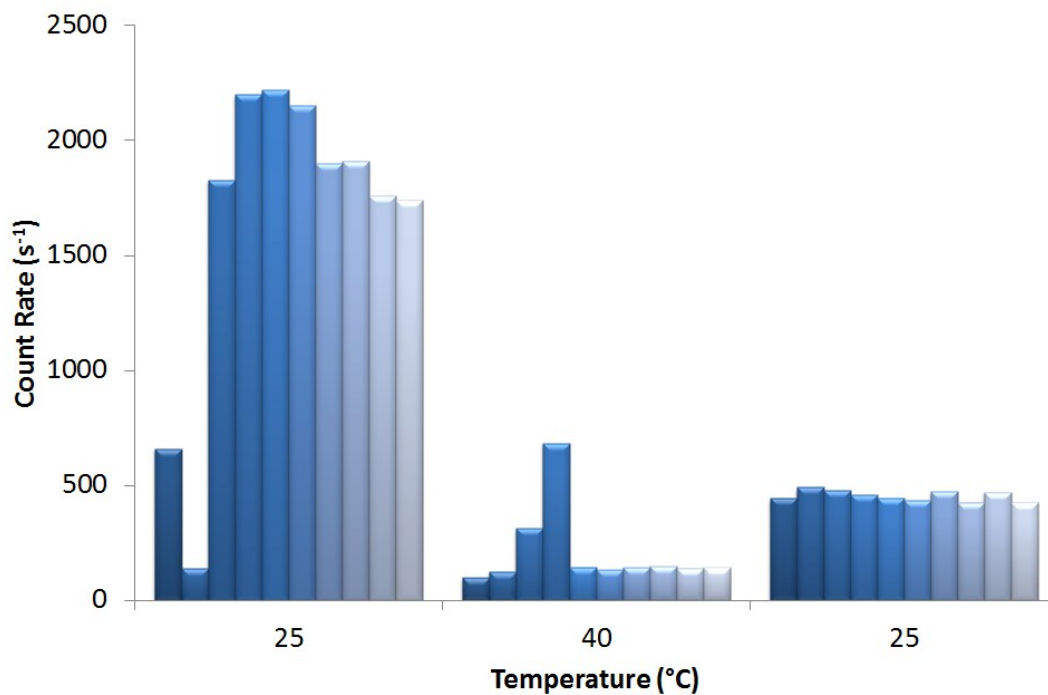


Figure S43 – Graph illustrating the count rate for each DLS run at a specific temperature with compound 1 (30.00 mg) and compound 2 (19.33 mg) in DMSO (1 mL).

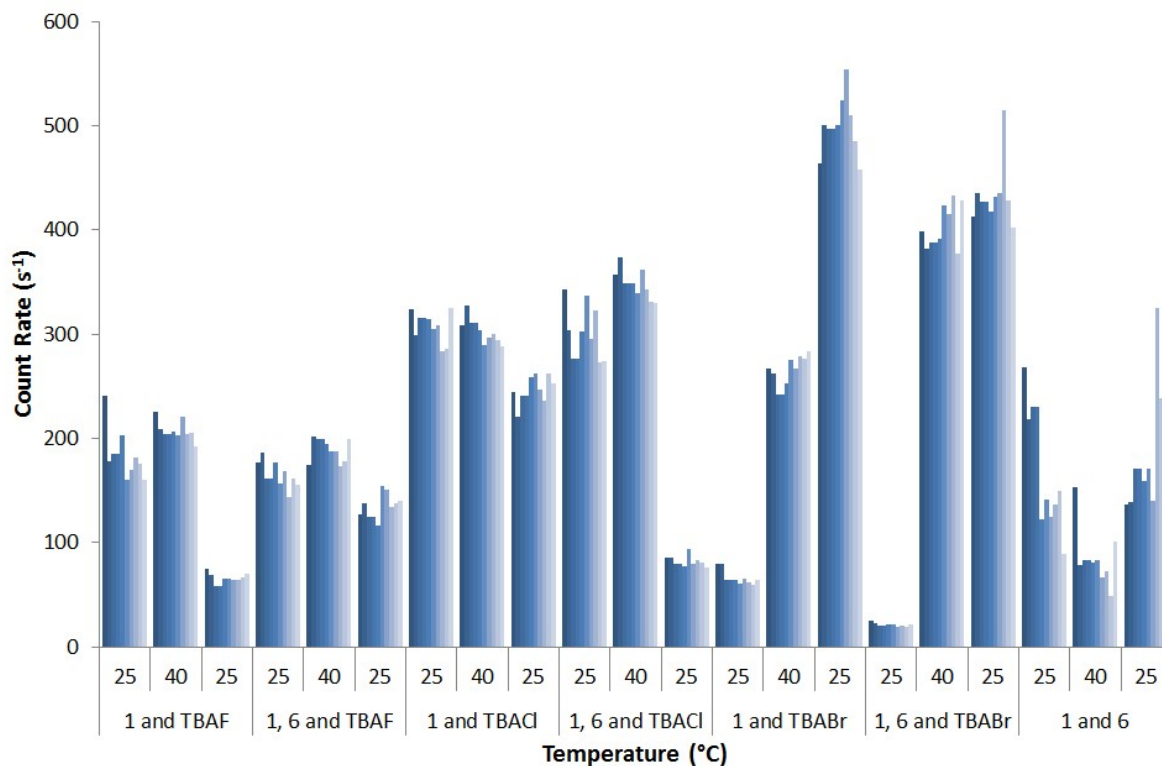


Figure S44 – Graph illustrating the count rate for each DLS run at a specific temperature with compound **1** (30.00 mg), TBA halide and compound **6** (19.33 mg) in DMSO (1 mL).

### Correlation data

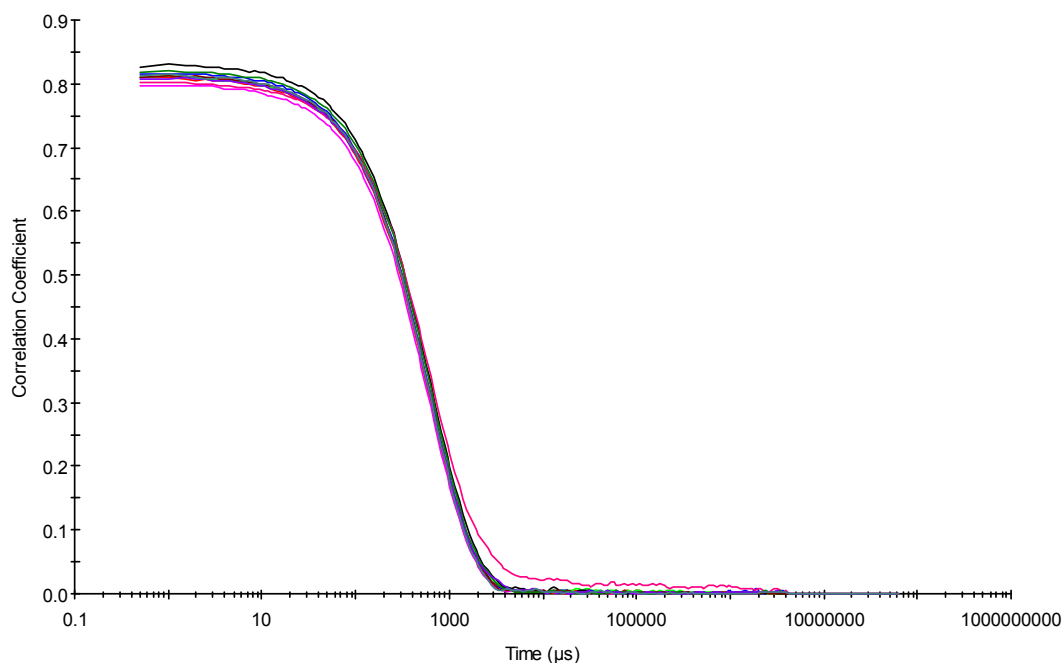


Figure S45 – Raw correlation data for 10 DLS runs at 25 °C before heating to 40 °C with compound **1** (60.00 mg) in DMSO (1 mL).

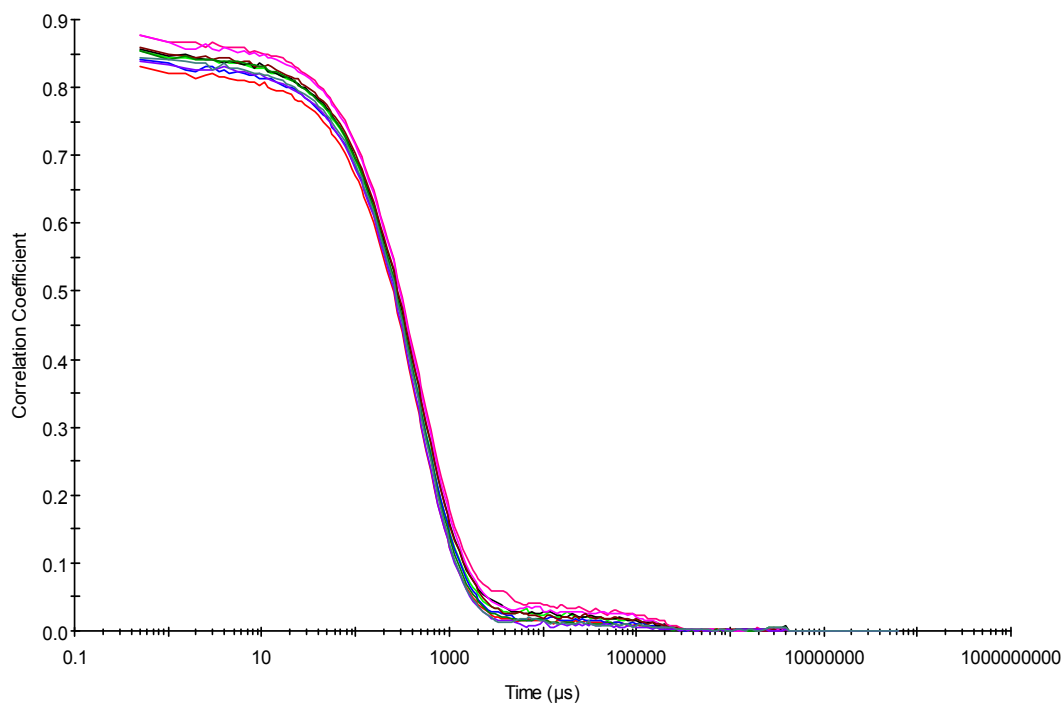


Figure S46 – Raw correlation data for 10 DLS runs at 40 °C with compound **1** (60.00 mg) in DMSO (1 mL).

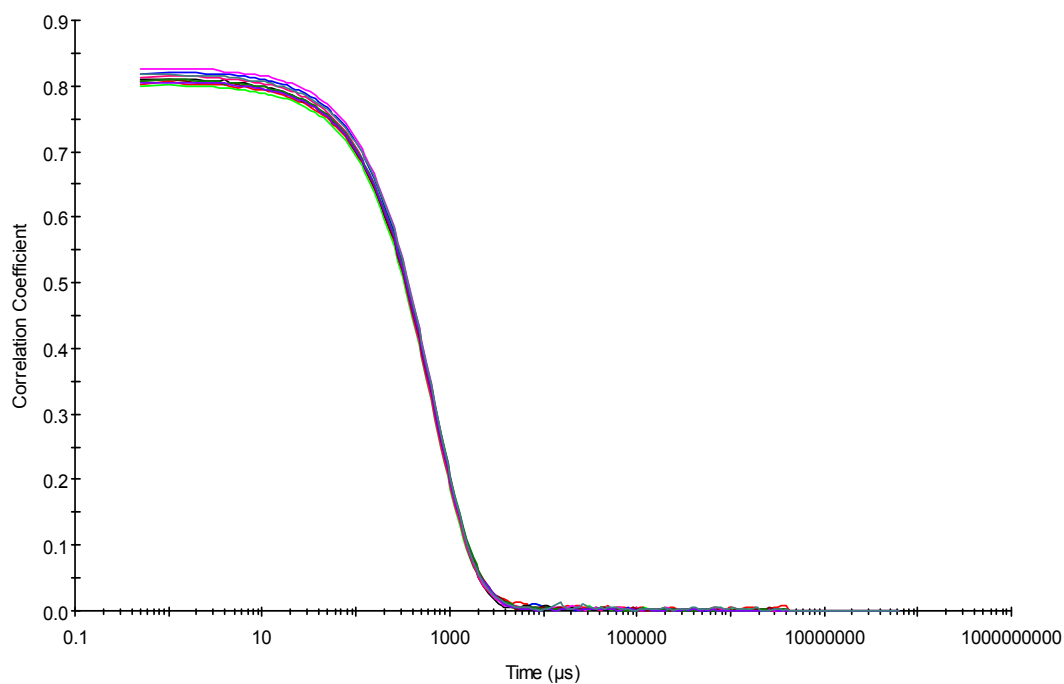


Figure S47 – Raw correlation data for 10 DLS runs at 25 °C after heating to 40 °C with compound **1** (60.00 mg) in DMSO (1 mL).

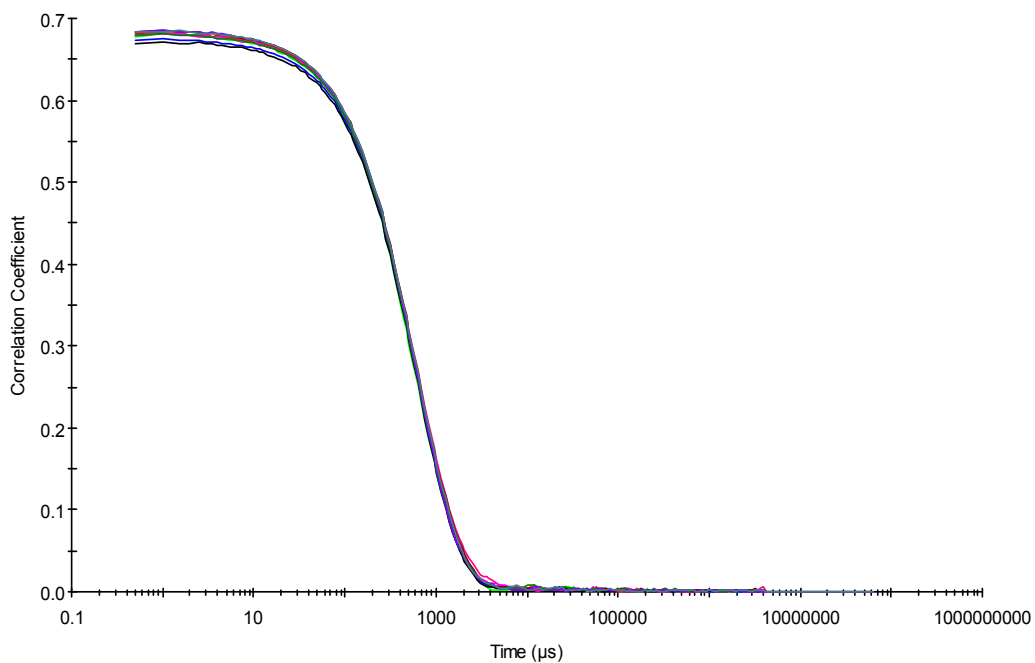


Figure S48 – Raw correlation data for 10 DLS runs at 25 °C before heating to 40 °C with compound **1** (30.00 mg) in DMSO (1 mL).

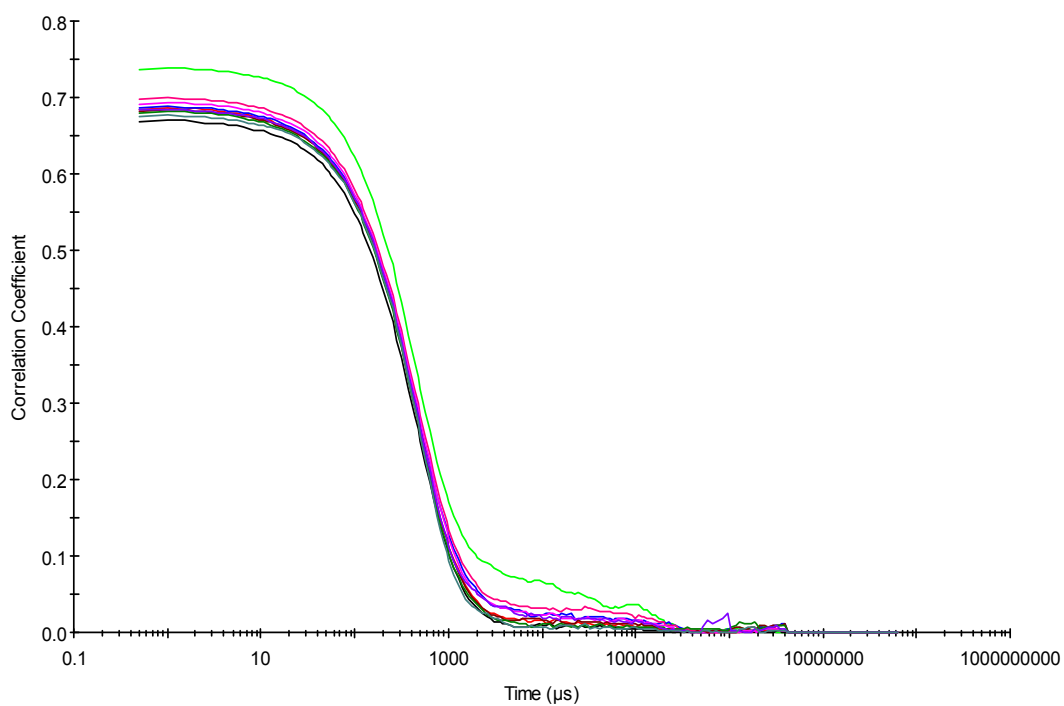


Figure S49 – Raw correlation data for 10 DLS runs at 40 °C with compound **1** (30.00 mg) in DMSO (1 mL).

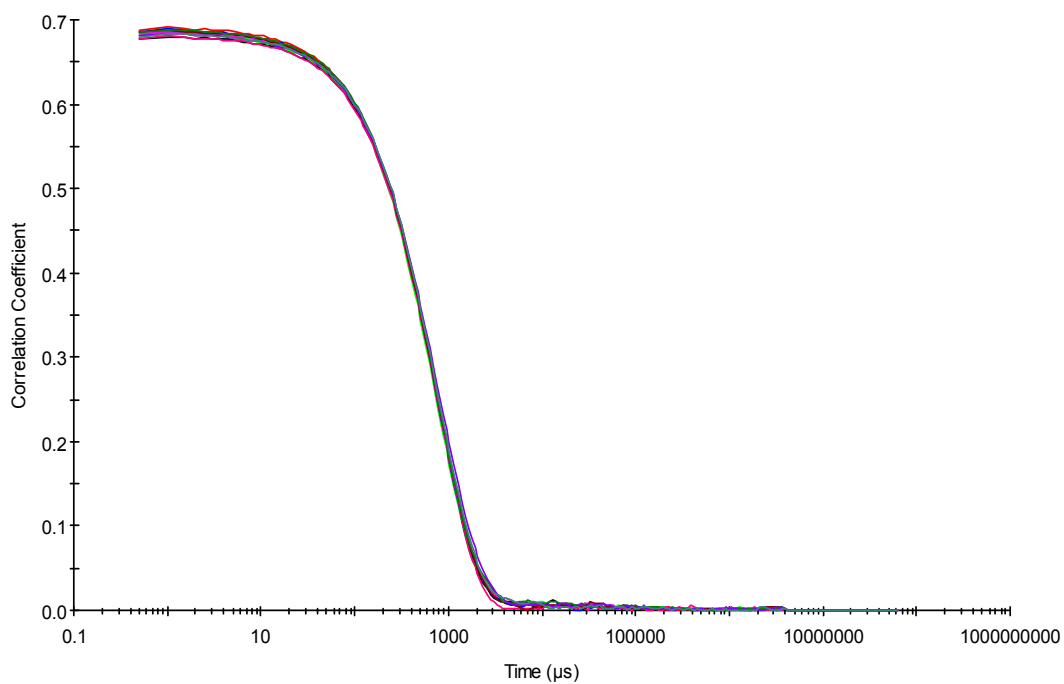


Figure S50 – Raw correlation data for 10 DLS runs at 25 °C after heating to 40 °C with compound **1** (30.00 mg) in DMSO (1 mL).

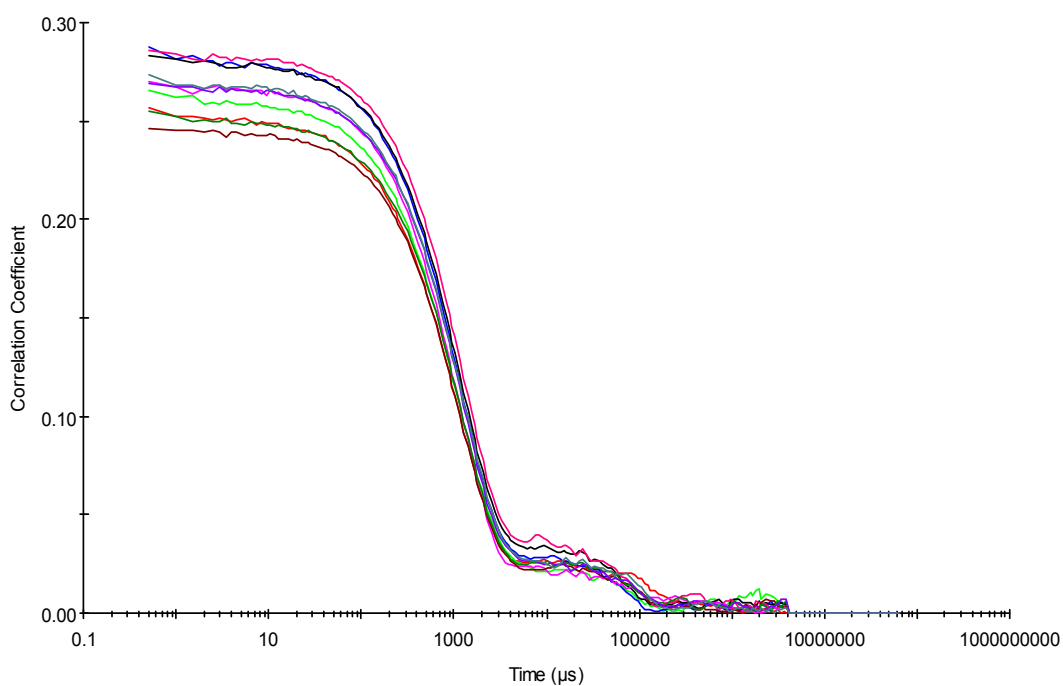


Figure S51 – Raw correlation data for 10 DLS runs at 25 °C before heating to 40 °C with compound **1** (3.00 mg) in DMSO (1 mL).

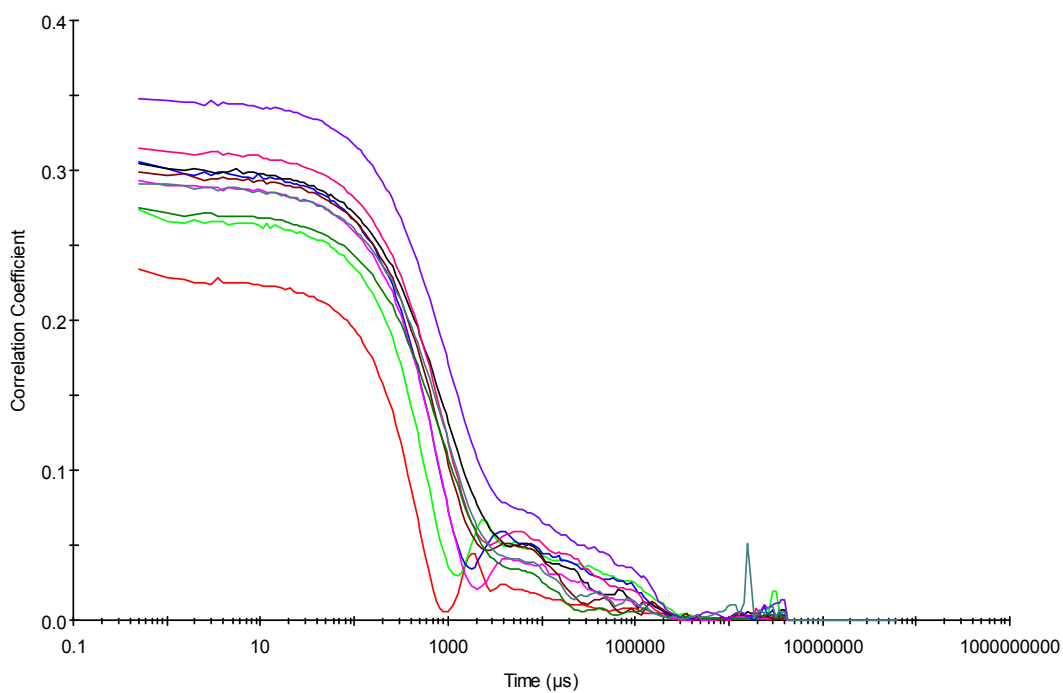


Figure S52 – Raw correlation data for 10 DLS runs at 40 °C with compound **1** (3.00 mg) in DMSO (1 mL).

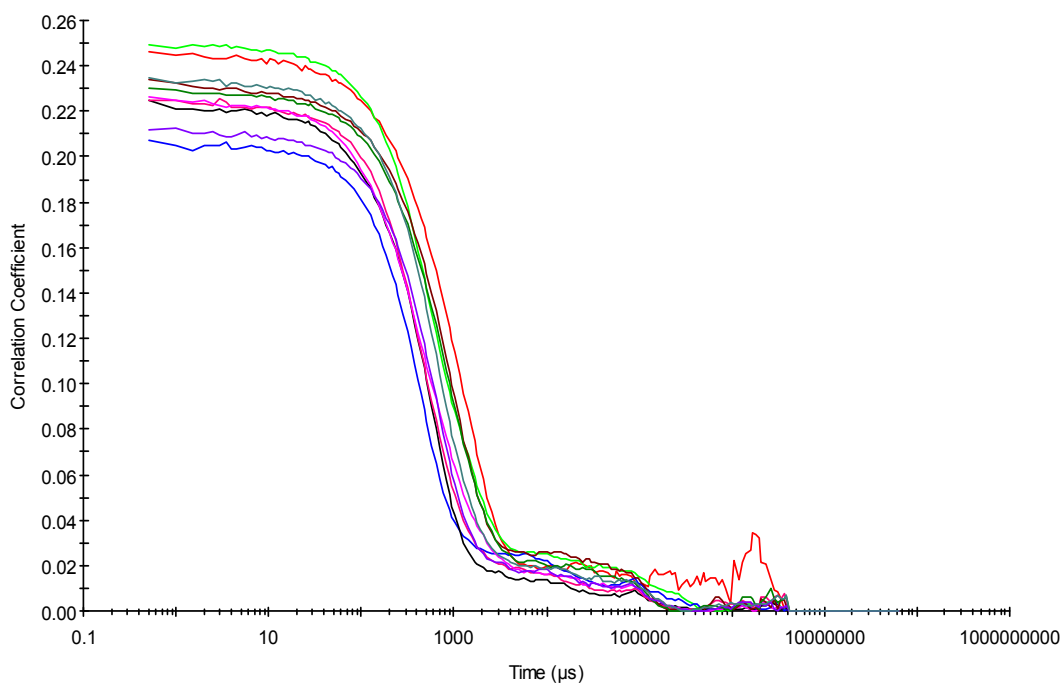


Figure S53 – Raw correlation data for 10 DLS runs at 25 °C after heating to 40 °C with compound **1** (3.00 mg) in DMSO (1 mL).

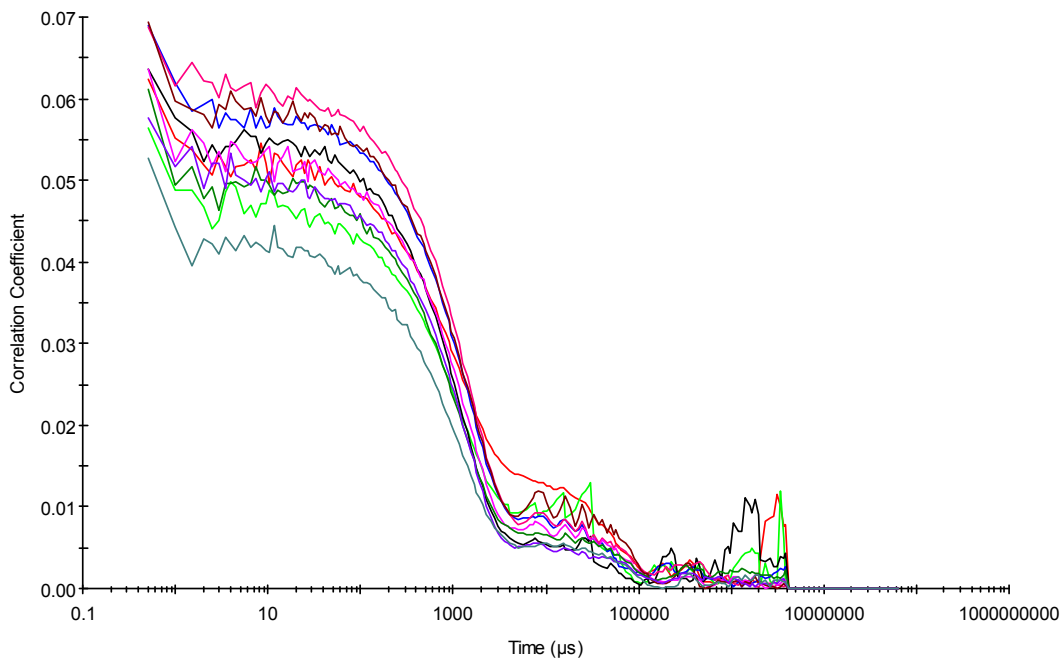


Figure S54 – Raw correlation data for 10 DLS runs at 25 °C before heating to 40 °C with compound **1** (0.30 mg) in DMSO (1 mL).

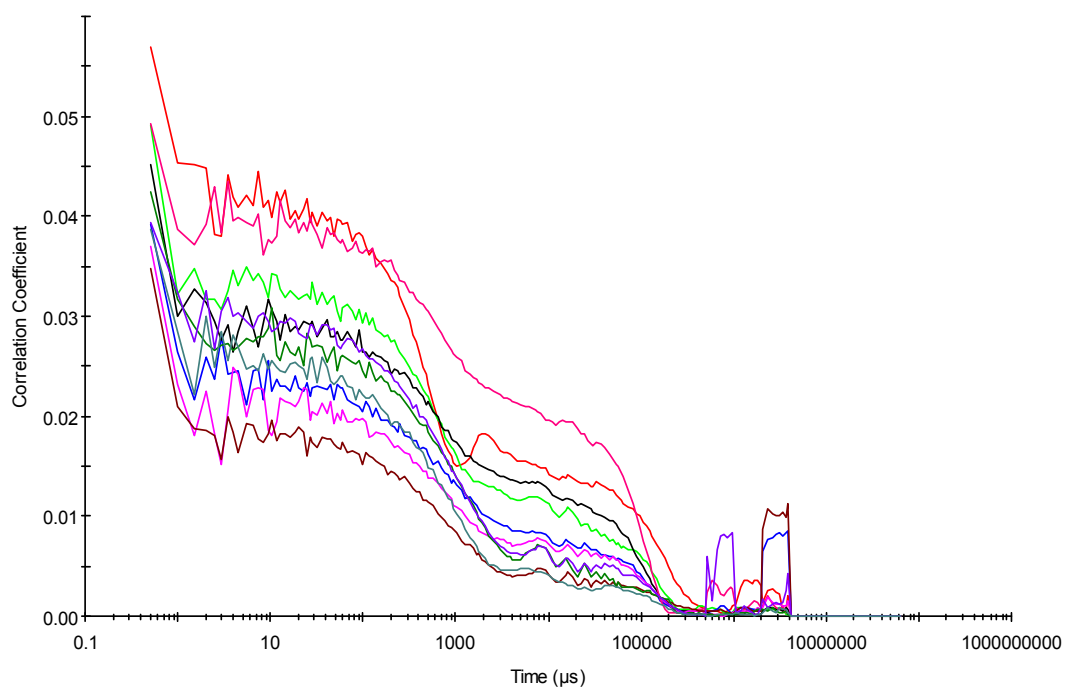


Figure S55 – Raw correlation data for 10 DLS runs at 40 °C with compound **1** (0.30 mg) in DMSO (1 mL).

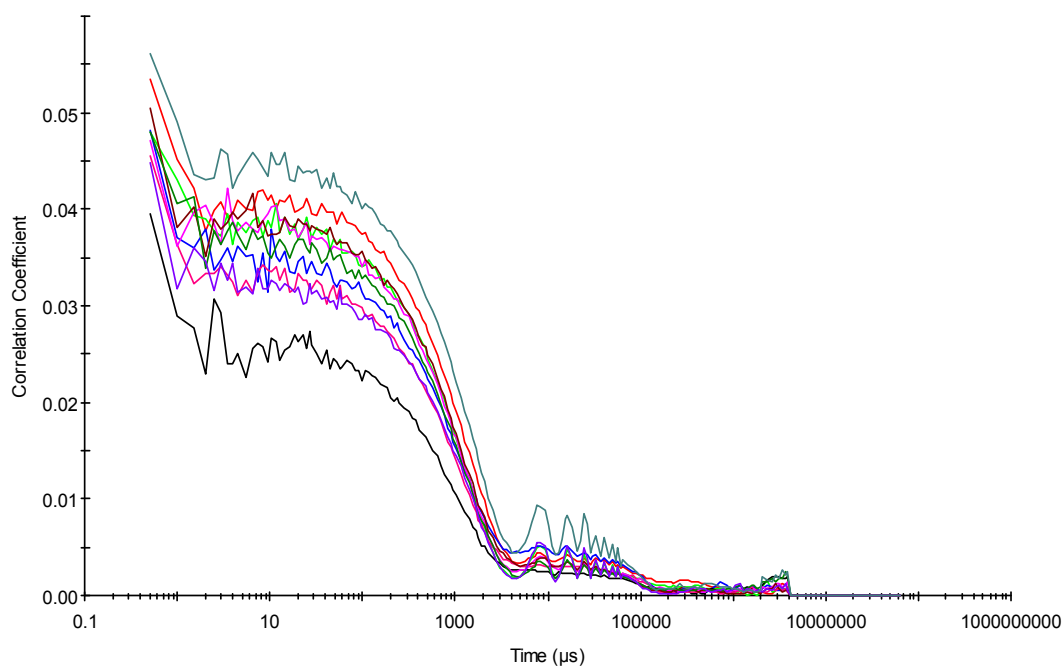


Figure S56 – Raw correlation data for 10 DLS runs at 25 °C after heating to 40 °C with compound **1** (0.30 mg) in DMSO (1 mL).

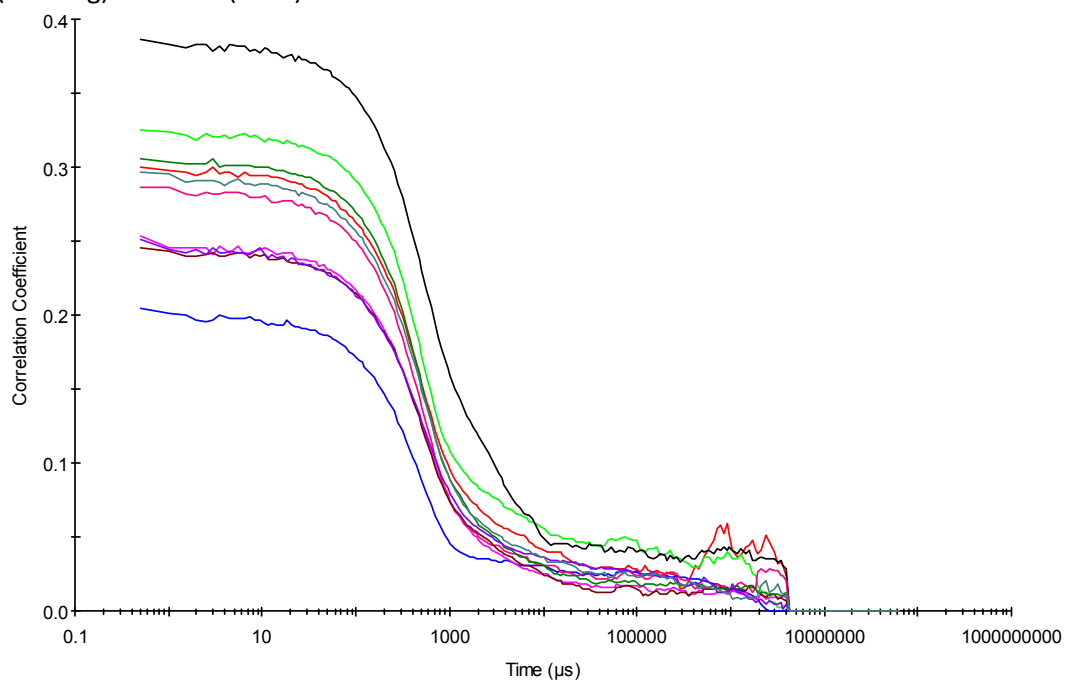


Figure S57 – Raw correlation data for 10 DLS runs at 25 °C before heating to 40 °C with compound **1** (0.03 mg) in DMSO (1 mL).

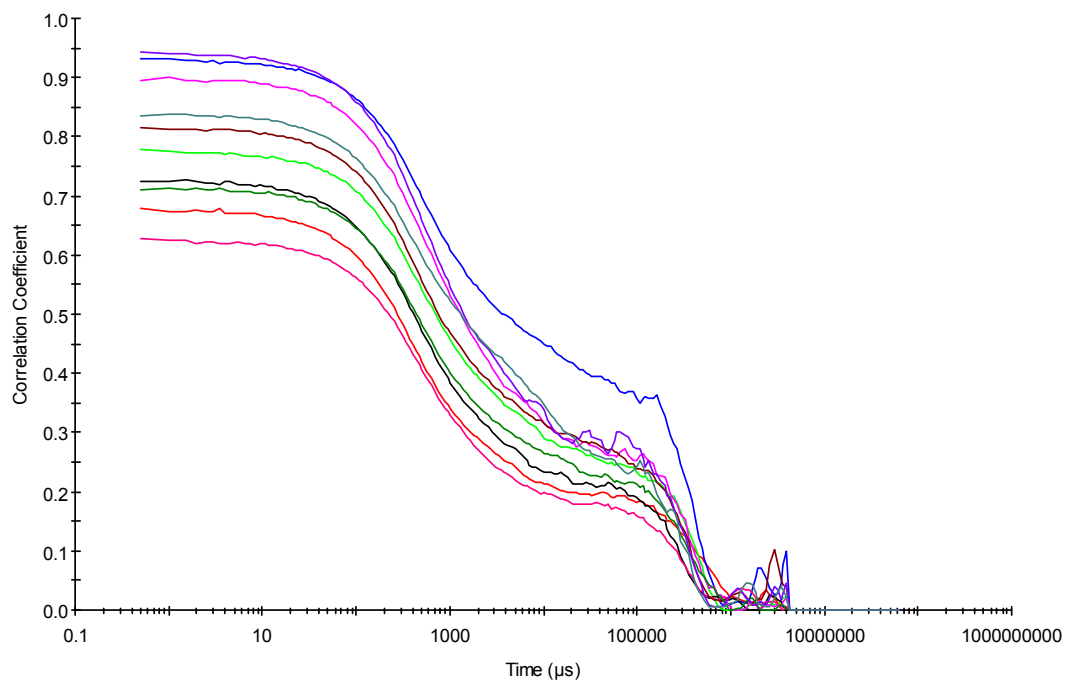


Figure S58 – Raw correlation data for 10 DLS runs at 40 °C with compound **1** (0.03 mg) in DMSO (1 mL).

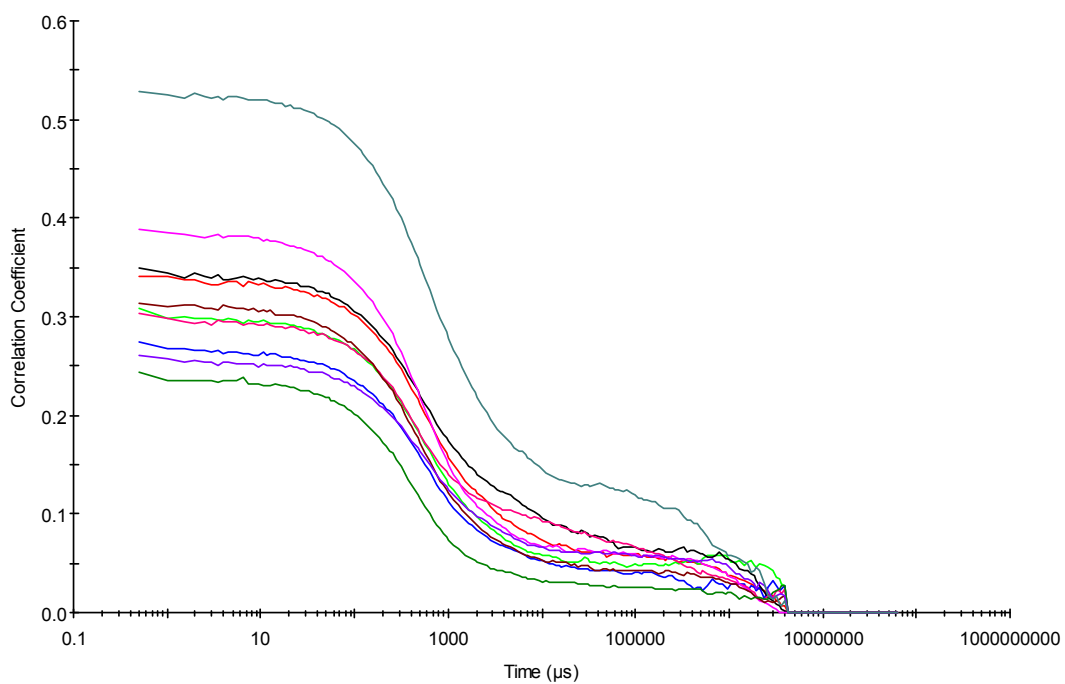


Figure S59 – Raw correlation data for 10 DLS runs at 25 °C after heating to 40 °C with compound **1** (0.03 mg) in DMSO (1 mL).

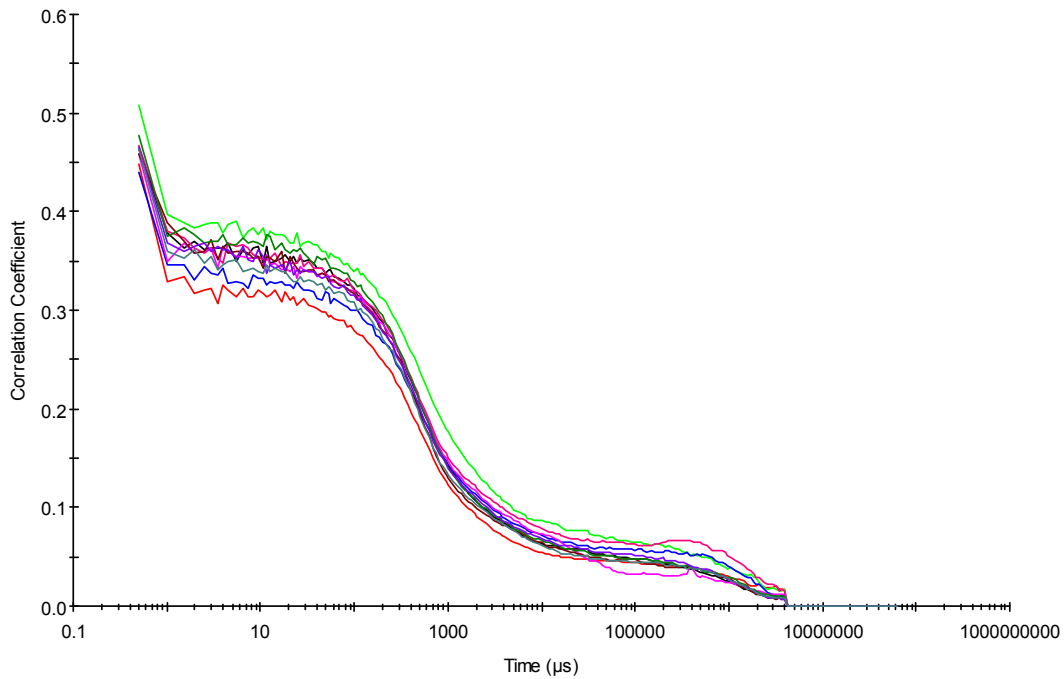


Figure S60 – Raw correlation data for 10 DLS runs at 25 °C before heating to 40 °C with compound **1** (0.003 mg) in DMSO (1 mL).

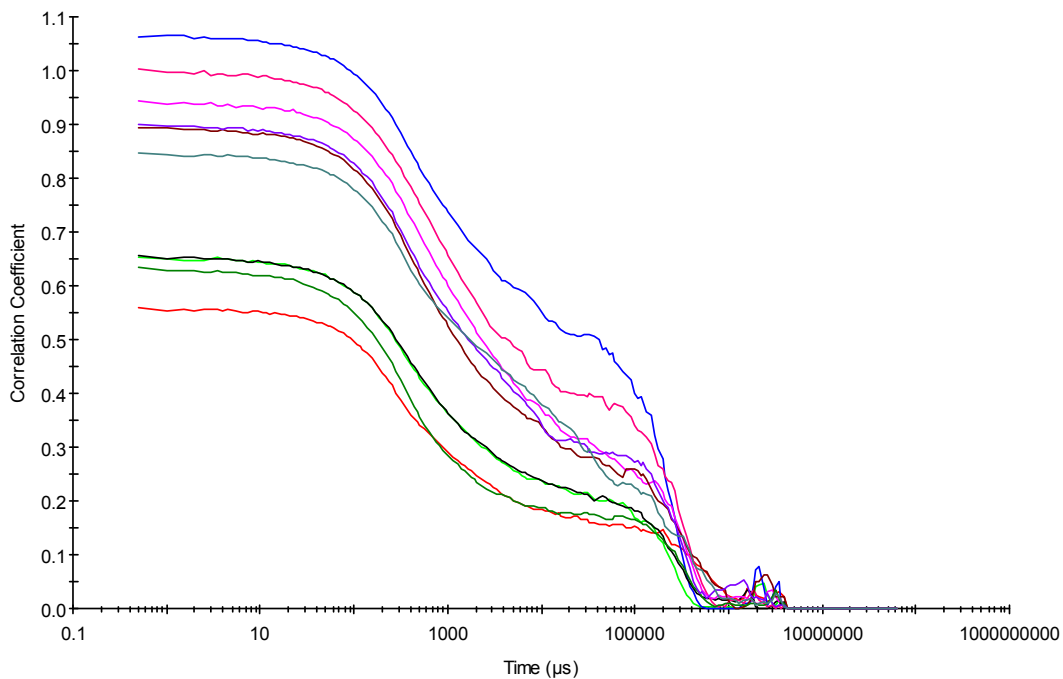


Figure S61 – Raw correlation data for 10 DLS runs at 40 °C with compound **1** (0.003 mg) in DMSO (1 mL).

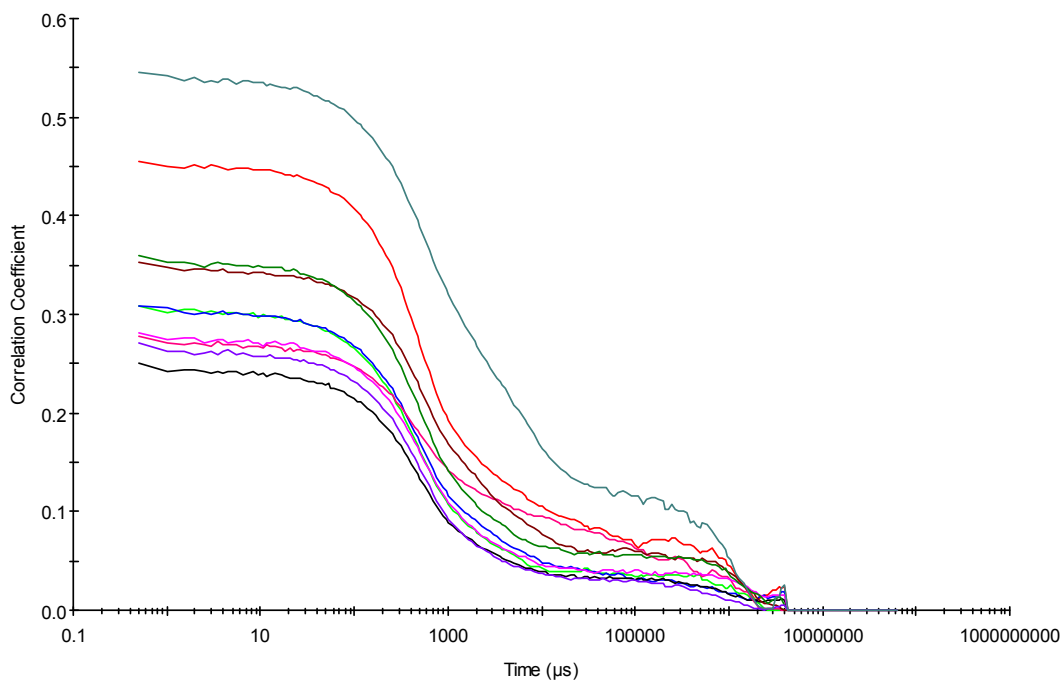


Figure S62 – Raw correlation data for 10 DLS runs at 25 °C after heating to 40 °C with compound **1** (0.003 mg) in DMSO (1 mL).

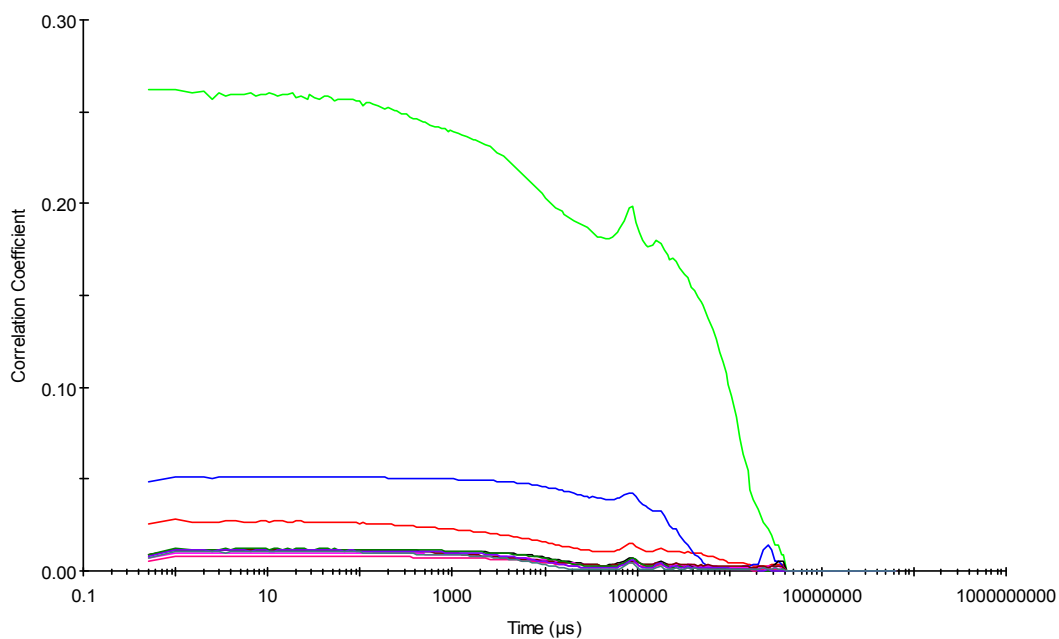


Figure S63 – Raw correlation data for 10 DLS runs at 25 °C before heating to 40 °C with compound **1** (30.00 mg) and compound **2** (19.33 mg) in DMSO (1 mL).

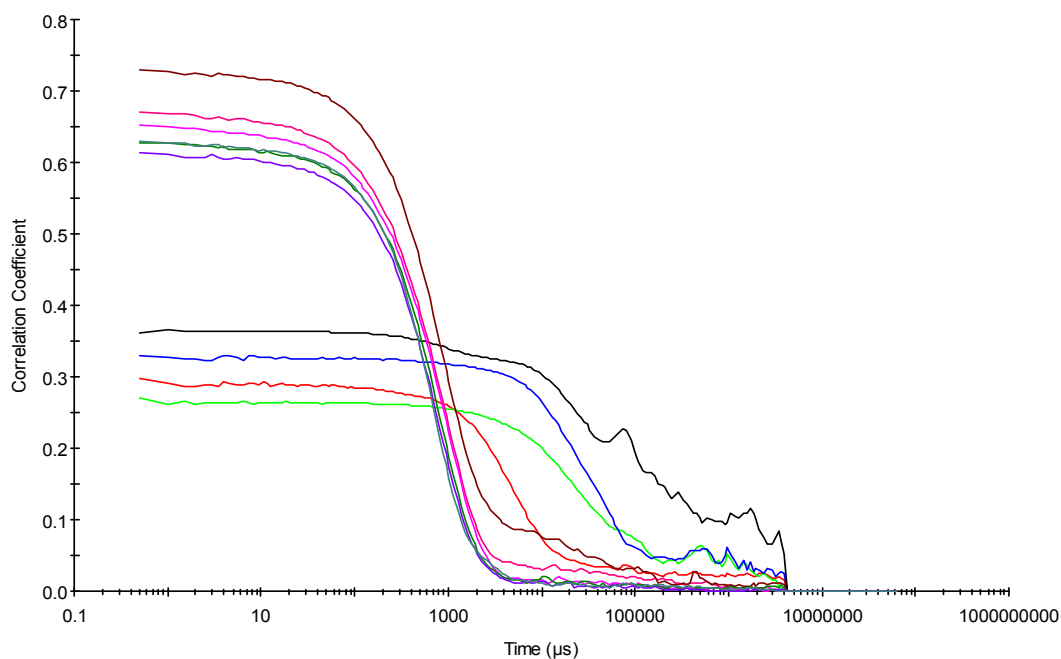


Figure S64 – Raw correlation data for 10 DLS runs at 40 °C with compound **1** (30.00 mg) and compound **2** (19.33 mg) in DMSO (1 mL).

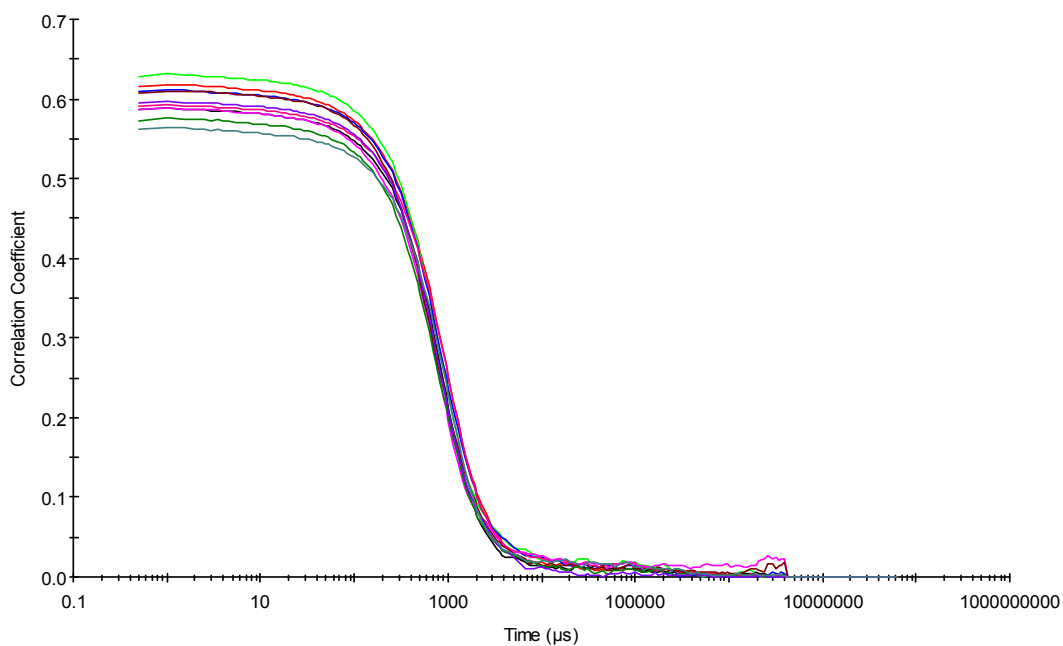


Figure S65 – Raw correlation data for 10 DLS runs at 25 °C after heating to 40 °C with compound **1** (30.00 mg) and compound **2** (19.33 mg) in DMSO (1 mL).

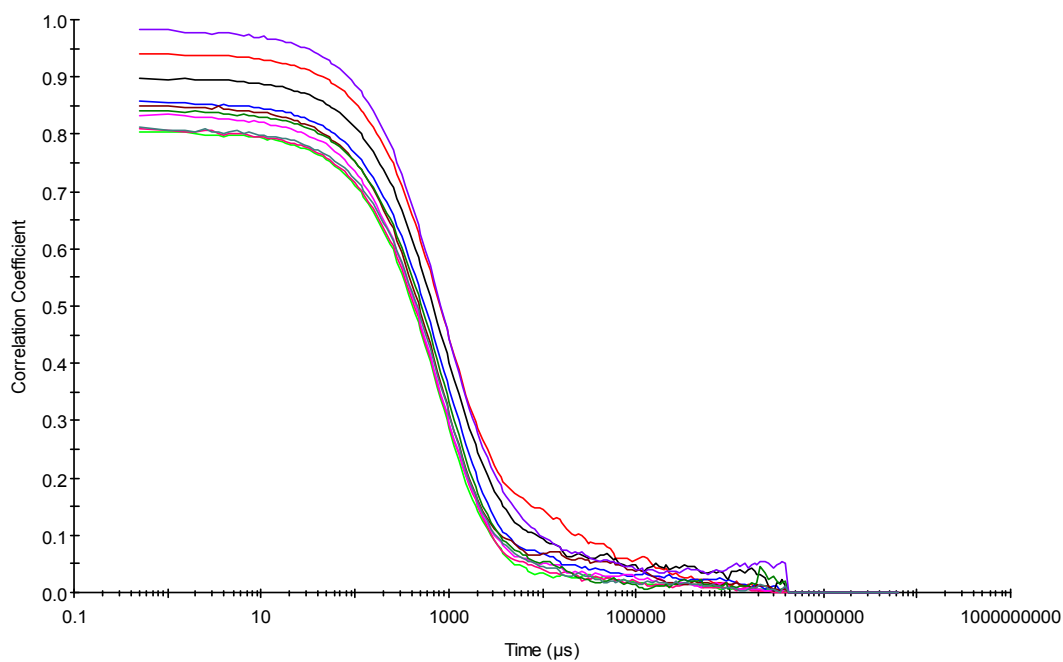


Figure S66 – Raw correlation data for 10 DLS runs at 25 °C before heating to 40 °C with compound **1** (30.00 mg) and 1 molar equivalent of TBAF in DMSO (1 mL).

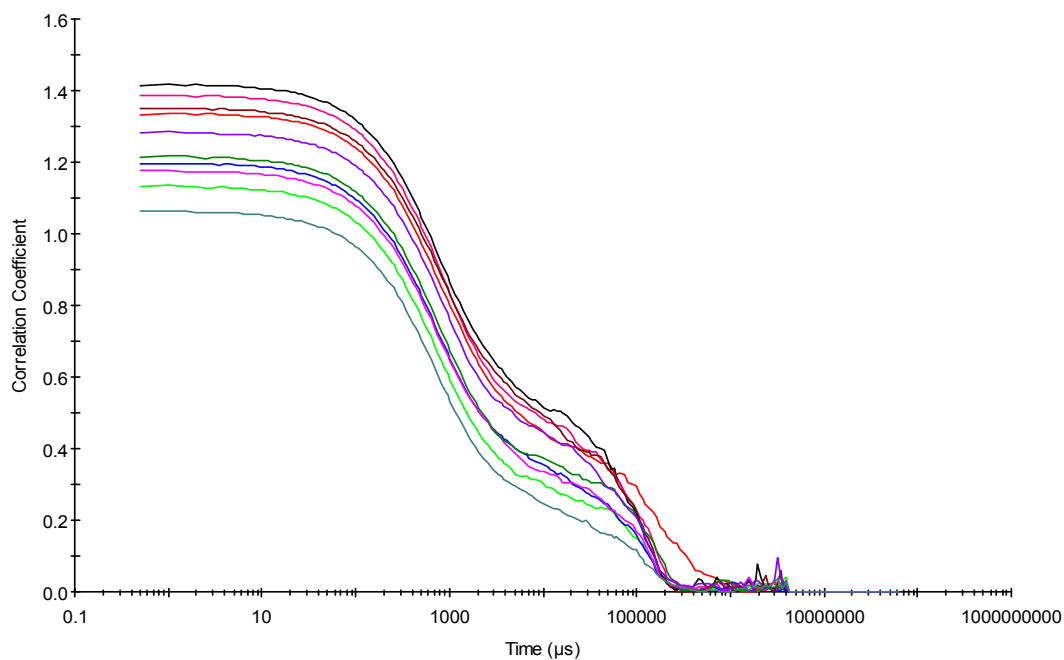


Figure S67 – Raw correlation data for 10 DLS runs at 40 °C with compound **1** (30.00 mg) and 1 molar equivalent of TBAF in DMSO (1 mL).

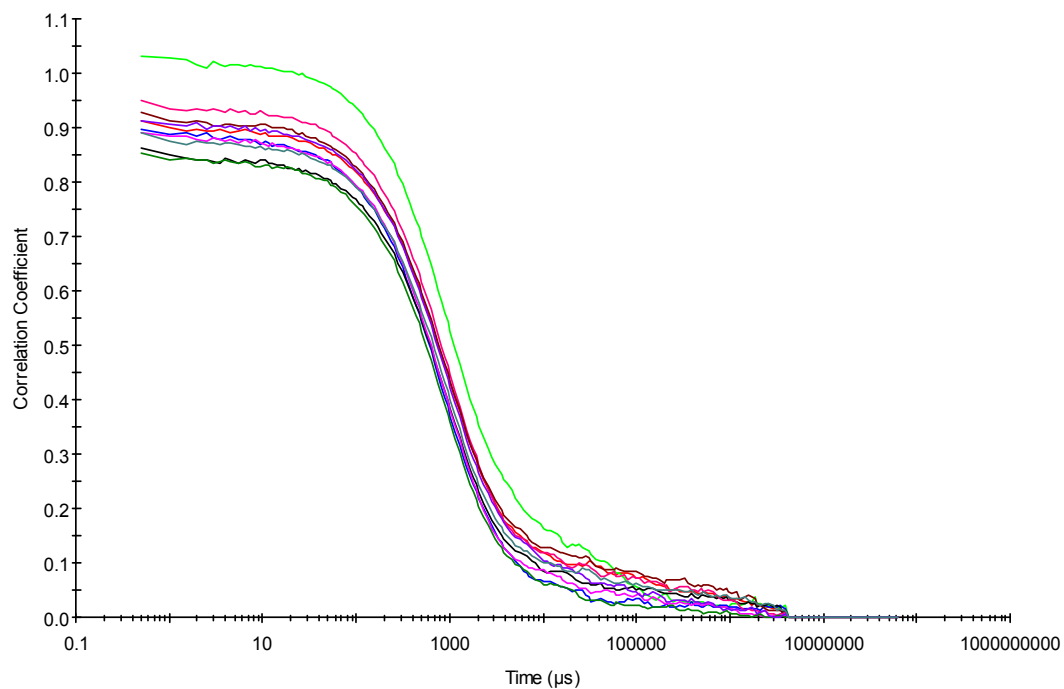


Figure S68 – Raw correlation data for 10 DLS runs at 25 °C after heating to 40 °C with compound **1** (30.00 mg) and 1 molar equivalent of TBAF in DMSO (1 mL).

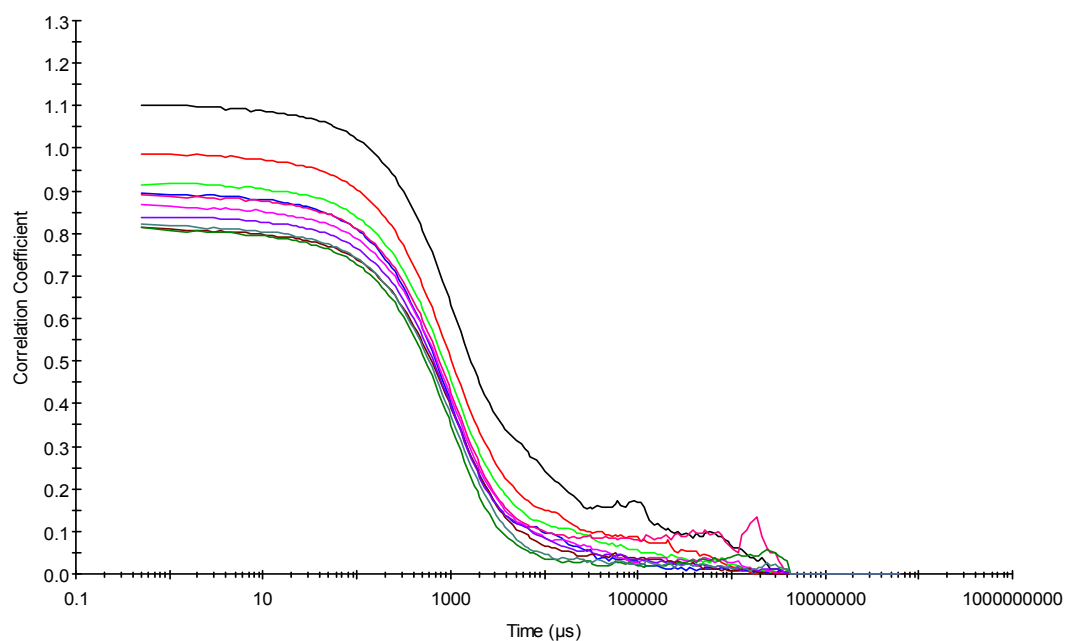


Figure S69 – Raw correlation data for 10 DLS runs at 25 °C before heating to 40 °C with compound **1** (30.00 mg) and 1 molar equivalent of TBAF and compound **6** in DMSO (1 mL).

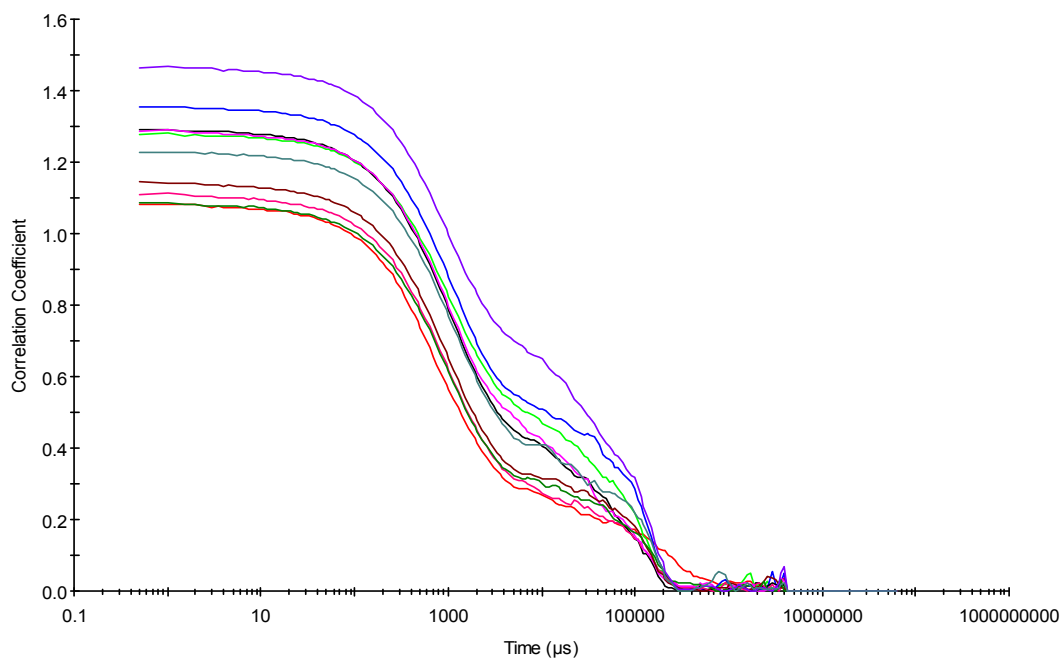


Figure S70 – Raw correlation data for 10 DLS runs at 40 °C with compound **1** (30.00 mg) and 1 molar equivalent of TBAF and compound **6** in DMSO (1 mL).

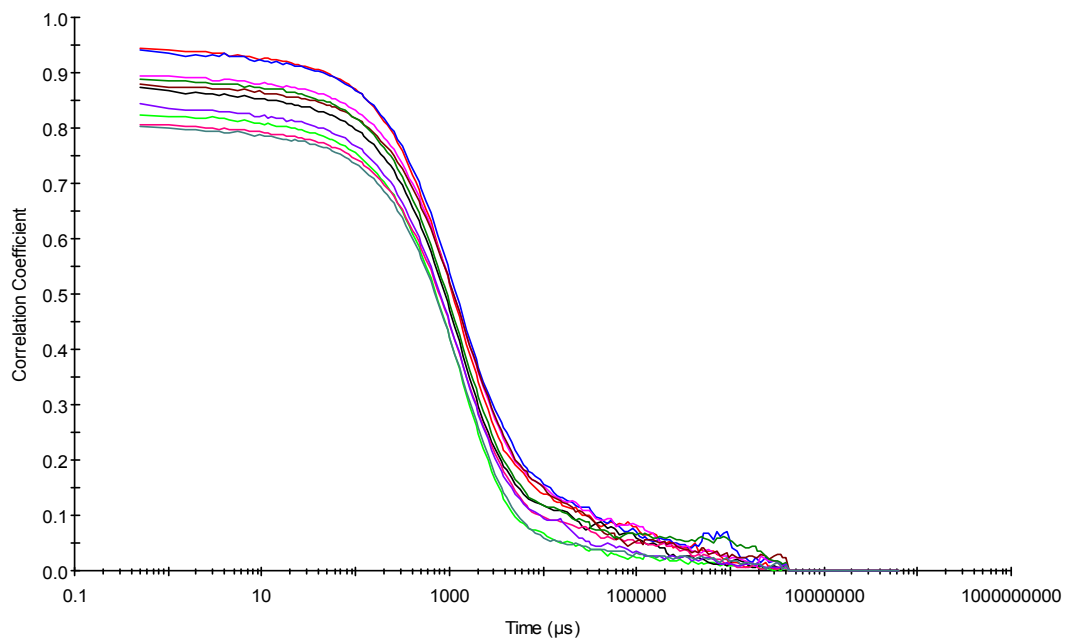


Figure S71 – Raw correlation data for 10 DLS runs at 25 °C after heating to 40 °C with compound **1** (30.00 mg) and 1 molar equivalent of TBAF and compound **6** in DMSO (1 mL).

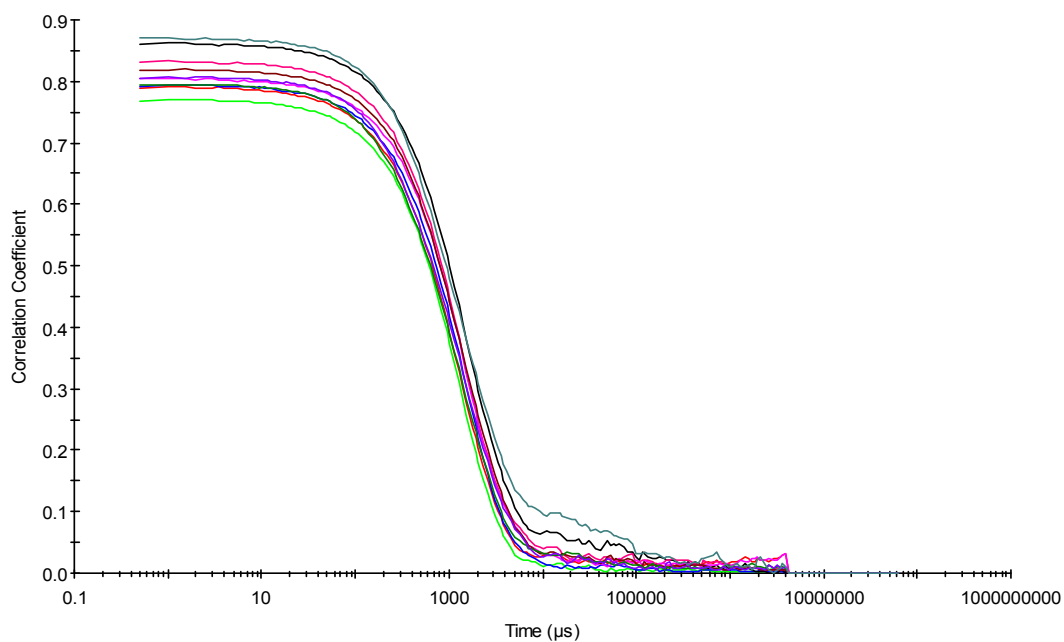


Figure S72 – Raw correlation data for 10 DLS runs at 25 °C before heating to 40 °C with compound **1** (30.00 mg) and 1 molar equivalent of TBACl in DMSO (1 mL).

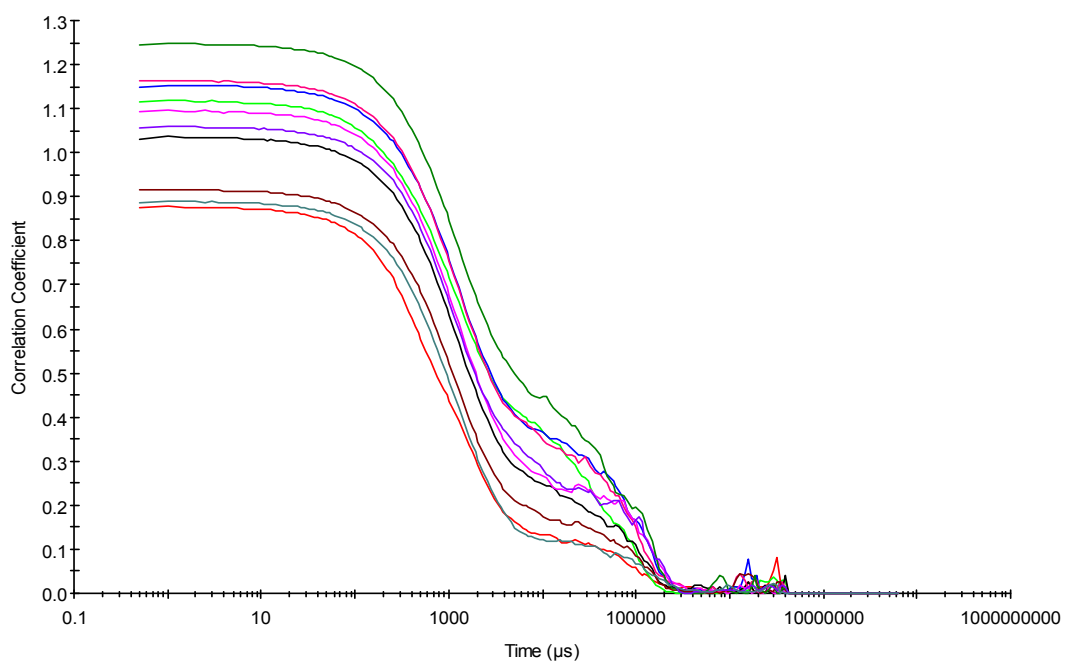


Figure S73 – Raw correlation data for 10 DLS runs at 40 °C with compound **1** (30.00 mg) and 1 molar equivalent of TBACl in DMSO (1 mL).

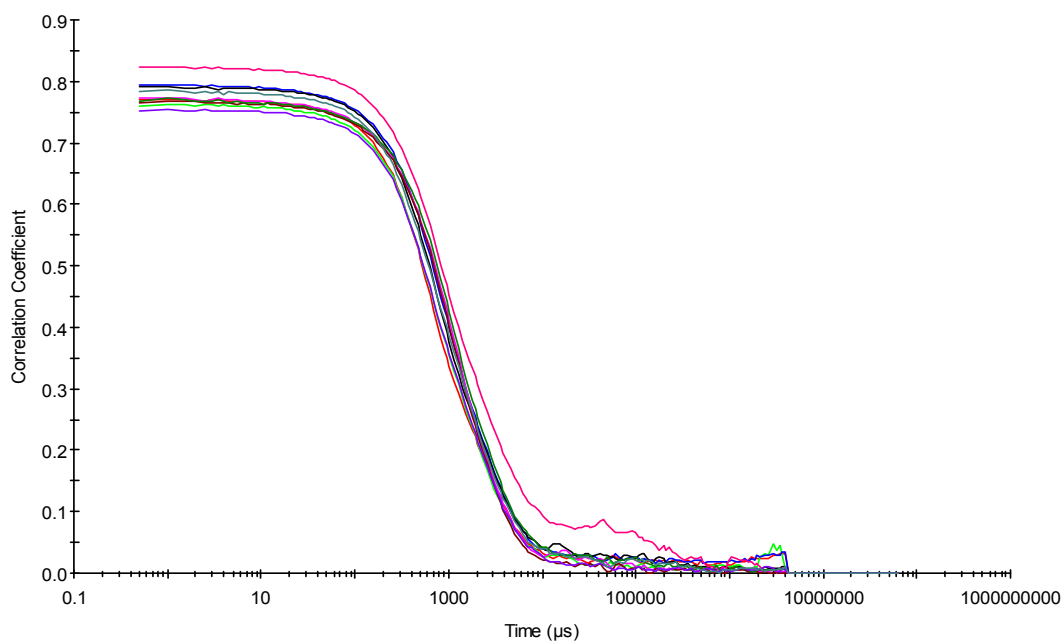


Figure S74 – Raw correlation data for 10 DLS runs at 25 °C after heating to 40 °C with compound **1** (30.00 mg) and 1 molar equivalent of TBACl in DMSO (1 mL).

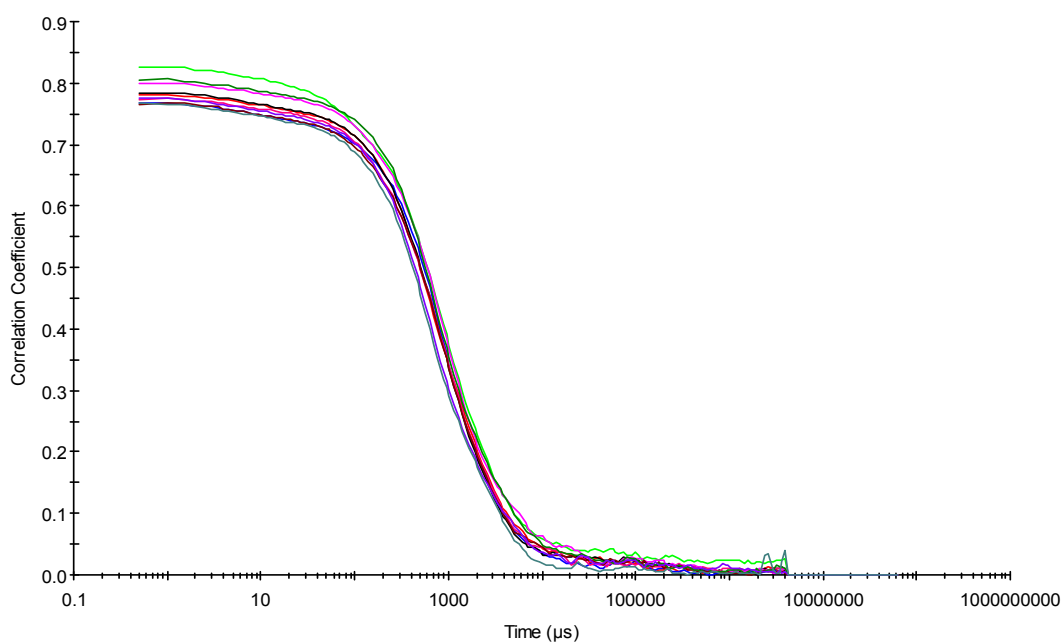


Figure S75 – Raw correlation data for 10 DLS runs at 25 °C before heating to 40 °C with compound **1** (30.00 mg) and 1 molar equivalent of TBACl and compound **6** in DMSO (1 mL).

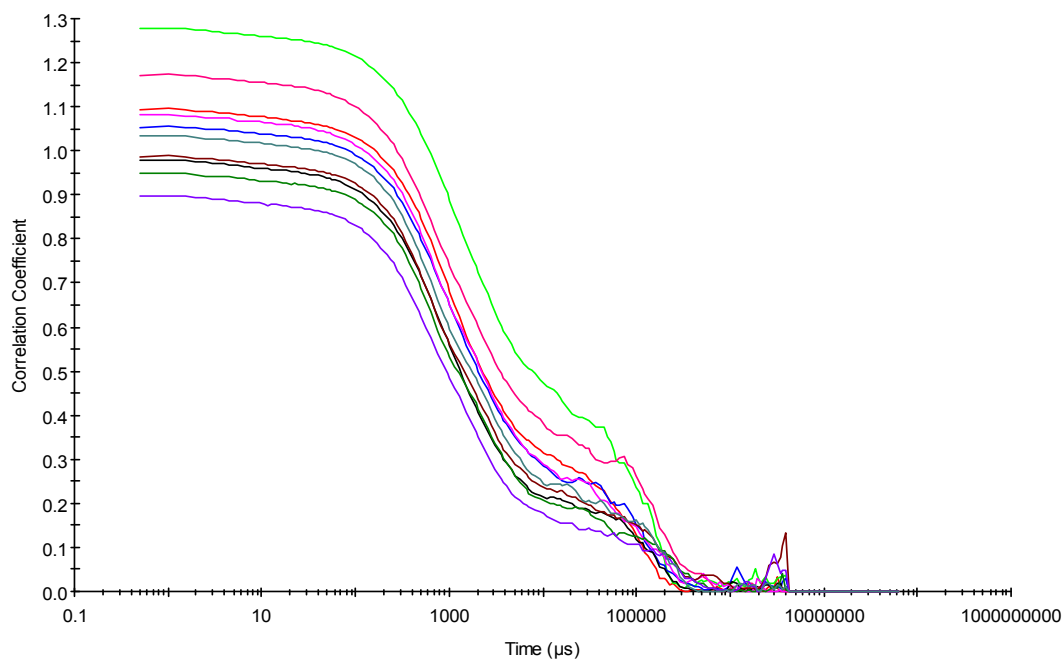


Figure S76 – Raw correlation data for 10 DLS runs at 40 °C with compound **1** (30.00 mg) and 1 molar equivalent of TBACl and compound **6** in DMSO (1 mL).

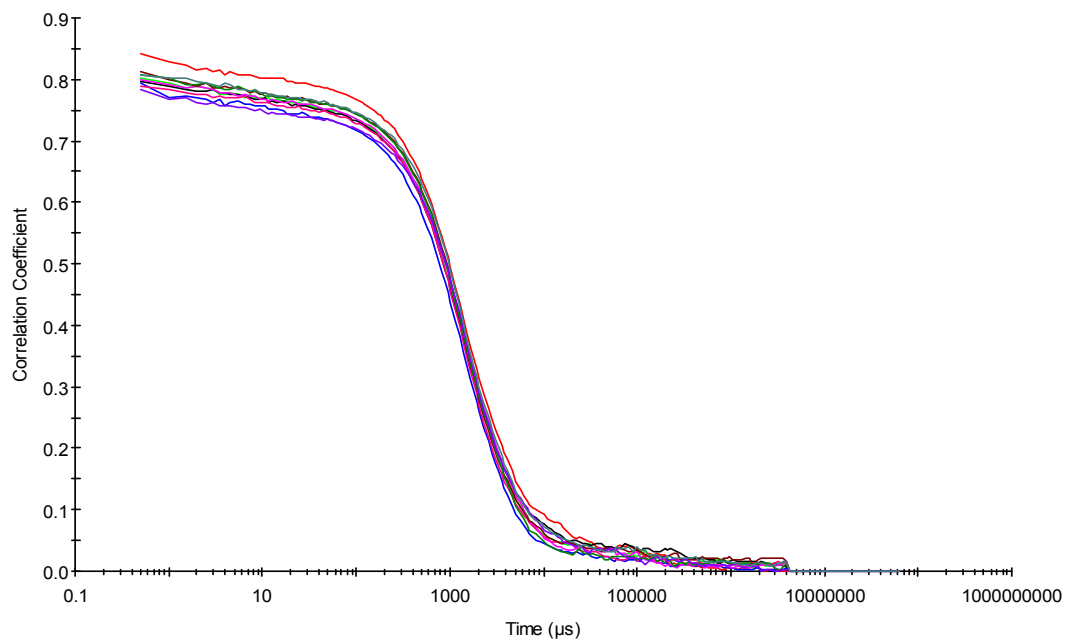


Figure S77 – Raw correlation data for 10 DLS runs at 25 °C after heating to 40 °C with compound **1** (30.00 mg) and 1 molar equivalent of TBACl and compound **6** in DMSO (1 mL).

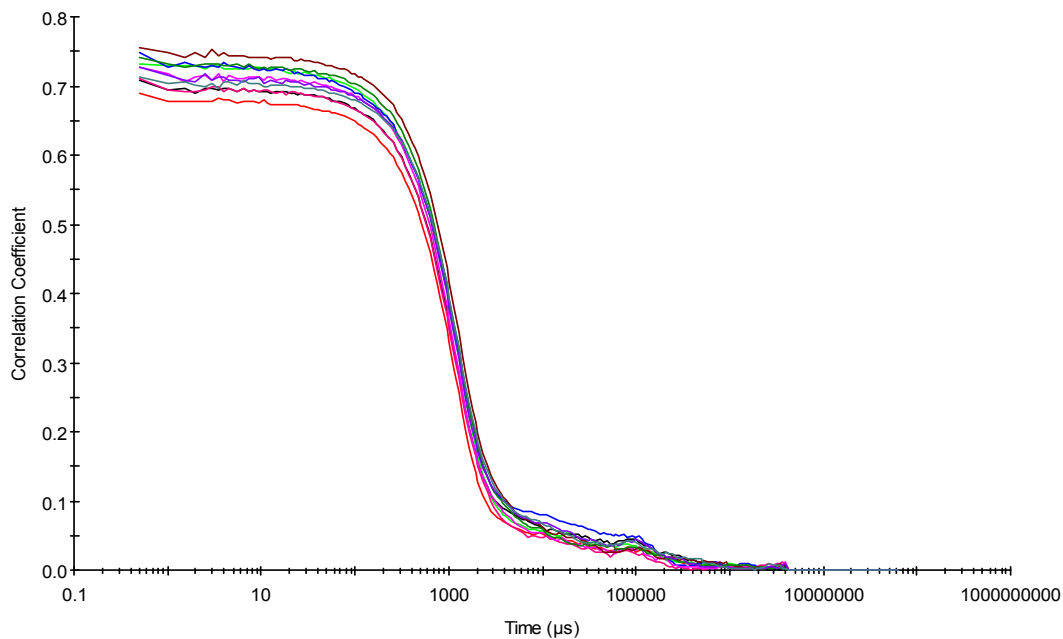


Figure S78 – Raw correlation data for 10 DLS runs at 25 °C before heating to 40 °C with compound **1** (30.00 mg) and 1 molar equivalent of TBABr in DMSO (1 mL).

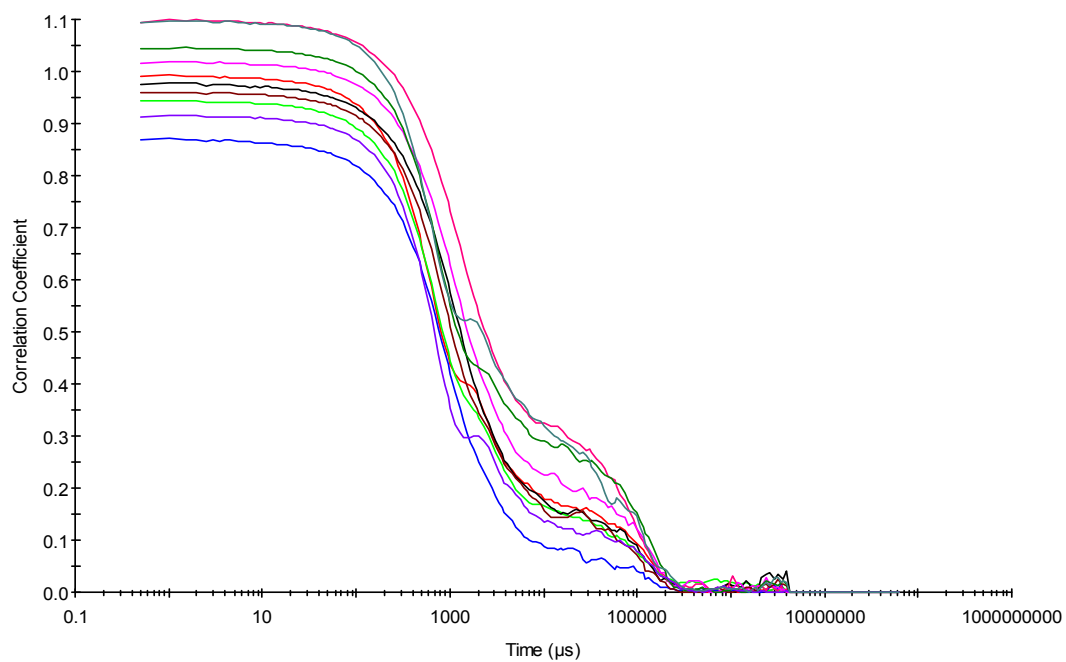


Figure S79 – Raw correlation data for 10 DLS runs at 40 °C with compound **1** (30.00 mg) and 1 molar equivalent of TBABr in DMSO (1 mL).

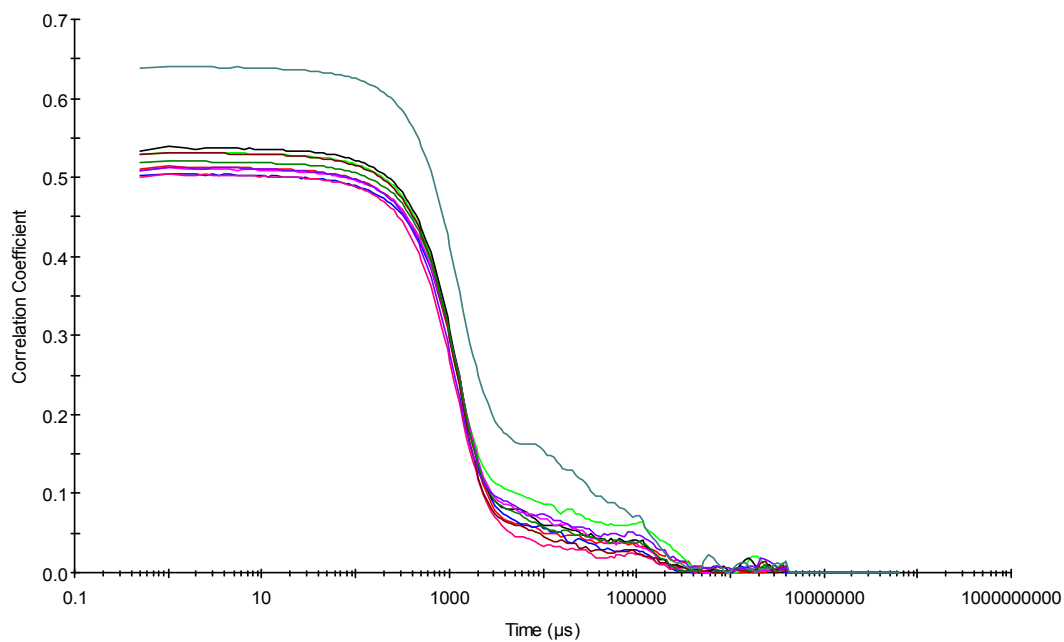


Figure S80 – Raw correlation data for 10 DLS runs at 25 °C after heating to 40 °C with compound **1** (30.00 mg) and 1 molar equivalent of TBABr in DMSO (1 mL).

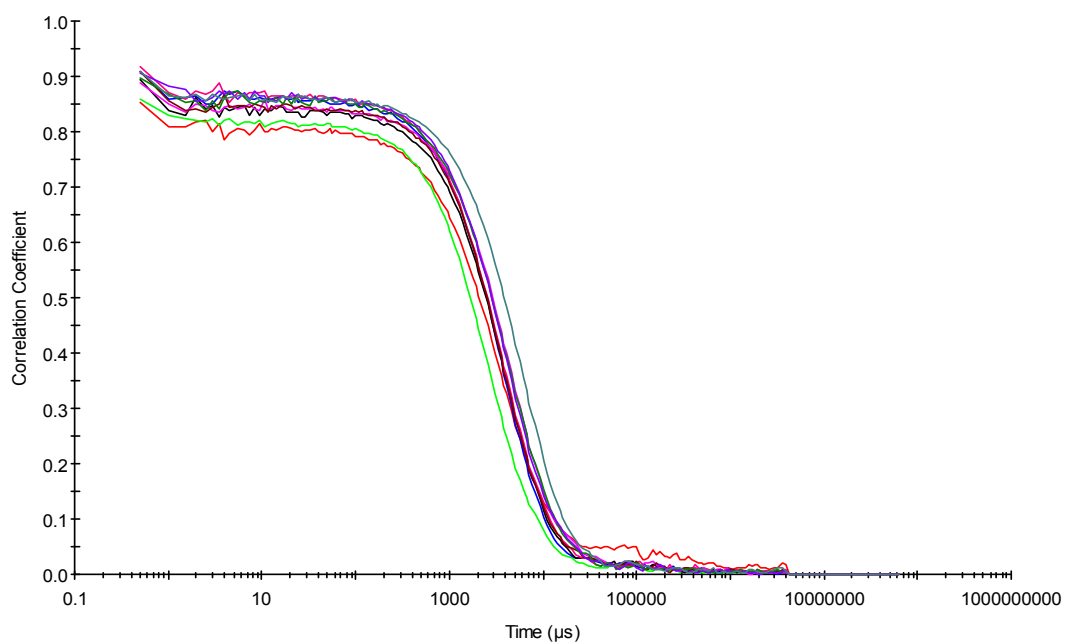


Figure S81 – Raw correlation data for 10 DLS runs at 25 °C before heating to 40 °C with compound **1** (30.00 mg) and 1 molar equivalent of TBABr and compound **6** in DMSO (1 mL).

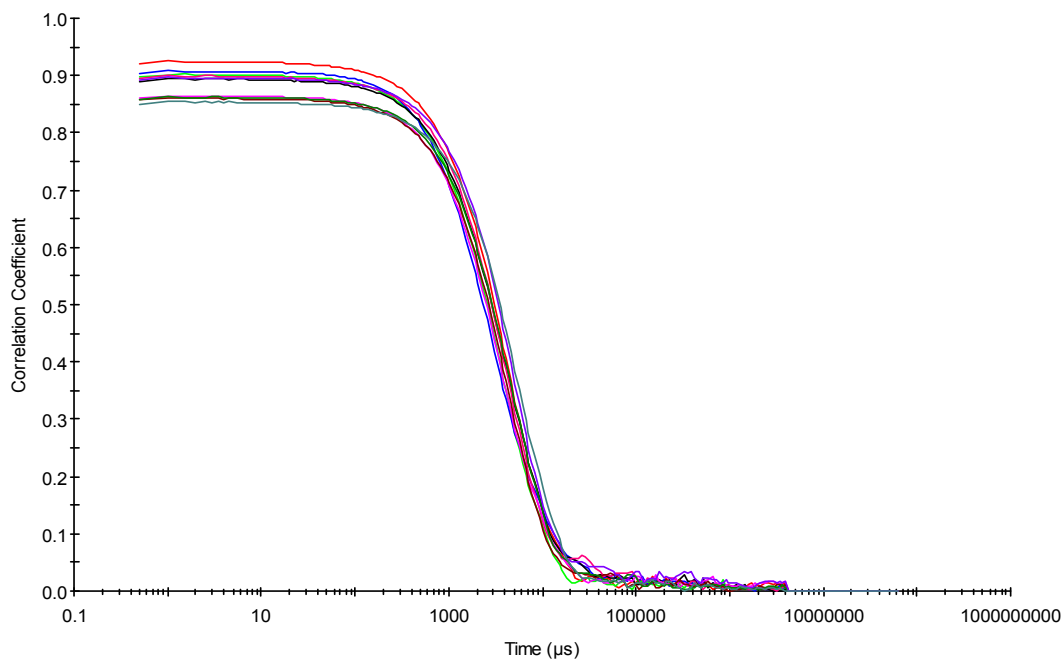


Figure S82 – Raw correlation data for 10 DLS runs at 40 °C with compound **1** (30.00 mg) and 1 molar equivalent of TBABr and compound **6** in DMSO (1 mL).

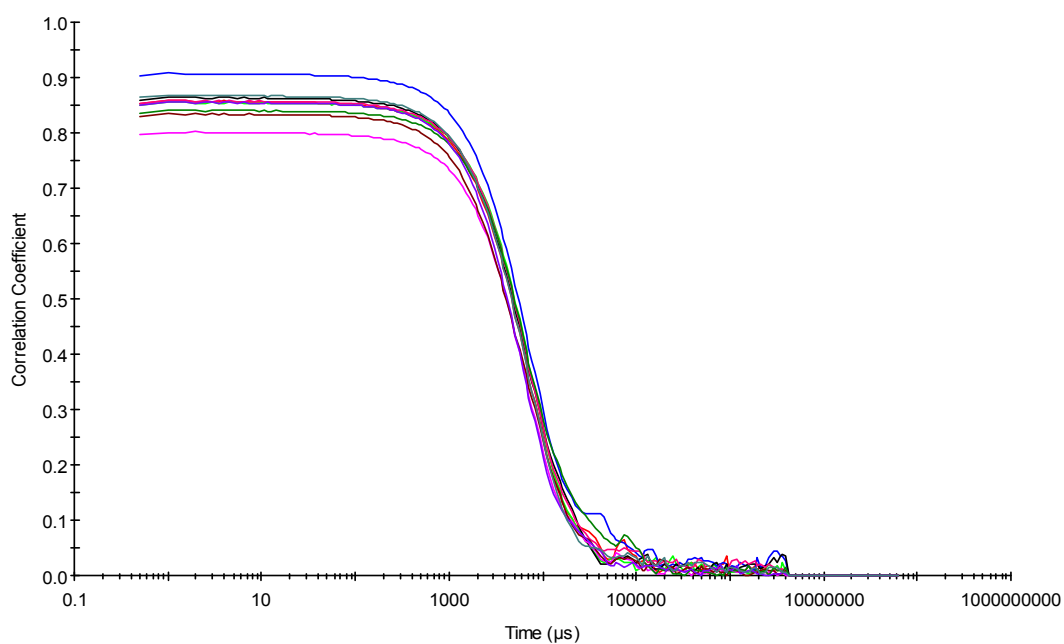


Figure S83 – Raw correlation data for 10 DLS runs at 25 °C after heating to 40 °C with compound **1** (30.00 mg) and 1 molar equivalent of TBABr and compound **6** in DMSO (1 mL).

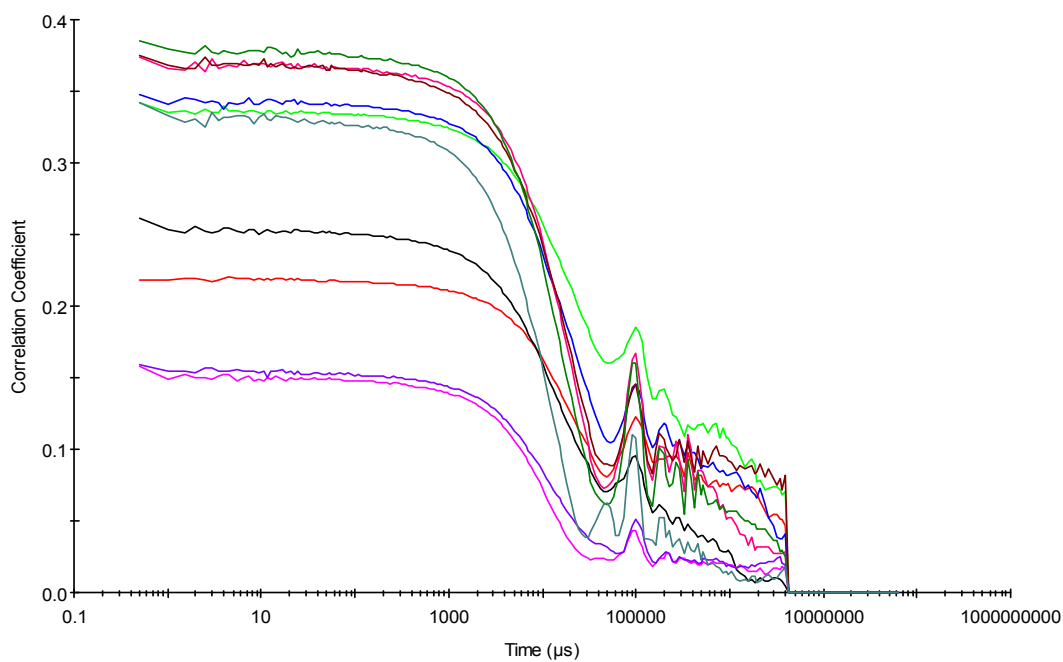


Figure S84 – Raw correlation data for 10 DLS runs at 25 °C before heating to 40 °C with compound **1** (30.00 mg) and 1 molar equivalent of compound **6** in DMSO (1 mL).

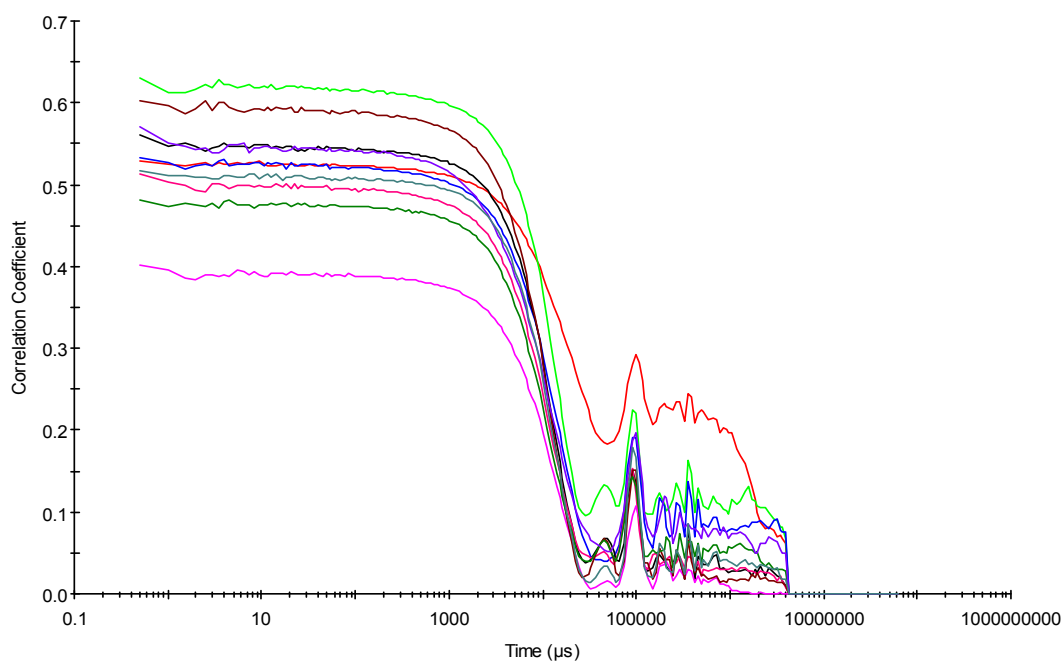


Figure S85 – Raw correlation data for 10 DLS runs at 40 °C with compound **1** (30.00 mg) and 1 molar equivalent of compound **6** in DMSO (1 mL).

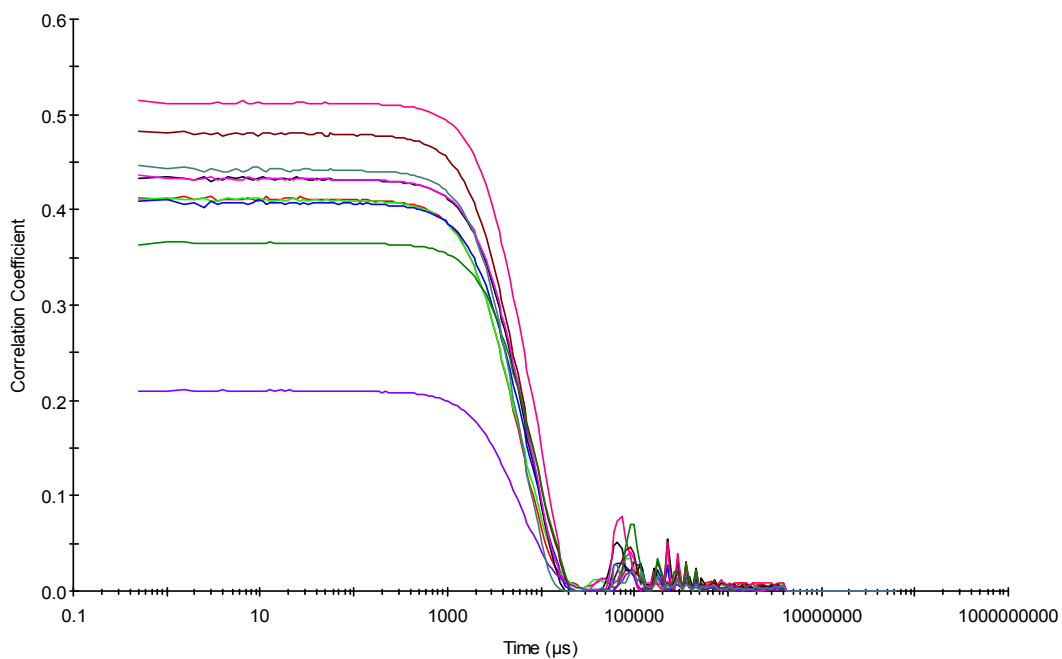


Figure S86 – Raw correlation data for 10 DLS runs at 25 °C after heating to 40 °C with compound **1** (30.00 mg) and 1 molar equivalent of compound **6** in DMSO (1 mL).

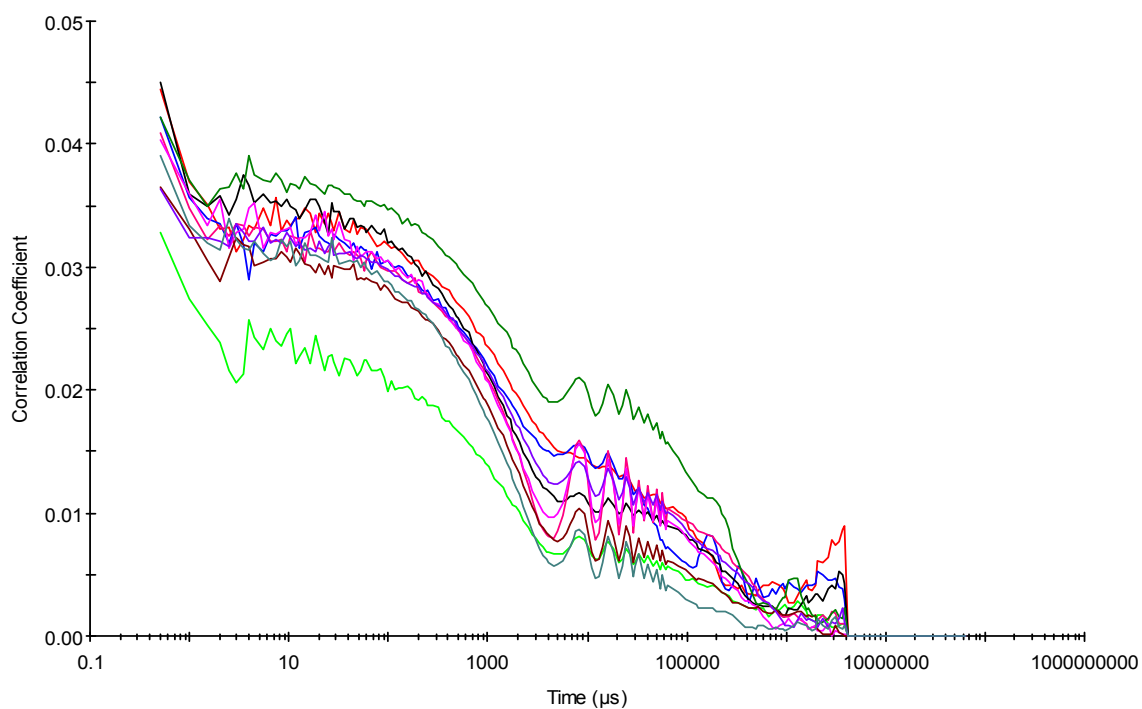


Figure S87 – Raw correlation data for 10 DLS runs at 25 °C before heating to 40 °C without compound **1** in DMSO (1 mL).

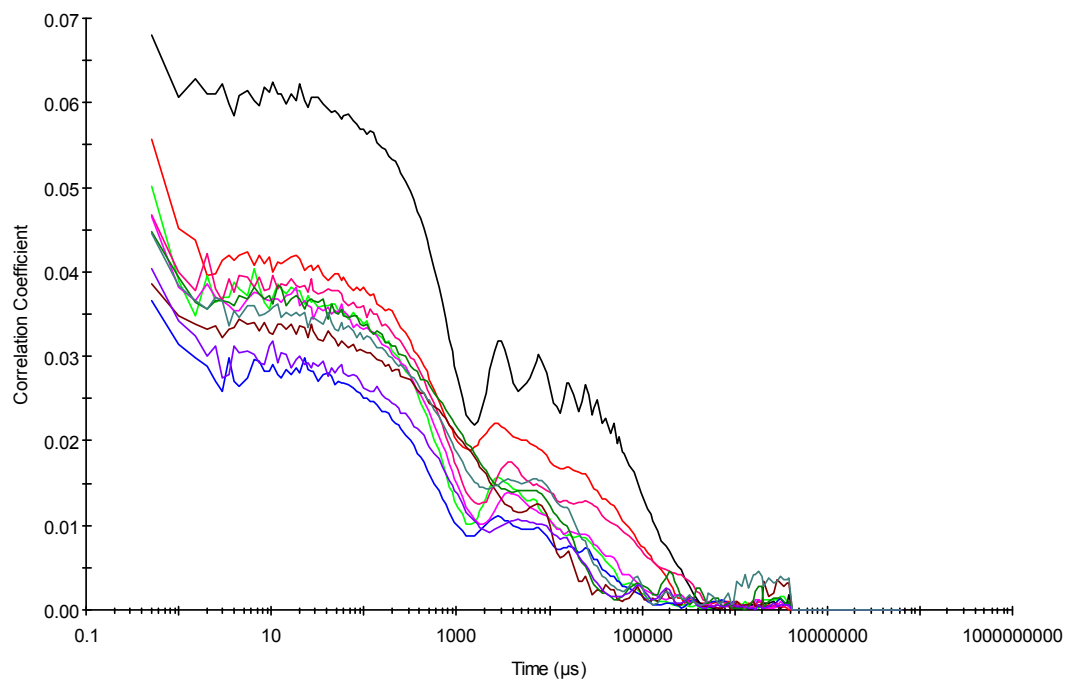


Figure S88 – Raw correlation data for 10 DLS runs at 40 °C without compound **1** in DMSO (1 mL).

## Size distribution calculated by DLS

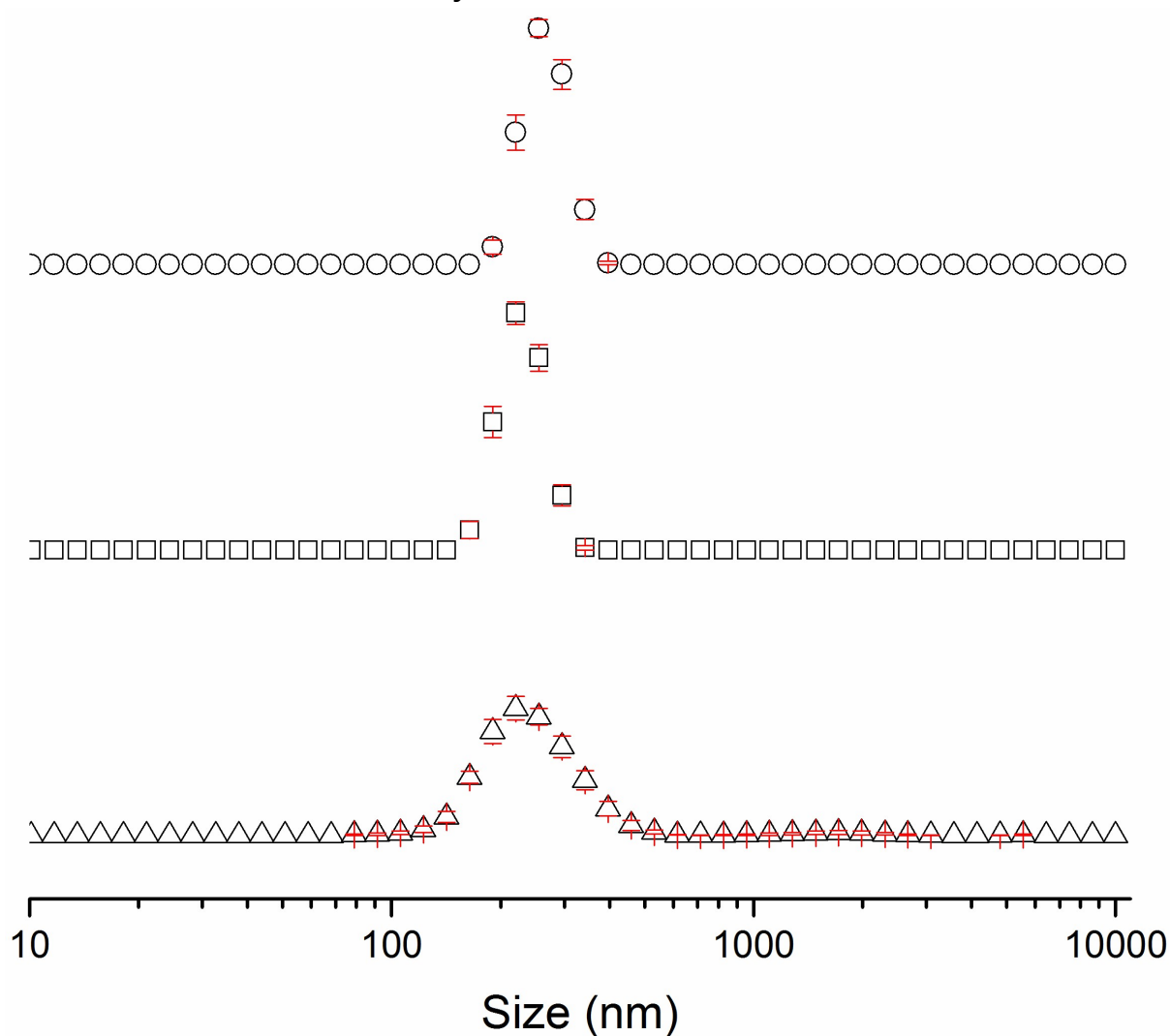


Figure S89 – Average intensity particle size distribution, calculated from 9 DLS runs, of supramolecular superstructures formed by dissolving **1** (60 mg) in DMSO (1 mL) at  $\Delta$  25 °C,  $\square$ ) heating to 40 °C and  $\circ$ ) cooling to 25 °C. Only 9 of the available 10 DLS runs were used as in some cases, due to the heating and cooling processes there were some obvious temperature equilibration issues for the first run.

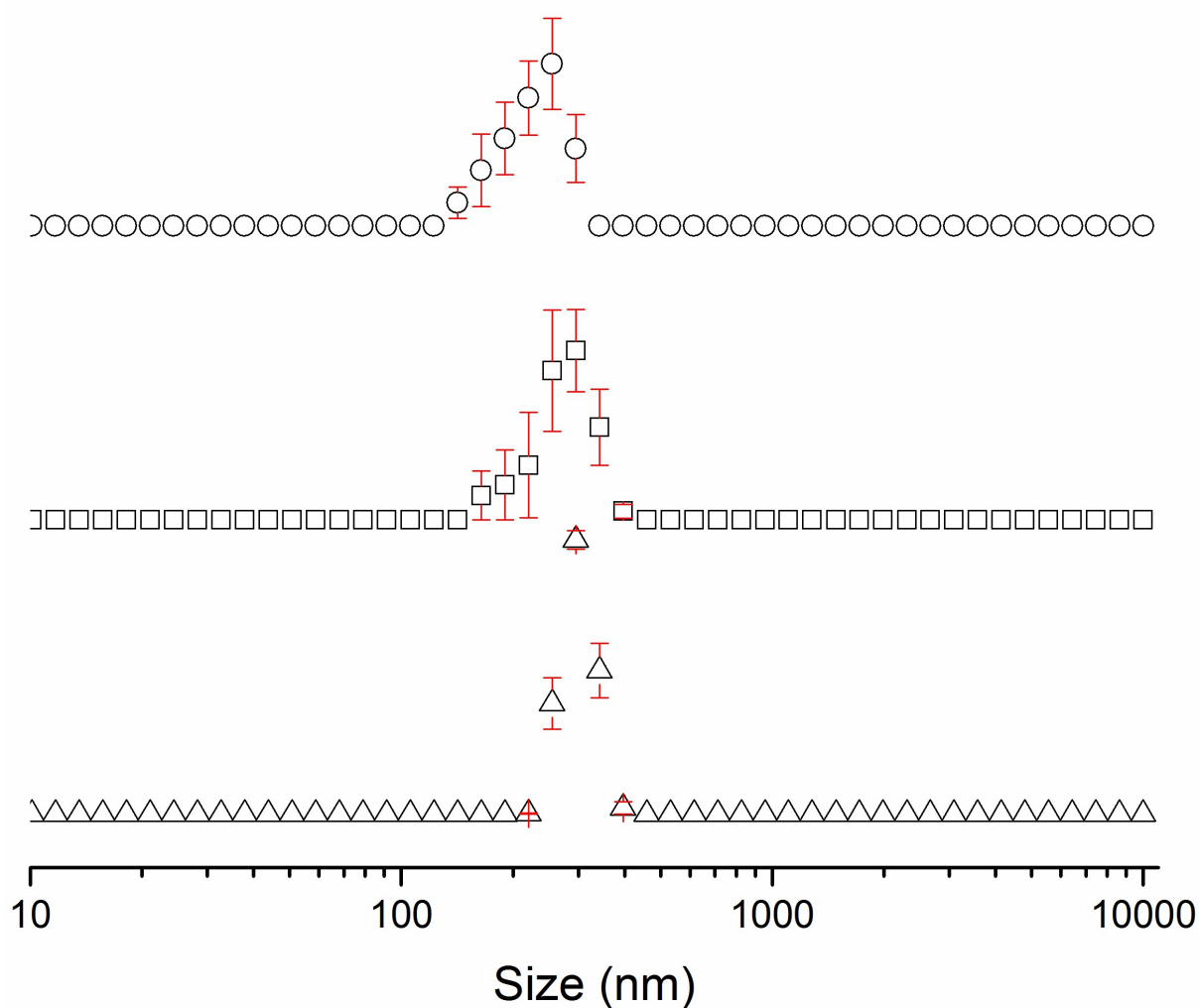


Figure S90 – Average intensity particle size distribution, calculated from 9 DLS runs, of supramolecular superstructures formed by dissolving **1** (3 mg) in DMSO (1 mL) at  $\Delta$  25 °C,  $\square$ ) heating to 40 °C and  $\circ$ ) cooling to 25 °C. Only 9 of the available 10 DLS runs were used as in some cases, due to the heating and cooling processes there were some obvious temperature equilibration issues for the first run.

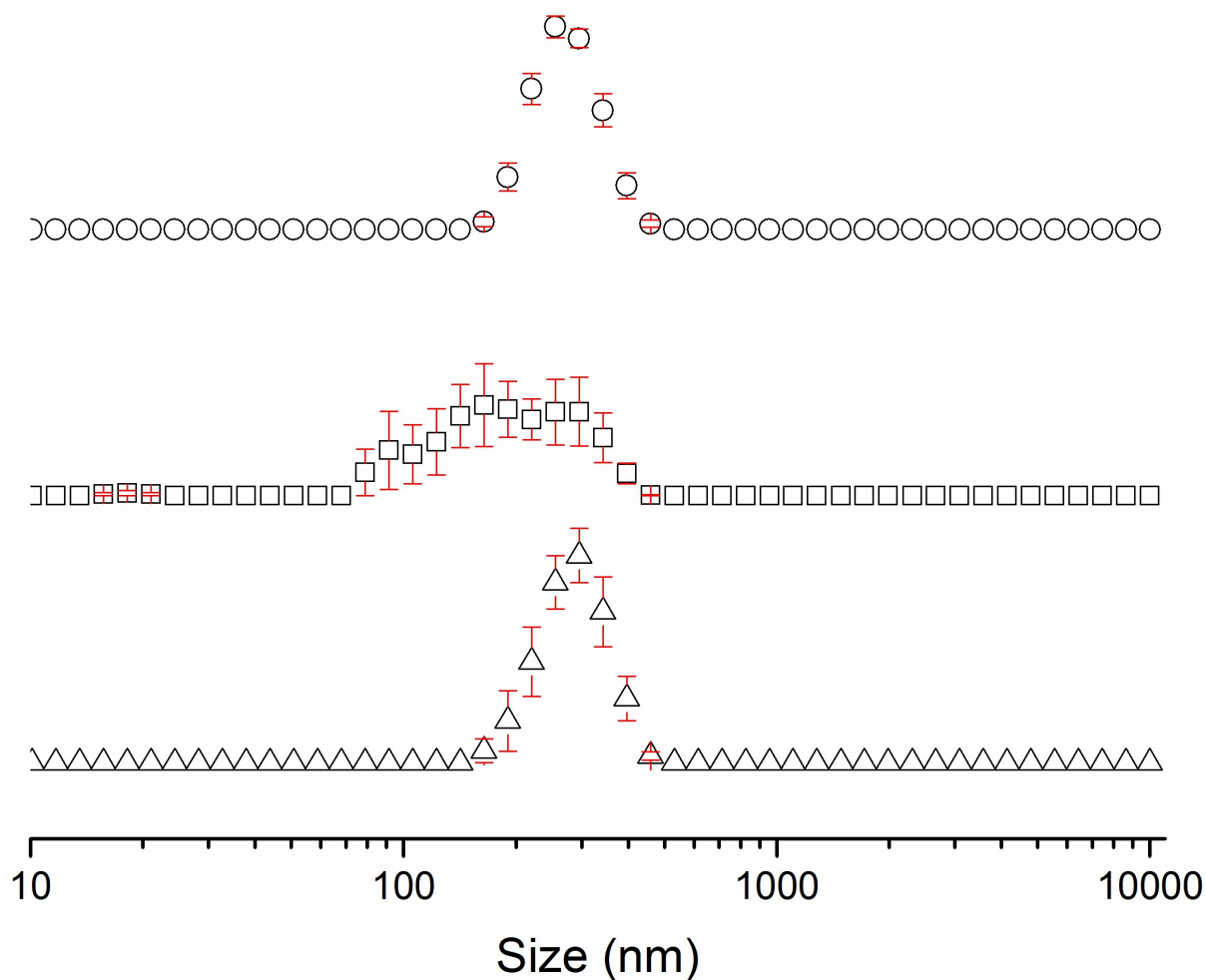


Figure S91 – Average intensity particle size distribution, calculated from 9 DLS runs, of supramolecular superstructures formed by dissolving **1** (0.3 mg) in DMSO (1 mL) at  $\Delta$ ) 25 °C,  $\square$ ) heating to 40 °C and  $\circ$ ) cooling to 25 °C. Only 9 of the available 10 DLS runs were used as in some cases, due to the heating and cooling processes there were some obvious temperature equilibration issues for the first run.

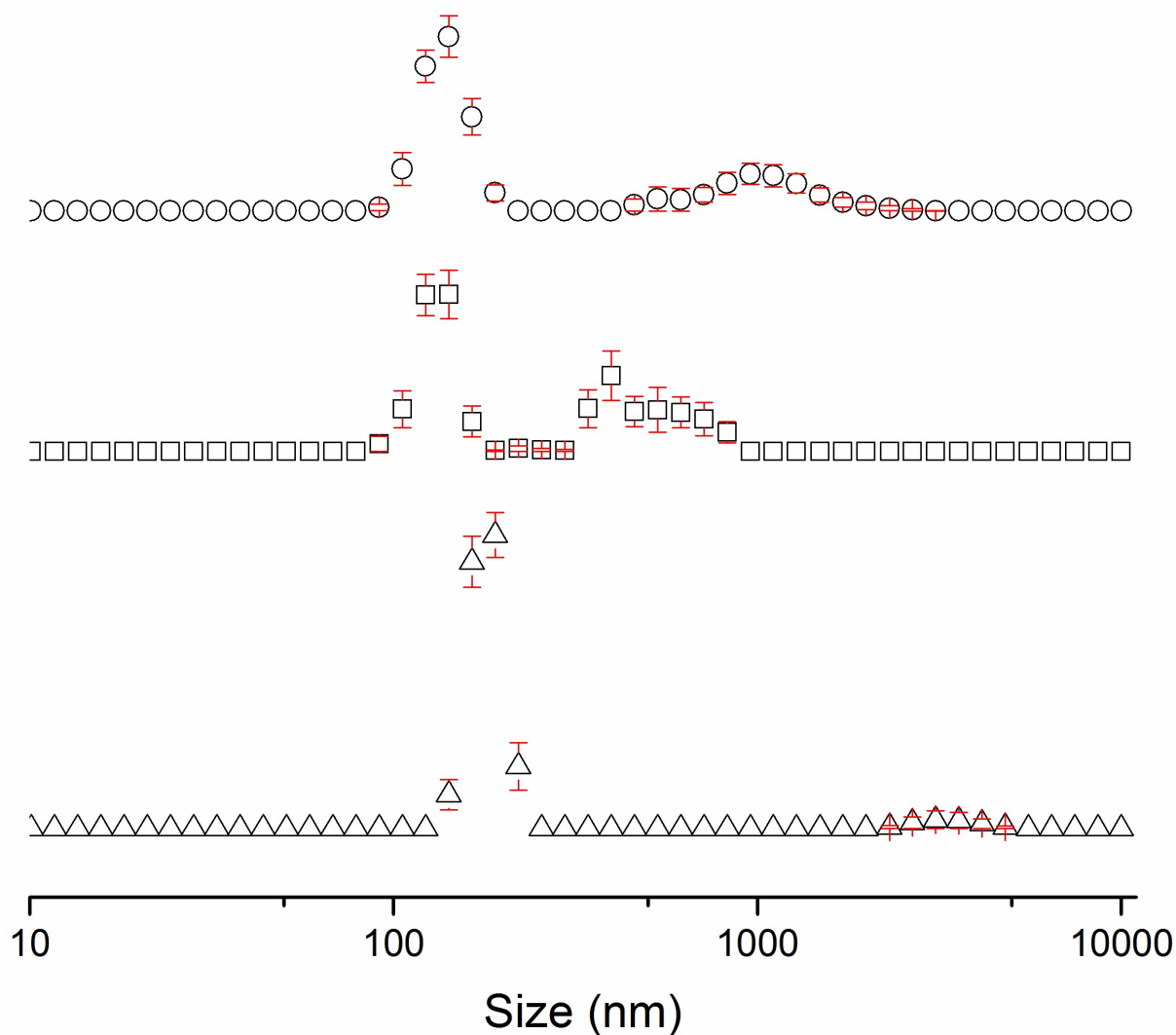


Figure S92 – Average intensity particle size distribution, calculated from 9 DLS runs, of supramolecular superstructures formed by dissolving **1** (0.03 mg) in DMSO (1 mL) at  $\Delta$ ) 25 °C,  $\square$ ) heating to 40 °C and  $\circ$ ) cooling to 25 °C. Only 9 of the available 10 DLS runs were used as in some cases, due to the heating and cooling processes there were some obvious temperature equilibration issues for the first run.

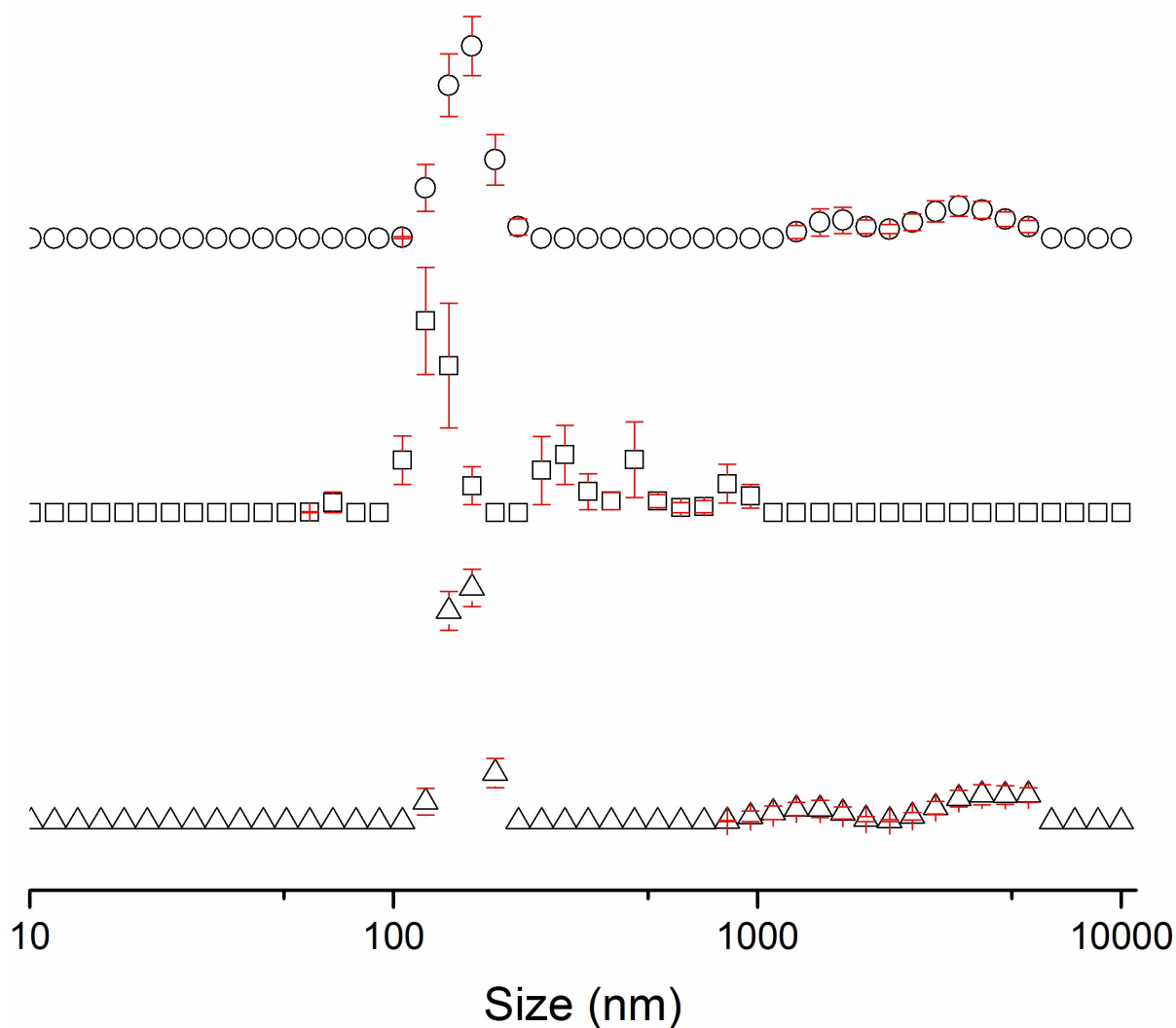


Figure S93 – Average intensity particle size distribution, calculated from 9 DLS runs, of supramolecular superstructures formed by dissolving **1** (0.003 mg) in DMSO (1 mL) at  $\Delta$  25 °C,  $\square$  heating to 40 °C and  $\circ$ ) cooling to 25 °C. Only 9 of the available 10 DLS runs were used as in some cases, due to the heating and cooling processes there were some obvious temperature equilibration issues for the first run.

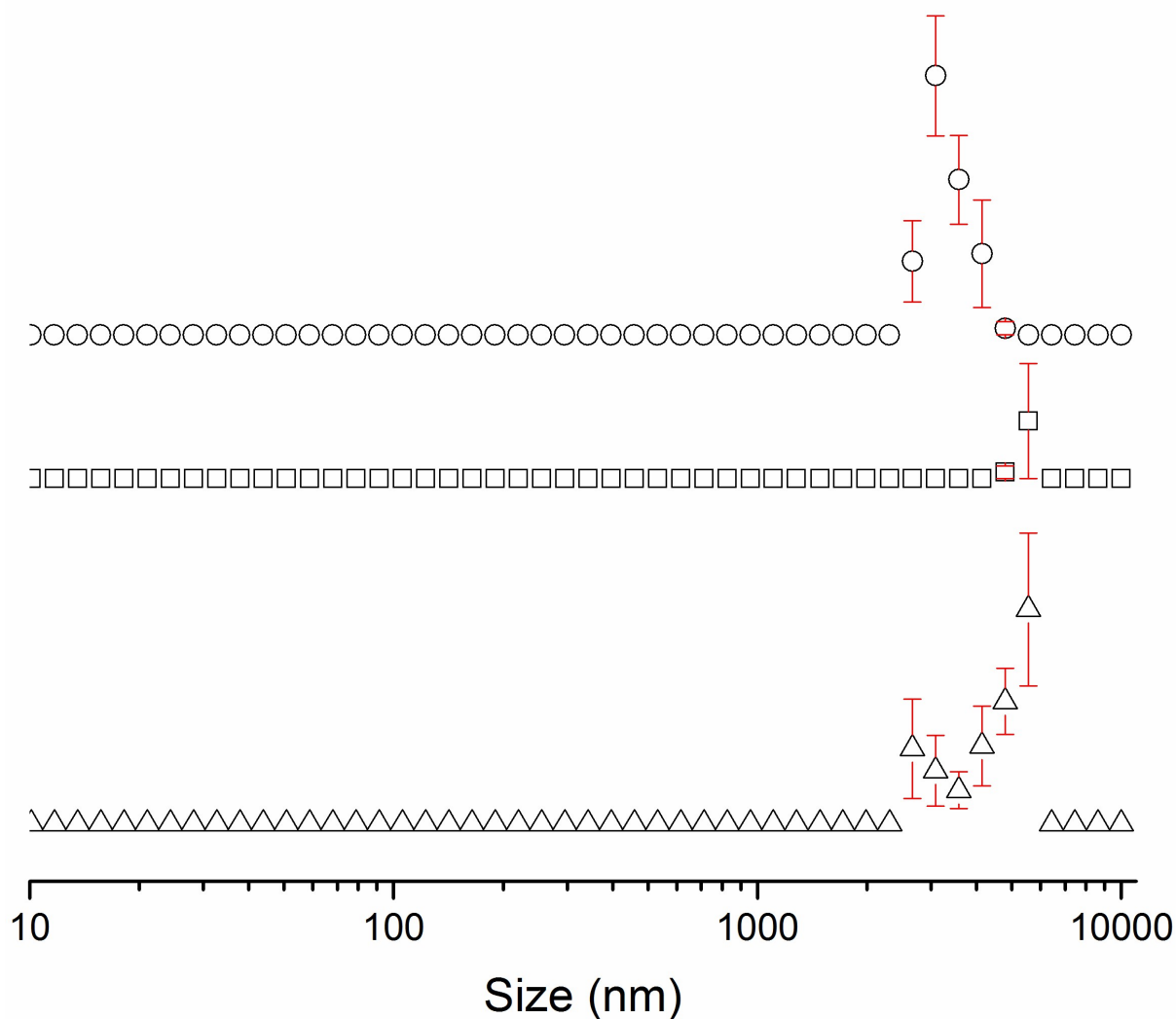


Figure S94 – Average intensity particle size distribution, calculated from 9 DLS runs, of supramolecular superstructures formed by dissolving **1** (30 mg) and 1 molar equivalent of compound **6** in DMSO (1 mL) at  $\Delta$ ) 25 °C,  $\square$ ) heating to 40 °C and  $o$ ) cooling to 25 °C. Only 9 of the available 10 DLS runs were used as in some cases, due to the heating and cooling processes there were some obvious temperature equilibration issues for the first run. Precipitation could be seen to occur during this process.

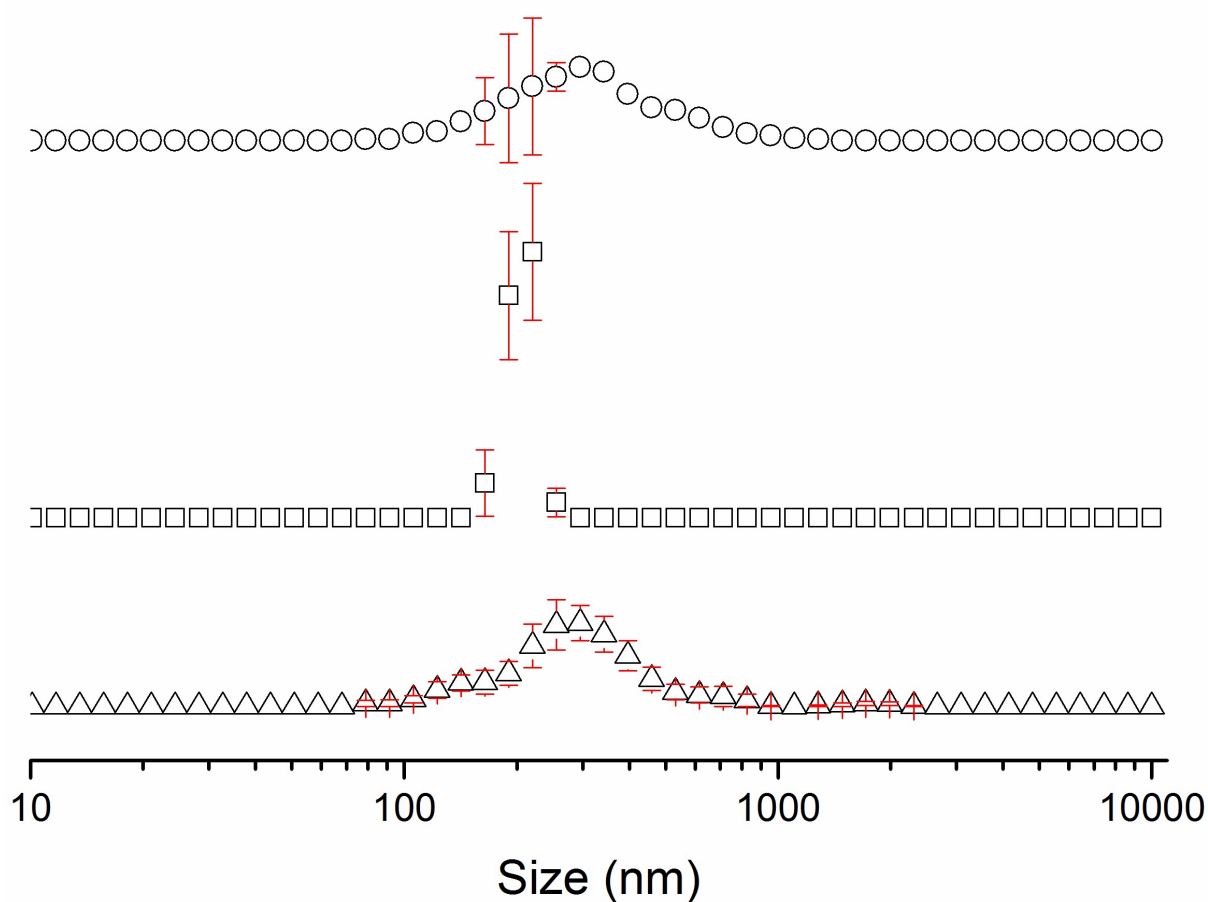


Figure S95 – Average intensity particle size distribution, calculated from 9 DLS runs, of supramolecular superstructures formed by dissolving **1** (30 mg) and 1 molar equivalent of TBAF in DMSO (1 mL) at  $\Delta$ ) 25 °C,  $\square$ ) heating to 40 °C and  $o$ ) cooling to 25 °C. Only 9 of the available 10 DLS runs were used as in some cases, due to the heating and cooling processes there were some obvious temperature equilibration issues for the first run.

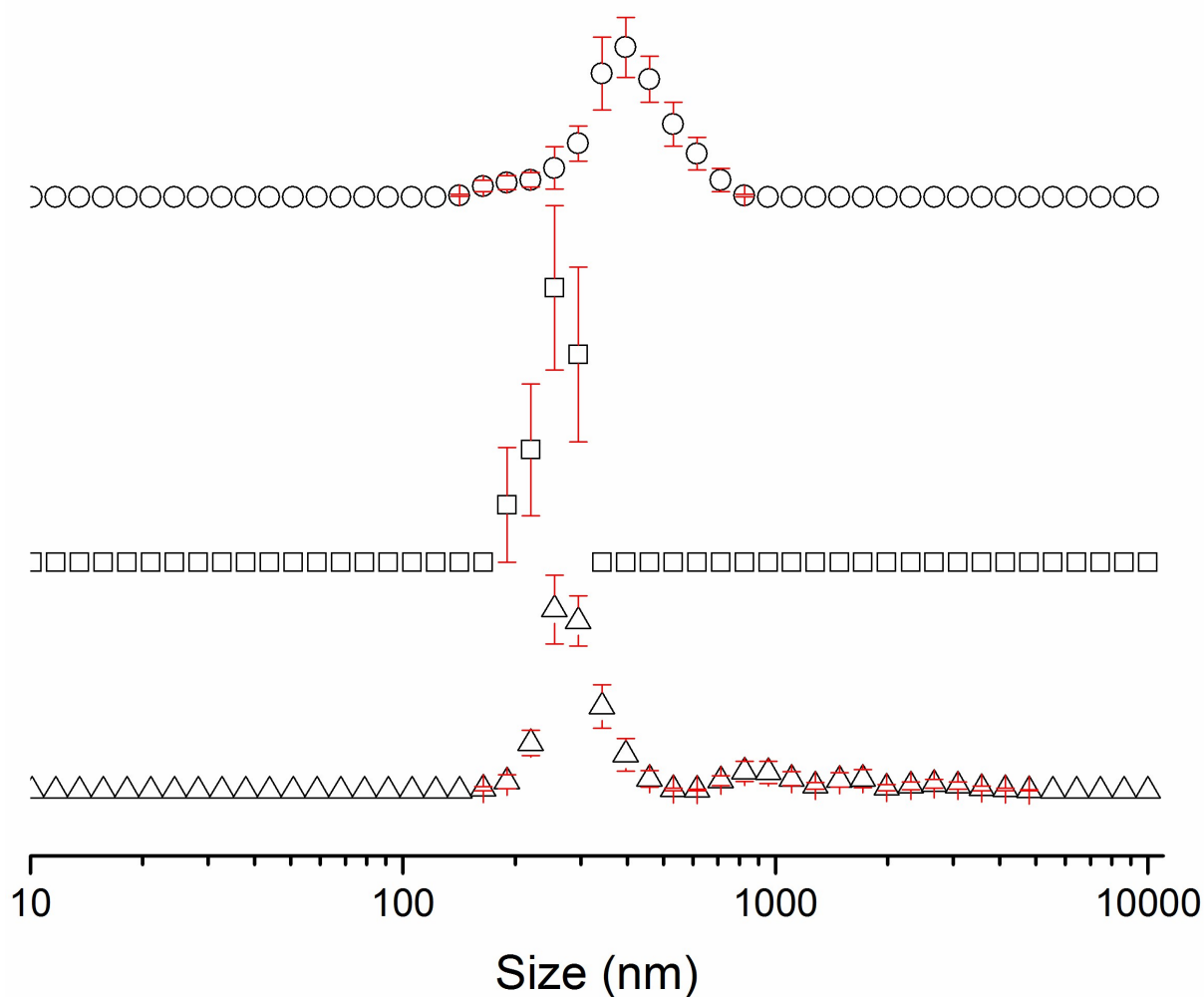


Figure S96 – Average intensity particle size distribution, calculated from 9 DLS runs, of supramolecular superstructures formed by dissolving **1** (30 mg) and 1 molar equivalent of TBAF and compound **6** in DMSO (1 mL) at  $\Delta$  25 °C,  $\square$ ) heating to 40 °C and  $\circ$ ) cooling to 25 °C. Only 9 of the available 10 DLS runs were used as in some cases, due to the heating and cooling processes there were some obvious temperature equilibration issues for the first run.

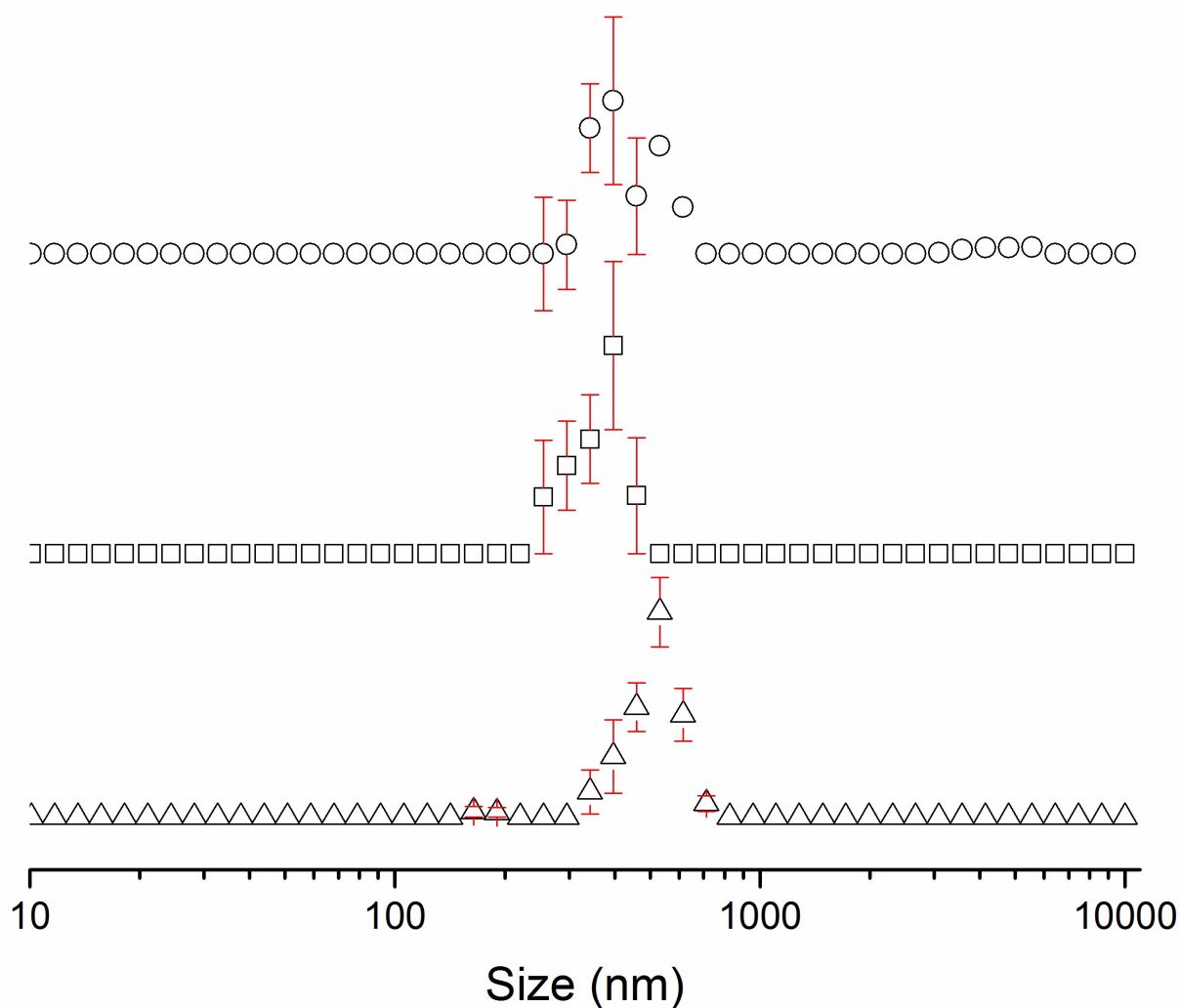


Figure S97 – Average intensity particle size distribution, calculated from 9 DLS runs, of supramolecular superstructures formed by dissolving **1** (30 mg) and 1 molar equivalent of TBACl in DMSO (1 mL) at  $\Delta$ ) 25 °C,  $\square$ ) heating to 40 °C and  $\circ$ ) cooling to 25 °C. Only 9 of the available 10 DLS runs were used as in some cases, due to the heating and cooling processes there were some obvious temperature equilibration issues for the first run.

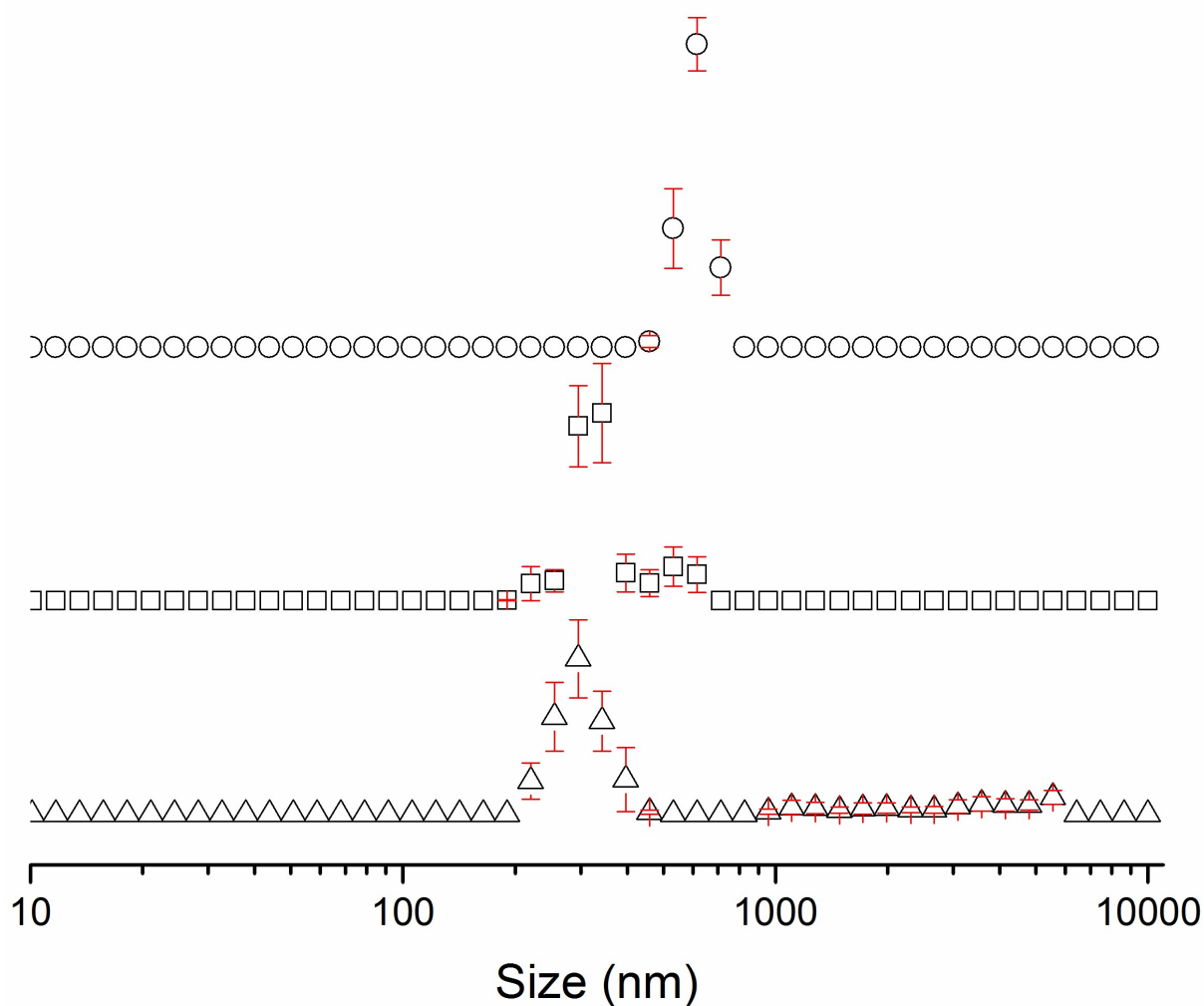


Figure S98 – Average intensity particle size distribution, calculated from 9 DLS runs, of supramolecular superstructures formed by dissolving **1** (30 mg) and 1 molar equivalent of TBACl and compound **6** in DMSO (1 mL) at  $\Delta$  25 °C,  $\square$ ) heating to 40 °C and  $\circ$ ) cooling to 25 °C. Only 9 of the available 10 DLS runs were used as in some cases, due to the heating and cooling processes there were some obvious temperature equilibration issues for the first run.

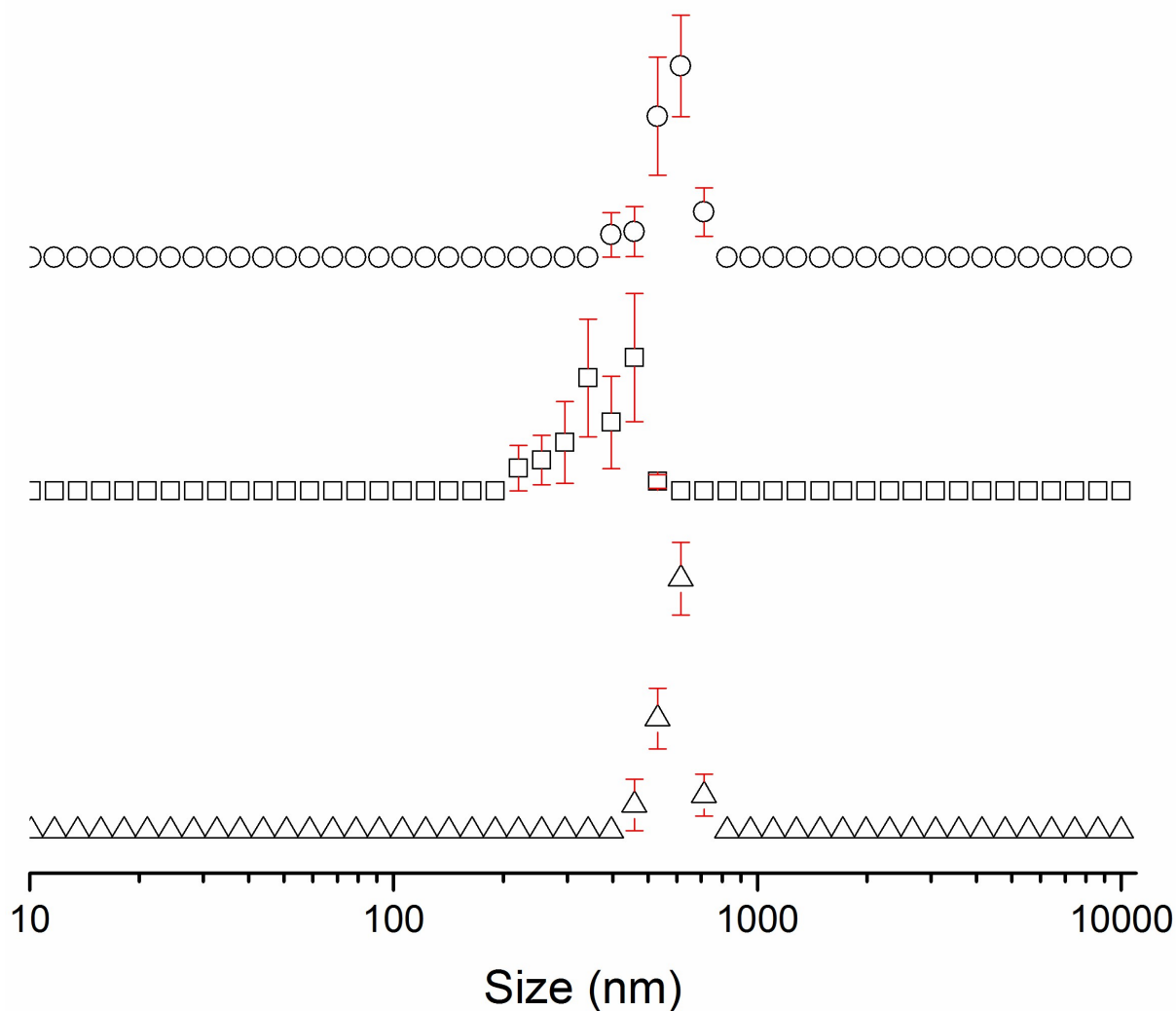


Figure S99 – Average intensity particle size distribution, calculated from 9 DLS runs, of supramolecular superstructures formed by dissolving **1** (30 mg) and 1 molar equivalent of TBABr in DMSO (1 mL) at Δ) 25 °C, □) heating to 40 °C and o) cooling to 25 °C. Only 9 of the available 10 DLS runs were used as in some cases, due to the heating and cooling processes there were some obvious temperature equilibration issues for the first run.

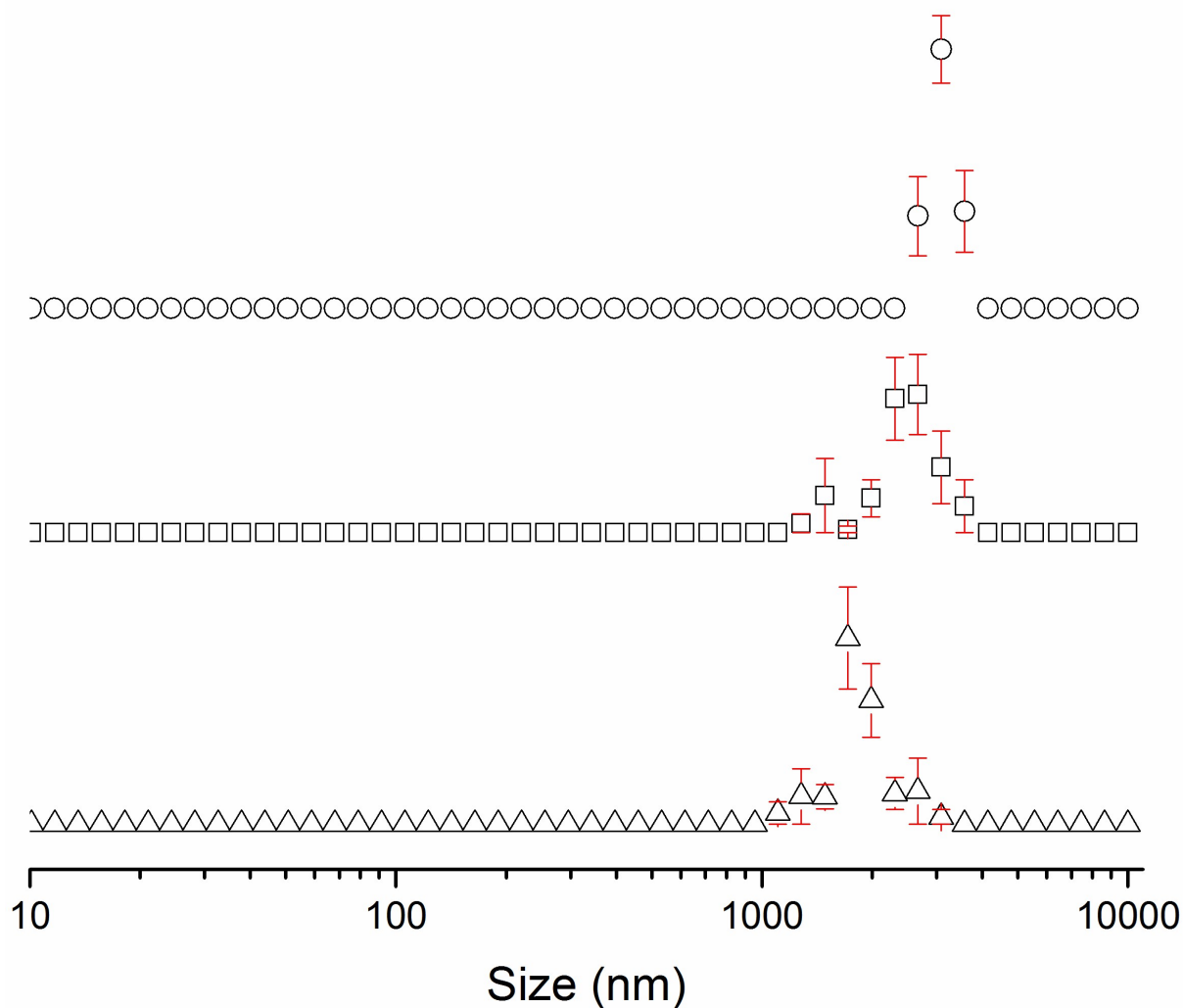


Figure S100 – Average intensity particle size distribution, calculated from 9 DLS runs, of supramolecular superstructures formed by dissolving **1** (30 mg) and 1 molar equivalent of TBABr and compound **6** in DMSO (1 mL) at  $\Delta$ ) 25 °C,  $\square$ ) heating to 40 °C and  $\circ$ ) cooling to 25 °C. Only 9 of the available 10 DLS runs were used as in some cases, due to the heating and cooling processes there were some obvious temperature equilibration issues for the first run.

## UV-Vis spectra

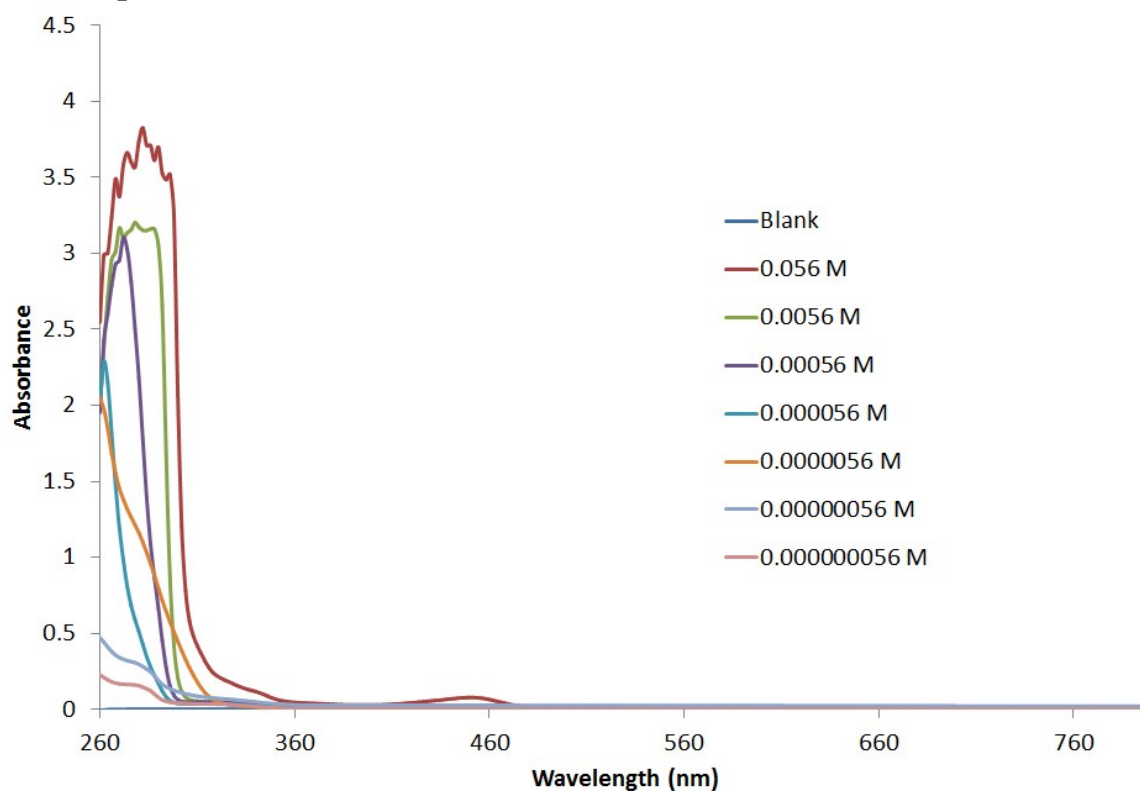


Figure S101 – UV-Vis spectra of compound 1 in DMSO.

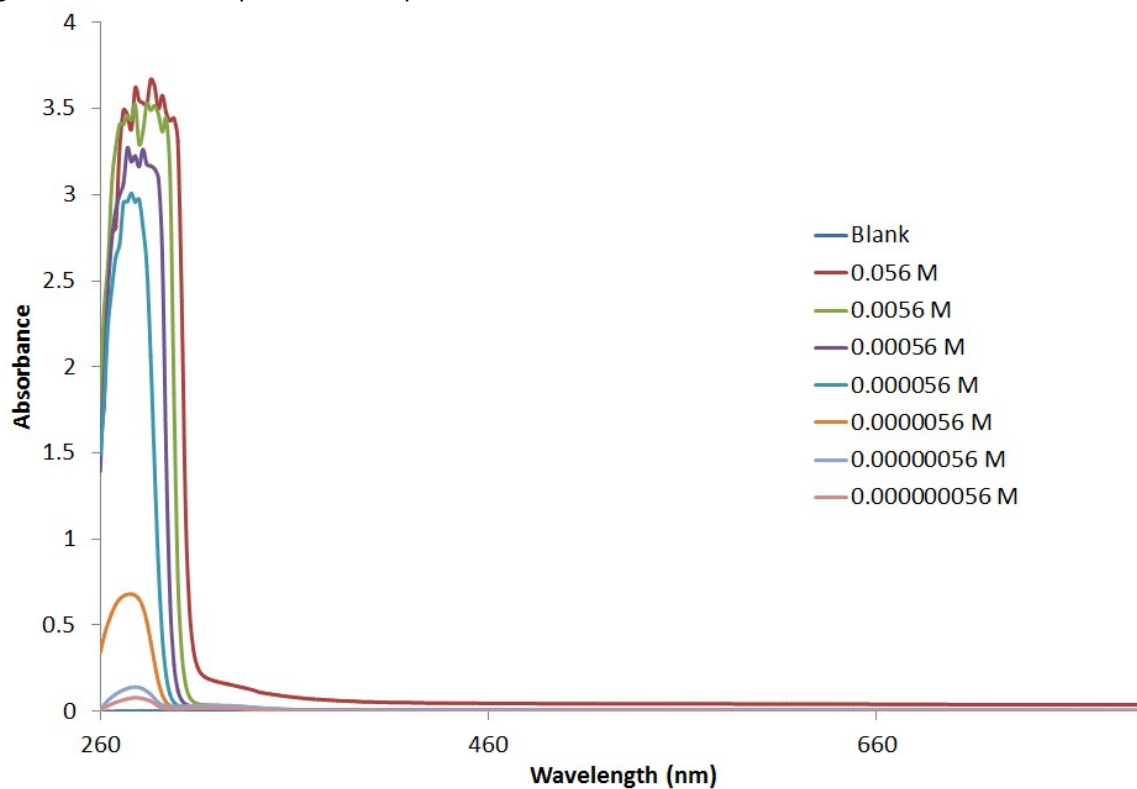


Figure S102 – UV-Vis spectra of compound 2 in DMSO.

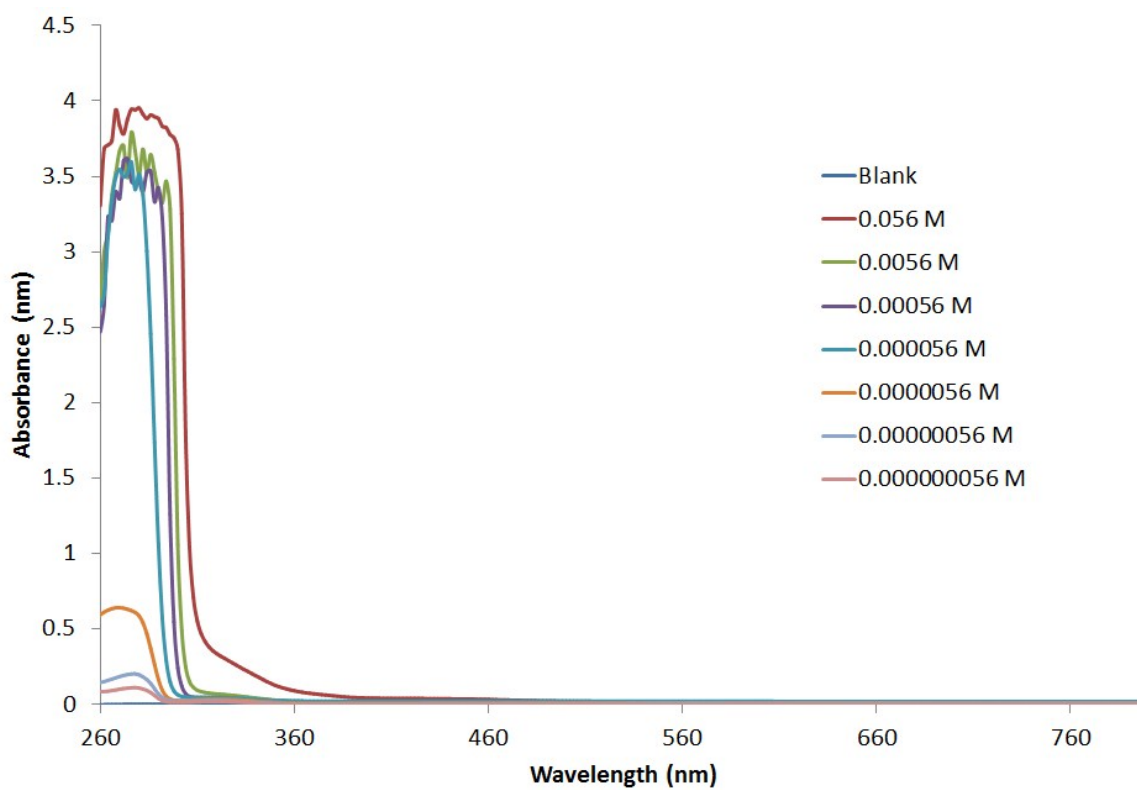


Figure S103 – UV-Vis spectra of compounds **1** and **2** in DMSO.

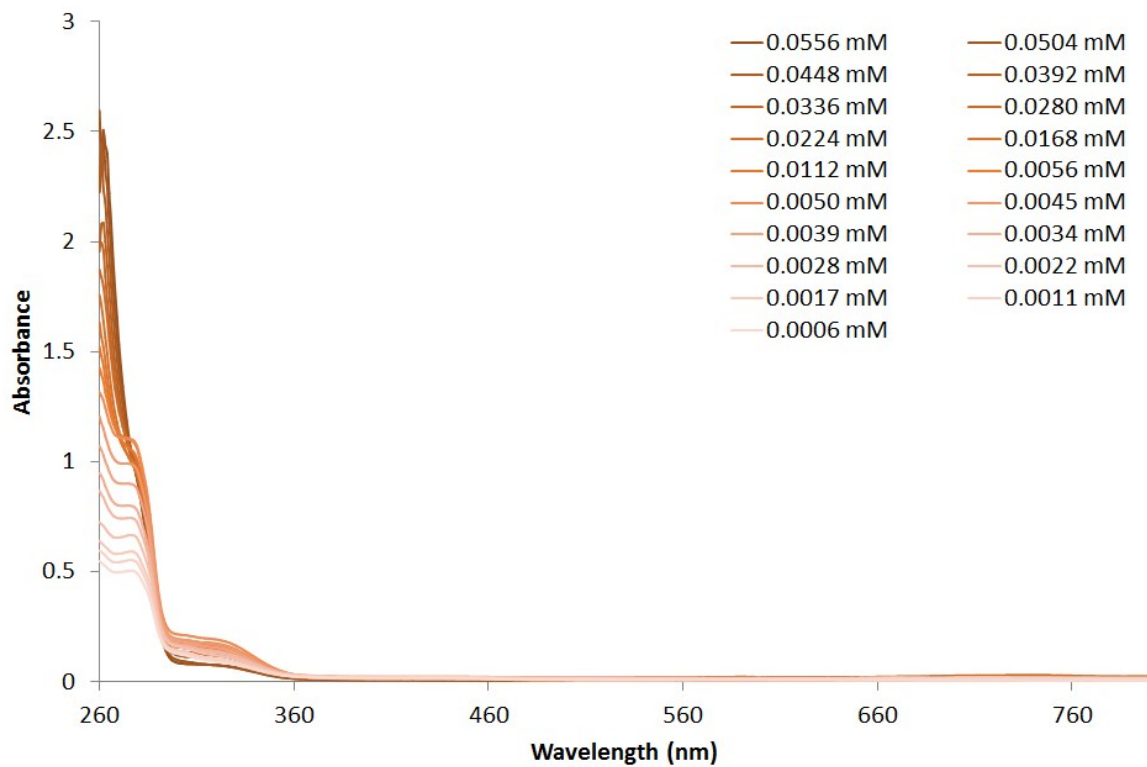


Figure S104 – Full UV-Vis spectra shown in Figure 3 of **1** in DMSO.

# Powder X-ray diffraction

## General procedure

Powder X-ray diffraction was used to examine the phase purity of compounds **4** and **5** created during this study in the solid state. This was carried out using a Rigaku MiniFlex diffractometer, operating in Bragg-Brentano geometry, with Cu K $\alpha$  radiation and a D/teX Ultra 1D detector. Samples were held on a Si zero-background sample holder at ambient temperatures. The sample obtained from compound **4**, which was close to a single phase was fitted using the Le Bail method<sup>3</sup> in the program Rietica<sup>4</sup> and shown in Figure S105 and S106, showing its purity. A comparison of a powder diffraction pattern calculated from the single crystal structure determined in this study for compound **5** with its powder diffraction pattern clearly indicated that it was not a single phase, see Figure S107.

## Compound 4

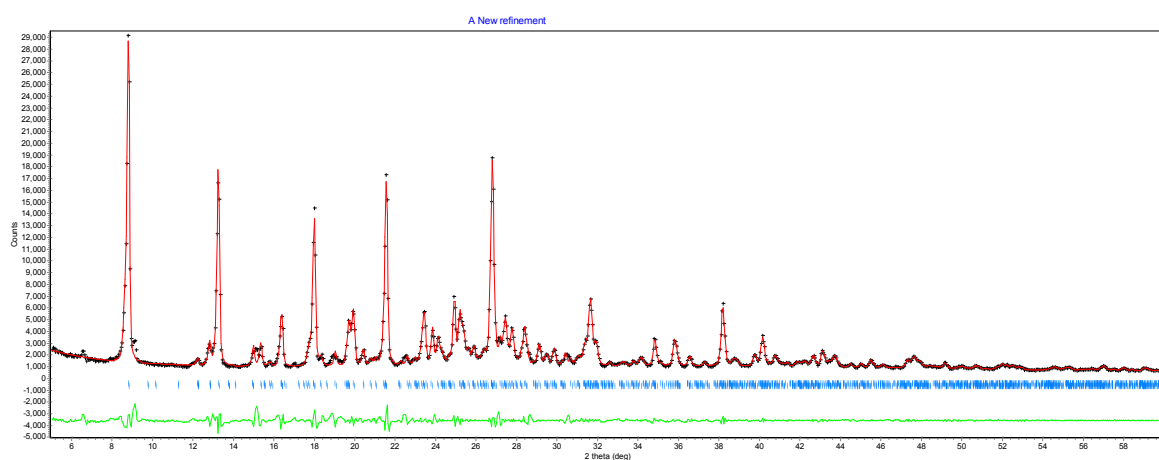


Figure S105 – Full powder X-ray diffraction pattern of compound **4**. Red – actual data. Black – predicted diffraction pattern from single crystal data. Green – difference between experimental and predicted powder diffraction pattern.

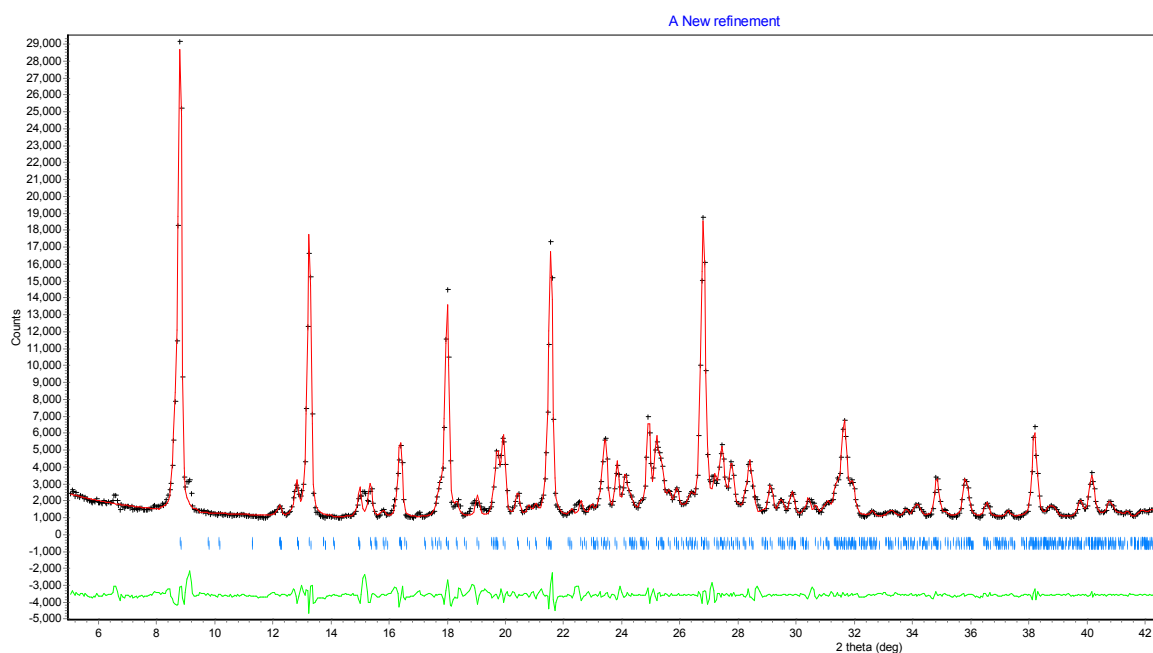


Figure S106 – Expanded powder X-ray diffraction pattern of compound **4**. Red – actual data. Black – predicted diffraction pattern from single crystal data. Green – difference between experimental and predicted powder diffraction pattern.

### Compound 5

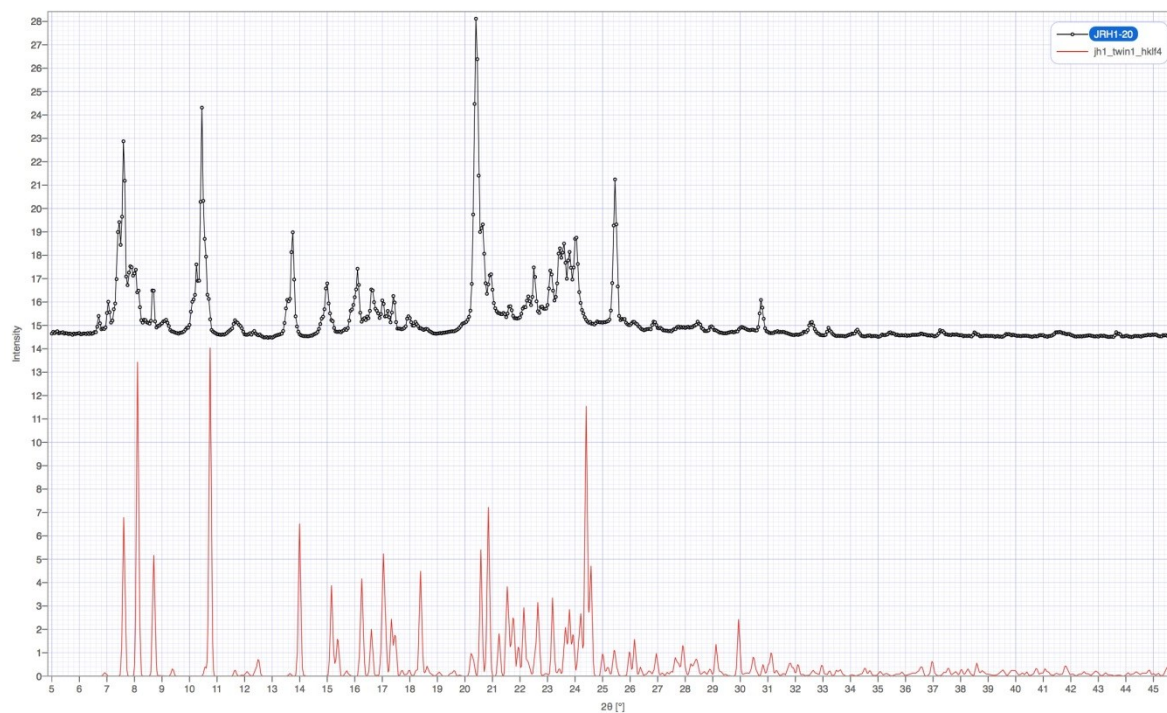


Figure S107 – Full powder X-ray diffraction pattern of compound **5**. Red – actual data. Black – predicted diffraction pattern from single crystal data.

## TEM data

### Sample preparation

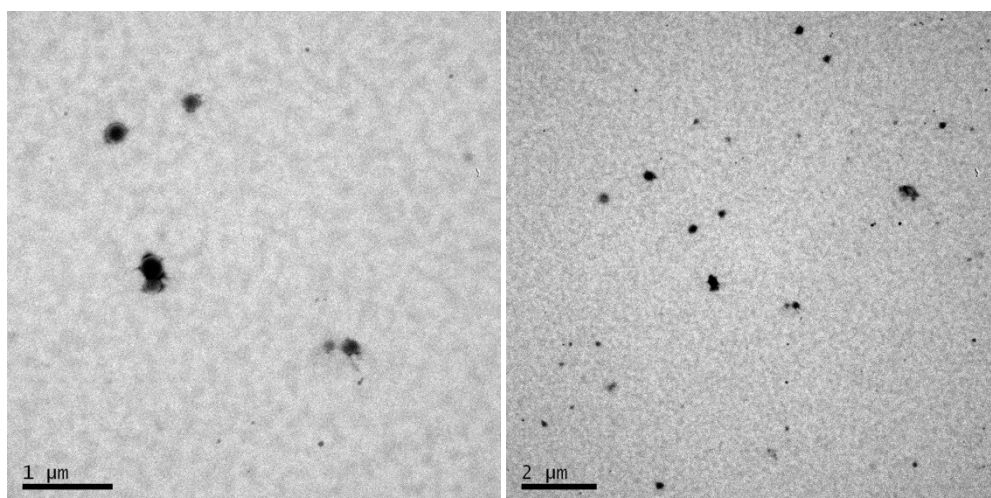
Samples were mounted on formvar/carbon coated 600mesh copper grids and were negatively stained with 2% aqueous uranyl acetate. Samples were obtained from DMSO solutions of compounds **1** (56 mM), **2** (56 mM) and **6** (56 mM) in various combinations. The TEM samples were prepared without heating at any stage.

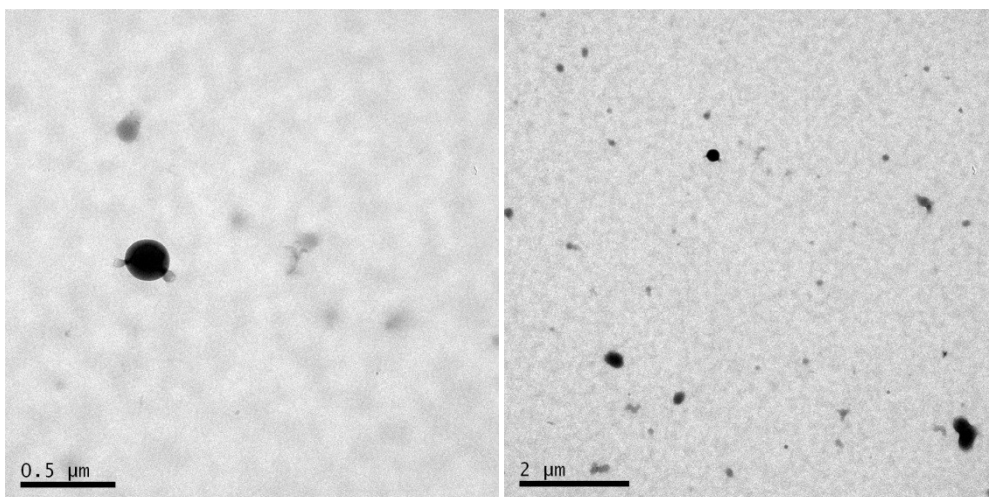
These TEM images do not appear in the main body of the text because they are of low quality; the staining process produced non uniform images that were also observed when the process was repeated. The images in the sections below were obtained from both the initial and repeated TEM imaging process. The images presented here are for consideration and should not be classed as definite representations of the nanostructures reported herein.

### Images

#### Filtered DMSO only

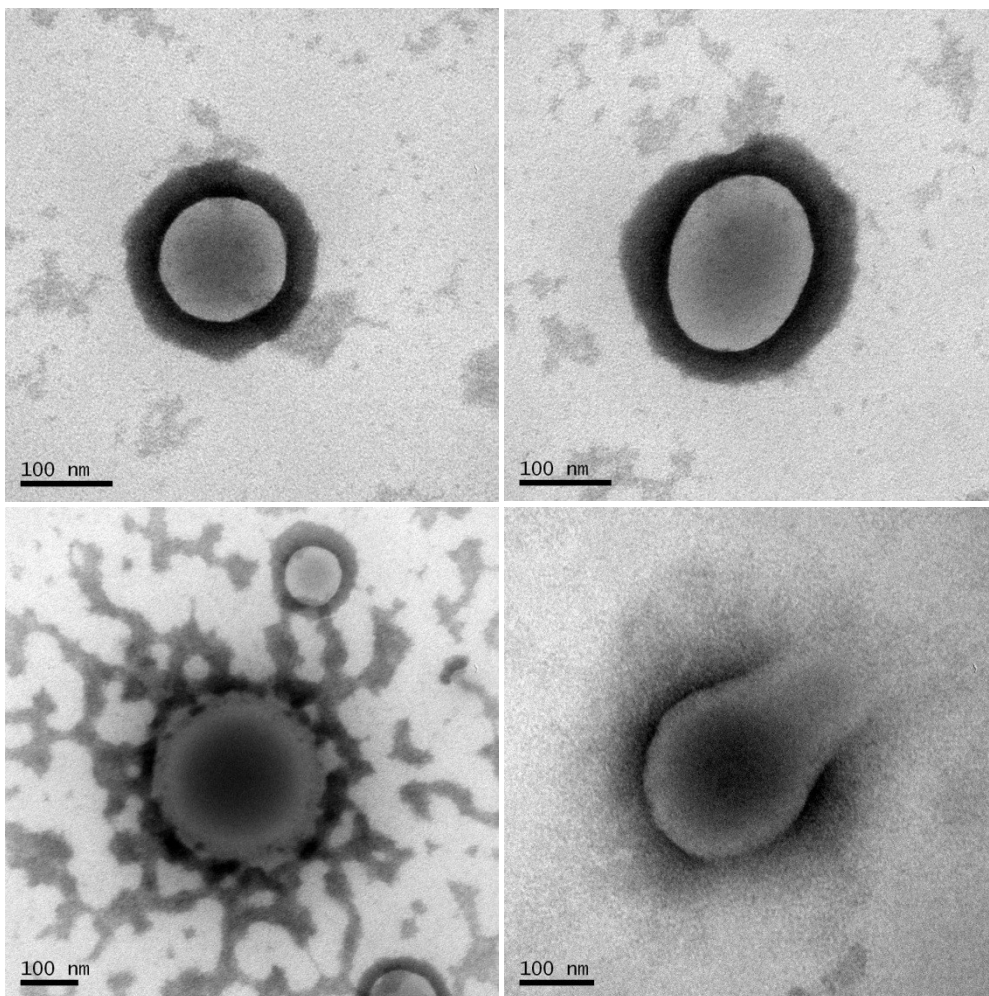
The images shown in this section were obtained by the direct addition of DMSO only to the TEM grids, followed by the staining methods previously mentioned. These images are included to illustrate the differences between those samples which contain compounds **1**, **2** and/or **6** and those which do not.

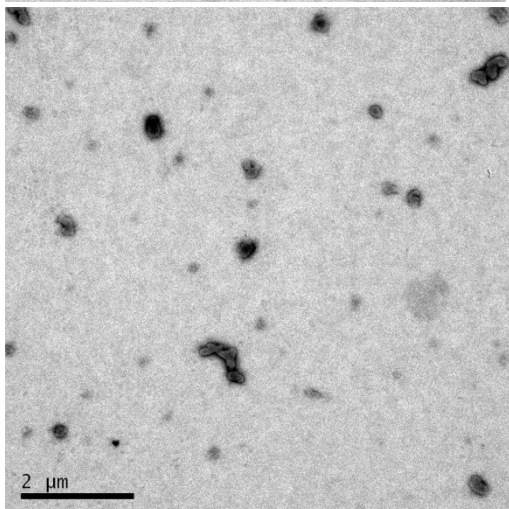
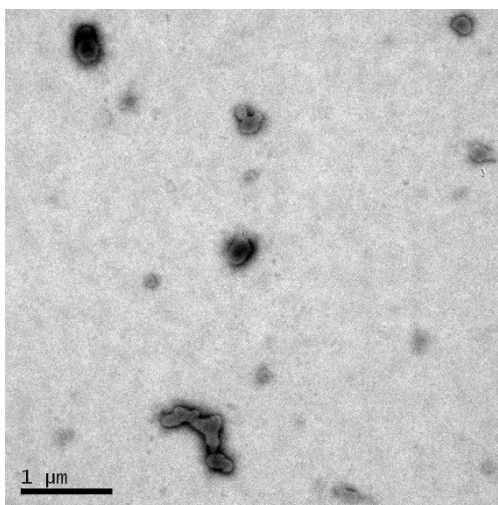
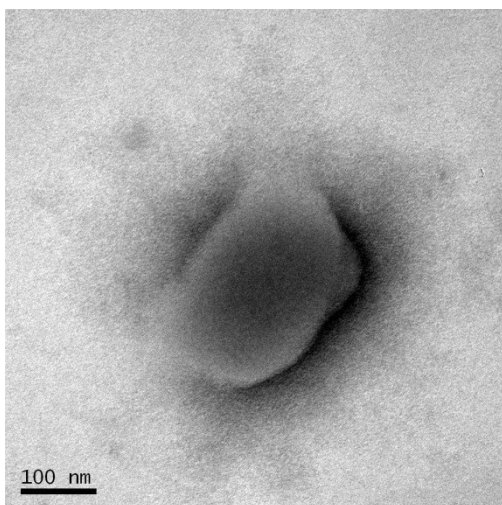
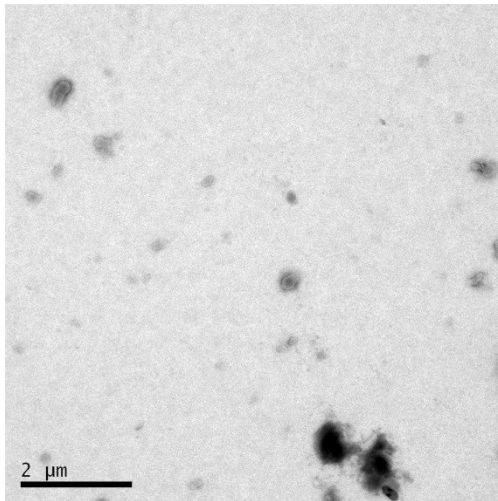
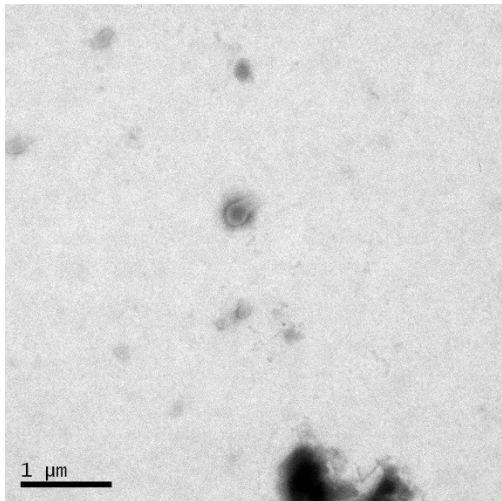




**Compound 1 only**

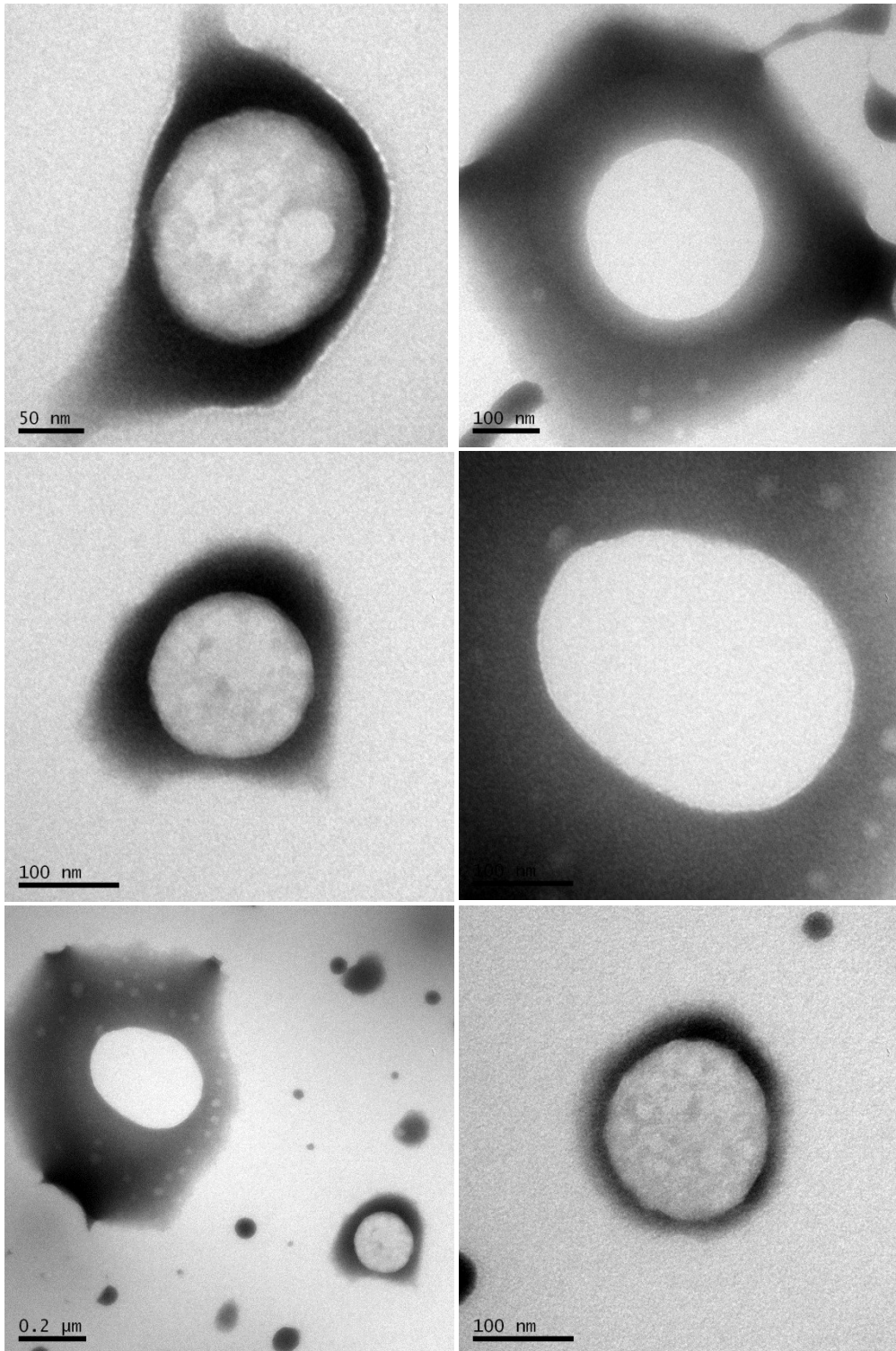
Here we see some possible evidence of those structures observed by analogous DLS experiments.

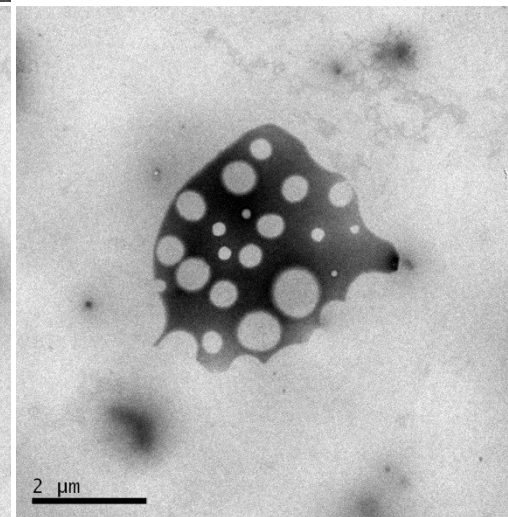
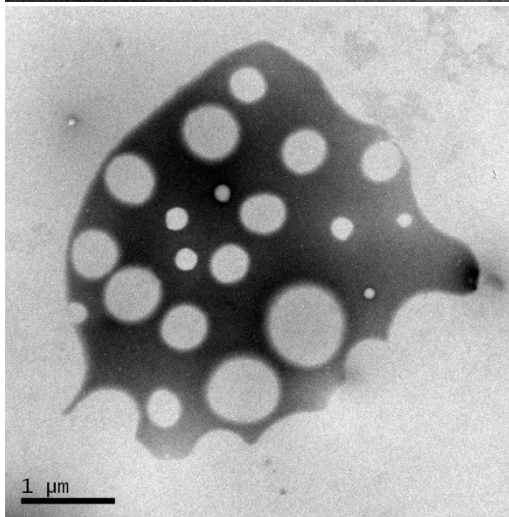
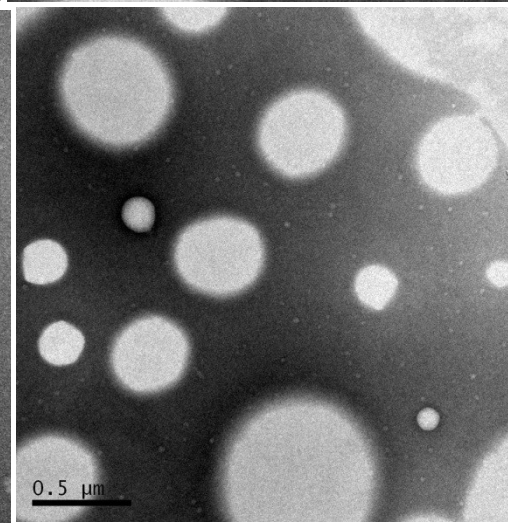
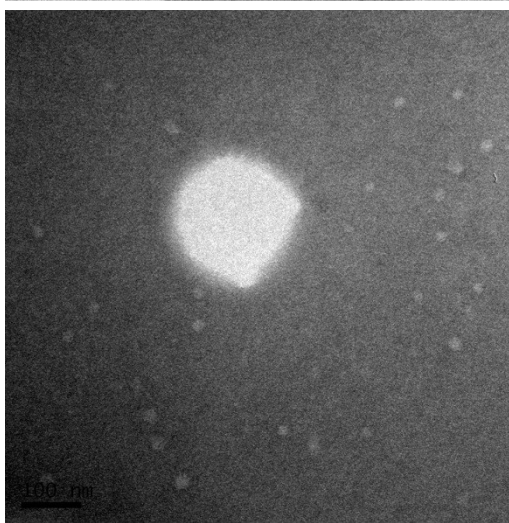
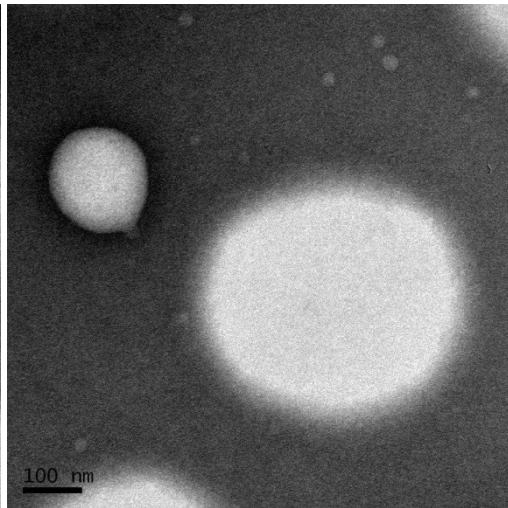
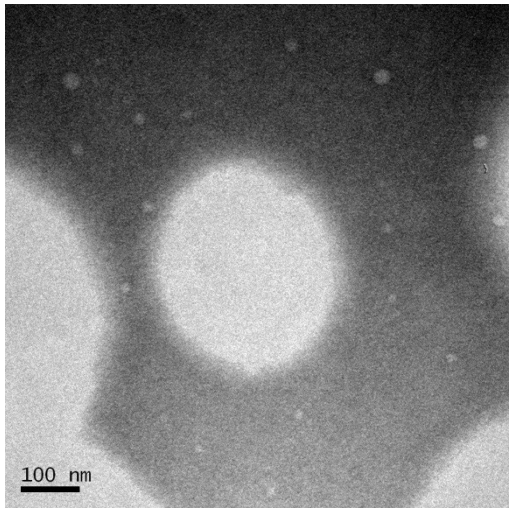


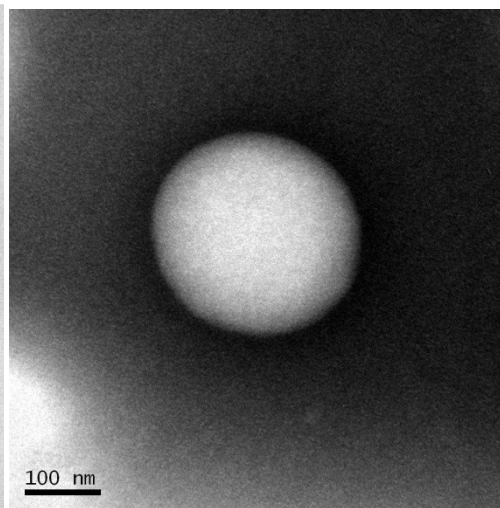
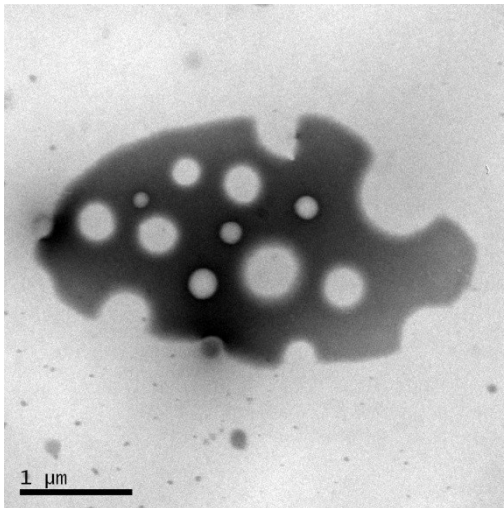
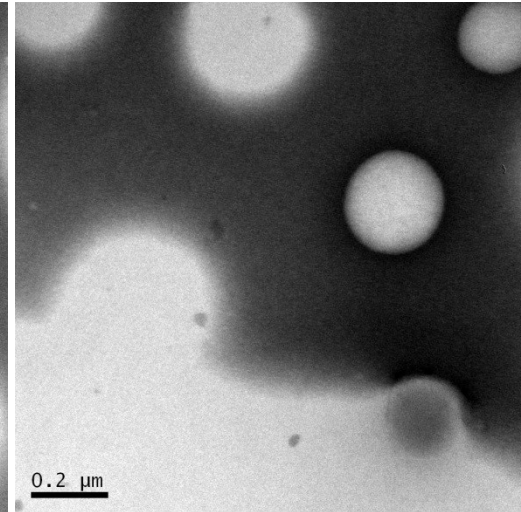
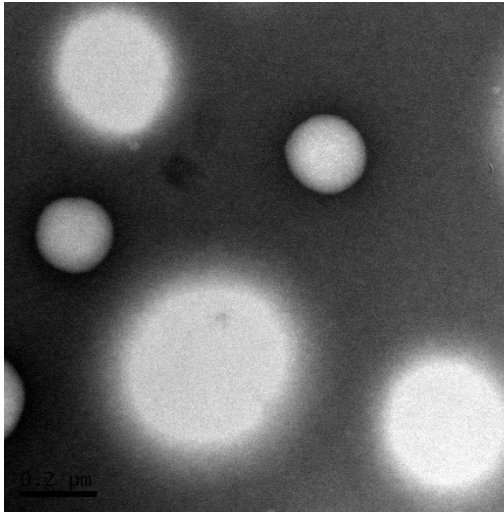
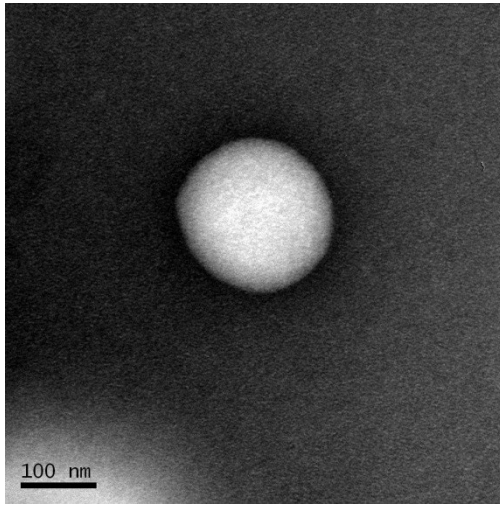
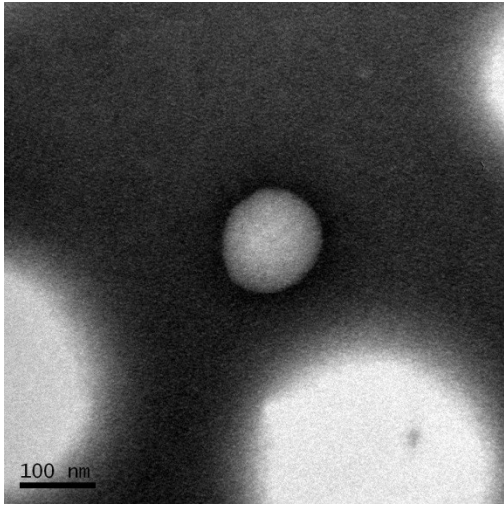


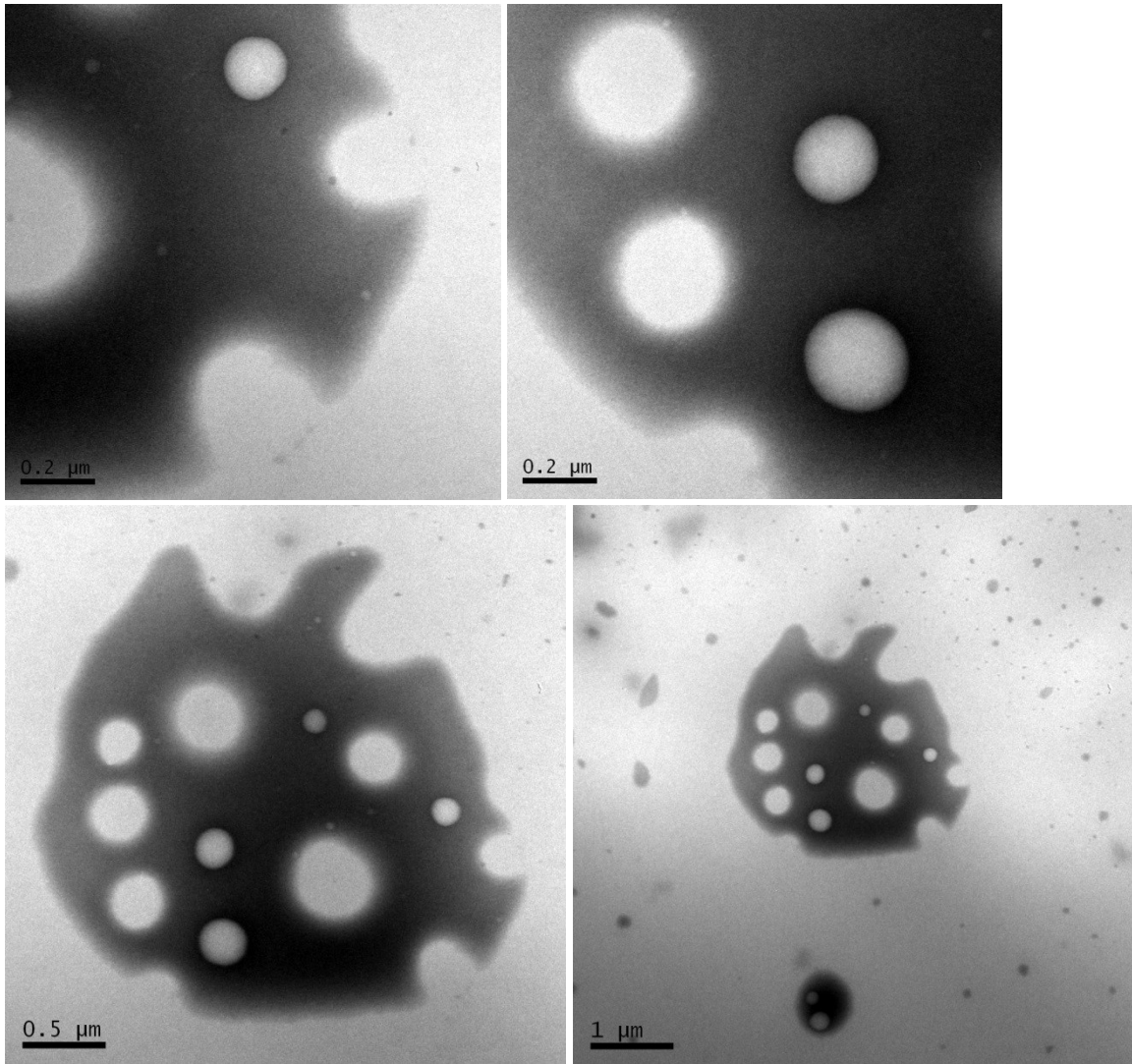
## Compound 1 and 2

Here we see some possible evidence of those structures observed by analogous DLS experiments.



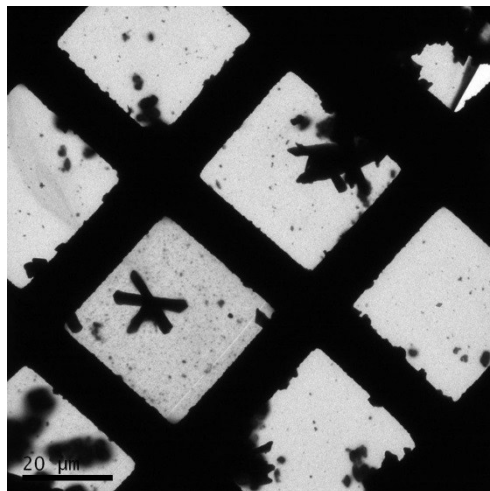






### Compound 1 and 6

This single image illustrates the precipitation of compound 6 from an equimolar solution of compounds 1 and 6. The aggregates here appear to be solid and form regular structures. This goes some way to explain the large structures observed in the analogous DSL samples.



## References

1. N. Busschaert, I. L. Kirby, S. Young, S. J. Coles, P. N. Horton, M. E. Light and P. A. Gale, *Angewandte Chemie-International Edition*, 2012, **51**, 4426-4430.
2. J. A. Shriver and S. G. Westphal, *Journal of Chemical Education*, 2006, **83**, 1330-1332.
3. A. Le Bail, H. Duroy and J. L. Fourquet, *Mater. Res. Bull.*, 1988, **23**, 447-452.
4. B. A. Hunter and C. J. Howard, *A computer program for Rietveld analysis of X-ray and neutron powder diffraction patterns*, Lucas Heights Laboratories, 1998.